Flying-V Crashworthiness: a Preliminary Assessment

Master's Thesis

Marco Desiderio

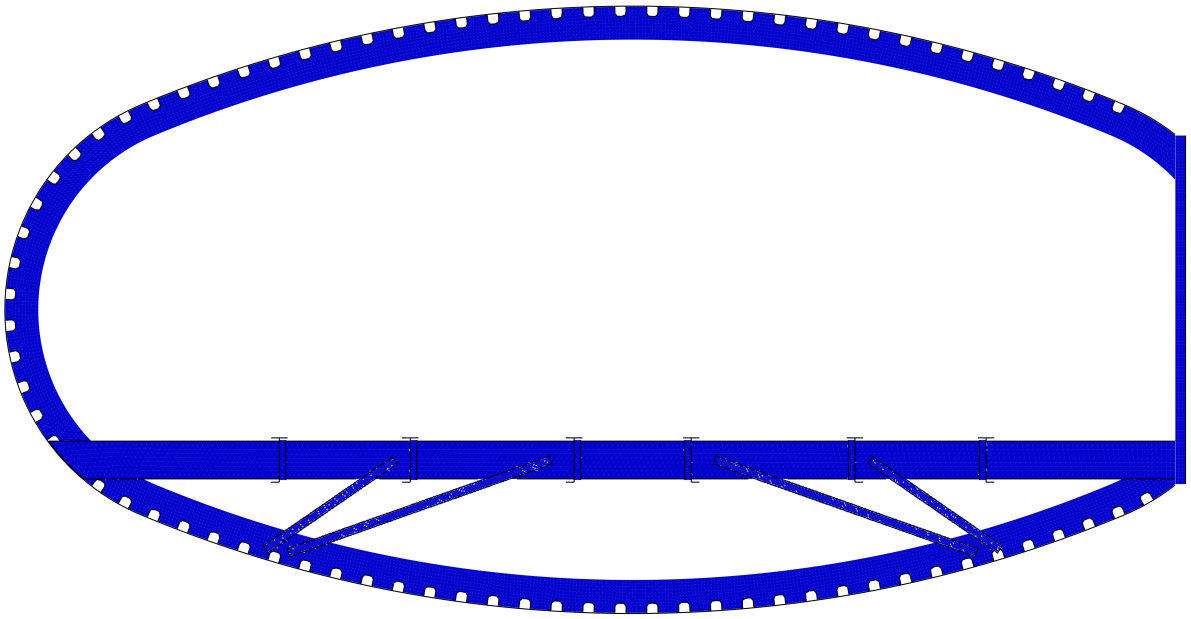

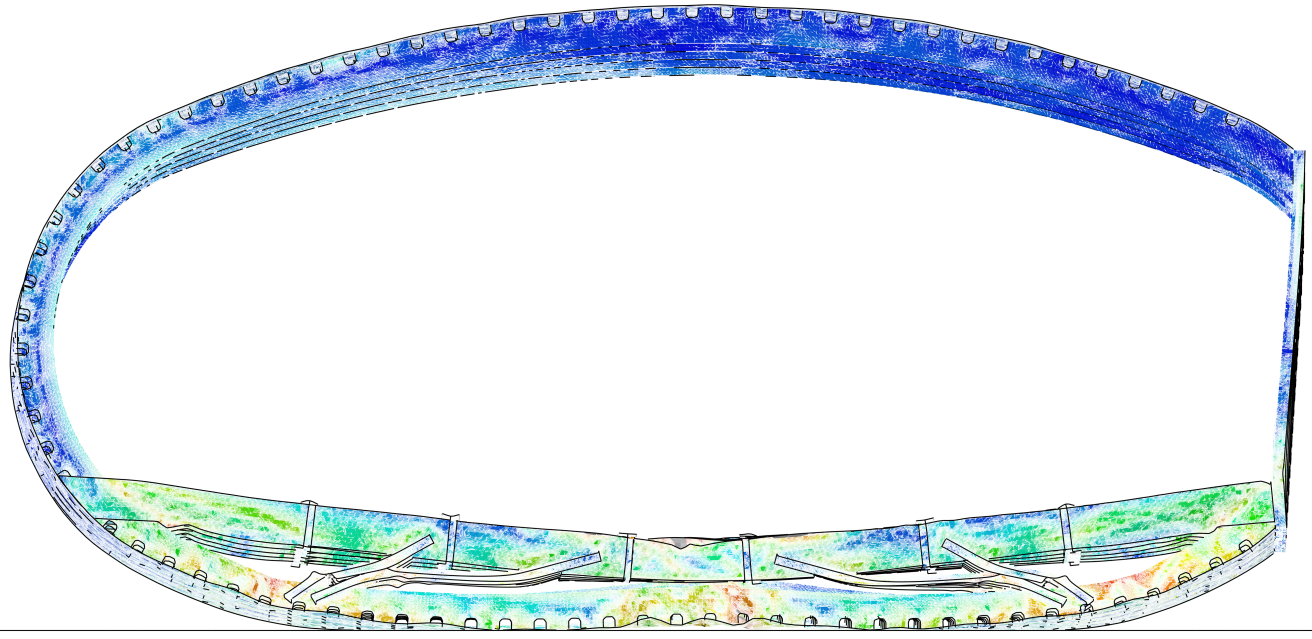

Technische Universiteit Delft

TU Delft

This page intentionally left blank.

Flying-V Crashworthiness: a Preliminary Assessment

Master's Thesis

of

Marco Desiderio

In fulfillment of the requirements to obtain the degree of
Master of Science in Aerospace Engineering,
at the Delft University of Technology

To be defended publicly at the Faculty of Aerospace Engineering, Lecture Room D,
on March 20, 2023, 9.00 am CET.

Student number:	4644150
Project Duration:	February 2022 – January 2023

Thesis Committee:		
Dr. Ing. S. G. P. Castro	Associate Professor	TU Delft
Dr. Ir. R. C. Alderliesten	Associate Professor	TU Delft
Ir. M. J. Schuurman	Assistant Professor	TU Delft
Dr. Ir. R. Vos	Associate Professor	TU Delft

A digital copy of this report is publicly available at `https://repository.tudelft.nl/`.

TU Delft

This page intentionally left blank.

I

Front Matter

This page intentionally left blank.

Preface and Acknowledgments

In August 2017 I moved here to Delft, in the Netherlands, to start my Bachelor of Science in Aerospace Engineering. I was 18 years old back then, and I looked a lot younger. I have nostalgic memories from the Bachelor's days, during which I have met plenty of inspiring, kind, and true friends. Some of them are still in Delft, or anyway elsewhere in the Netherlands. Some of them moved abroad. But the characteristics mentioned above remain and, while we might or might no longer meet sometime in the future, the simple fact of meeting such people has played a role in shaping me into the person I have became since August 2017.

Now that my Master of Science in Aerospace Engineering has come to an end, I cannot but be grateful to every single person that I have met along the way. I will however not be making any names since this thesis will be public, and I do not want to disappoint anyone. Above all, however, is of course my family. My parents, Marina and Roberto, and my brother, Alfredo. They have motivated me, supported me, inspired me, valued me and forged me in the person I am very happy to be today. I am and I will be grateful to you, forever. Thank you from the depth of my hearth.

I would additionally like to thank my daily supervisor, Saullo, and co-supervisors Michiel and Rene. Thank you Saullo for being available round the clock, even in your busiest periods, and always with a deep interest and excitement in and about the research. I really appreciated that! I could not have asked for a better supervisor. Thank you Rene for the always meaningful and spot-on suggestions, and awesome humor during the various reviews. And thank you Michiel for the equally valid and helpful discussions, and the care that you have always shown to have. Overall, I could not have asked for better supervisors, and I am grateful for that. If I have enjoyed working on this thesis for the past months, that is also thanks to you!

And, last but not least, thank you Daniel (Atherstone) for the awesome support provided to use the 3DX platform, that has enabled me to really speed up the workflow, and generate multiple finite element models within minutes, and for the VR set-up (for the defense - if you are in the graduation committee and reading this, I am sorry for the spoiler).

Have a happy reading.

Marco Desiderio
Delft, the Netherlands, March 6, 2023

This page intentionally left blank.

Abstract

The Flying-V (FV) is a novel aircraft configuration where the cabin and two half wings have been integrated to form a V-shaped aircraft, in a configuration that promises higher aerodynamic efficiency and an estimated 20% reduction in fuel burn. Compared to other blended wing-body designs, the Flying-V can be stretched to generate a family of designs, thus rendering this concept more palatable from a commercial standpoint. Contrarily to conventional aircraft configurations, the Flying-V cabin's typical section presents a significant eccentricity, making the crashworthiness aspect unique and the design more challenging.

Aircraft crashworthiness is the ability of an airplane to protect the occupants in the event of a crash. Airworthiness regulators, for CS-25 aircraft, namely large passenger aircraft, require four main criteria to be addressed when it comes to occupant protection: (1) guarantee of a survivable volume; (2) guarantee of acceptable acceleration and loads sustained by the occupants; (3) retention of items of mass; (4) preservation of occupants' egress paths. To highlight the importance of such requirement, one can simply note how, according to Boeing's 2020 statistical summary of commercial jet airplane accidents, considering the 2011-2020 time-frame, 54% of fatal crashes occurred during the final approach and landing phases, but these only account for about 40% of total casualties.

The aforementioned criteria are generally validated by means of a drop test of the aircraft's typical fuselage section. The scope of this research is to provide an initial assessment of the crashworthiness characteristics of the FV in terms of loads and accelerations sustained by the occupants and render recommendations for future design iterations, to directly incorporate crashworthiness requirements during the preliminary design of the airframe.

Firstly, to understand the influence of fuselage ovalization, and the distance of the floor structure from the keel of the fuselage (hereinafter referred to as 'floor beam height' for brevity), a series of parametric studies have been performed on the fuselage section of a conventional aircraft, the Fokker F-28. The parametric CAD model of the F-28 typical section is generated based on a readily accessible airframe in possession of the Faculty of Aerospace Engineering at TU Delft. Based on the CAD, a FEM directly linked to the CAD geometry is generated. The analysis consists of a virtual drop test, at a velocity of $9.1\,\mathrm{m/s}$, and is solved using the commercially available Abaqus software.

During the ovalization studies, the ellipse eccentricity parameter e, initially set to 0.0 to represent a circular fuselage, is progressively increased until 0.75, which is the approximate eccentricity of the FV typical section. During the parametric studies on the effects of the vertical floor location, instead, the fuselage eccentricity is kept constant, while the floor beam height is varied, in increments of $50\,\mathrm{mm}$. The crashworthiness properties are evaluated using three metrics: mean acceleration experienced by the occupants from the start of the impact until before the post-impact rebound; dynamic response index; energy absorption characteristics of the section. Data from the parametric studies show a strong increase in occupant accelerations, due to the reduction in crushable volume and impact time duration.

Regarding the FV's section design, the preliminary assessment is performed on a CAD model of the FV typical section with constant frame height and thickness. Previous research focused on a structural optimization of a different section with a more complete set of design variables, and airworthiness requirements, which resulted in variable height and thickness frames. However, this previous research did not consider crashworthiness aspects quantitatively. Based on the sizing results from previous work, a finite element model was built of the FV's typical section. Some simplifications to the geometry of the crash section have been applied, to account for future manufacturing constraints. A total of four different crash concepts have been developed and assessed: two conventional ones with six and four floor struts, respectively, and two unconventional ones with vertical crushable elements. The unconventional concepts were not able to absorb a sufficient about of energy, and this resulted in high accelerations experienced by the occupants, due to the lack of creation of plastic hinge on the frames, which, in conventional aircraft, is where a large portion of energy is dissipated. The six-struts

conventional concept also resulted being too stiff, and, thus, resulted in an increase in occupant accelerations. The four-struts concepts seemed to be the most promising one, although, within this research, a crashworthy design was not achieved. For future work recommendations, it is suggested to develop a coupled static-dynamic optimization, in order to fulfill requirements related to quasi-static operational loads, and the crashworthiness aspect.

Contents

Nomenclature

Abbreviations

AC	Advisory Circular
AM	Additive Manufacturing
AMC	Acceptable Means of Compliance
ARALL	Aramid Reinforced Aluminium Laminate
ATAG	Air Transport Action Group
CARALL	Carbon Reinforced Aluminium Laminate
CFRP	Carbon Fiber Reinforced Plastic
CPU	Central Processing Unit
CS	Certification Specifications
DLR	German Aerospace Center (Deutsches Zentrum für Luft- und Raumfahrt)
DRI	Dynamic Response Index
EASA	European Union Aviation Safety Agency
FAA	US Federal Aviation Administration
FE	Finite Element
FEA	Finite Element Analysis
FML	Fiber-Metal Laminate
FRP	Fiber-Reinforced Plastic
FV	Flying-V Aircraft
GA	General Aviation
GFRP	Glass Fiber Reinforced Plastic
GLARE	Glass Laminate and Aluminium Reinforced Epoxy
HIC	Head Injury Criterion
JC	Johnson-Cook Material Model
LDS	Lower Deck Seating
LL	Lumbar Loads
LTB	Lateral Torsional Buckling

MBA	Multi-Body Approach
MCF	Mean Crushing Force
MTOW	Maximum Take-Off Weight
NASA	National Aeronautics and Space Administration
NLES	No-leading edge spar concept from Dotman
NLR	Royal Netherlands Aerospace Center (Koninklijk Nederlands Lucht- en Ruimtevaartcentrum)
OEM	Original Equipment Manufacturer
PCF	Peak Crushing Force
SC	Special Conditions
SEA	Specific Energy Absorption
TACDWG	Transport Aircraft Crashworthiness and Ditching Working Group
TiCaPEEK	Titanium Carbon Fiber PEEK Laminate
USAF	United States Air Force

Greek Symbols

ϵ_f	Fracture Strain	–
μ	Friction Coefficient	–
σ_u	Ultimate Tensile Stress	MPa

Abaqus Keywords

ALLFD	Frictional dissipation energy	J
ALLKE	Global model kinetic energy	J
ALLPD	Plastic deformation dissipation energy	J

Latin Symbols

$\dot{W}_c$	Crack Propagation Energy Release Rate	$\mathrm{J\,s^{-1}}$
$\dot{W}_f$	Friction Energy Release Rate	$\mathrm{J\,s^{-1}}$
$\dot{W}_s$	Transverse Shearing Energy Release Rate	$\mathrm{J\,s^{-1}}$
A	Area	$\mathrm{m^2}$
a	Acceleration	$\mathrm{m\,s^{-2}}$
CFE	Crush Force Efficiency	–
D	Diameter	m
DRI	Dynamic Response Index	–

E_s	Specific Energy	kJ kg^{-1}
F	Force	N
F_{mean}	Mean Crushing Force	N
F_{peak}	Peak Crushing Force	N
g	Earth Gravitational Acceleration	m s^{-2}
G_{IC}	Interlaminar Fracture Toughness	MPa m$^{0.5}$
HIC	Head Injury Criterion	–
l	Length	m
m	Mass	kg
t	Thickness	m
t	Time	s
v	Velocity	m s^{-1}

This page intentionally left blank.

List of Figures

This page intentionally left blank.

List of Tables

This page intentionally left blank.

Introduction

Aircraft crashworthiness is the ability of an airplane to protect the occupants in the event of a crash. Airworthiness regulators, for CS-25 aircraft, namely large passenger aircraft, require four main criteria to be addressed when it comes to occupant protection: (1) guarantee of a survivable volume; (2) guarantee of acceptable acceleration and loads sustained by the occupants; (3) retention of items of mass; (4) preservation of occupants' egress paths. To highlight the importance of such requirement, one can simply note how, according to Boeing's 2020 statistical summary of commercial jet airplane accidents, considering the 2011-2020 time-frame, 54% of fatal crashes occurred during the final approach and landing phases, but these only account for about 40% of total casualties.

The Flying-V aircraft is a novel aircraft configuration, which integrates the lifting surface and fuselage in a single shell. Contrary to other blended-wing body concepts, the Flying-V fuselage can be stretched and shortened with relative ease, to make a family of Flying-V aircraft, which thereby makes it palatable from a commercial standpoint. On the other hand, as opposed to conventional cylindrical fuselage and wing aircraft, the Flying-V cabin presents a significant eccentricity (considering the dual purpose of passenger seating area and lifting surface), which thereby makes the crashworthiness aspect a design challenge. Conventional, full-metal fuselages are indeed able to provide sufficient passenger protection thanks to the large crumple zone available below the passenger seating area. For the FV aircraft, the space available is limited.

The purpose of this research project is thereby to generate a feasible design proposal regarding the crashworthiness of the Flying-V aircraft. In order to achieve so, a literature study has been first performed as part of this research. The scope of the literature study was to provide insights into 1) regulatory requirements and crash injury criteria to evaluate aircraft crashworthiness; 2) crashworthiness of conventional aircraft configurations (metal, fiber-metal laminated, and fiber-reinforced polymers); 3) typical modeling approaches used; 4) future developments for energy-absorbing structures. While the literature study report was a separate deliverable[1]. in this report, a small extract on the most relevant parts of the literature study will be presented.

This report will document all the activities performed in the context of this research, present the obtained results and generate recommendations for future design iterations. The report is structured in multiple parts, with each part being constituted by multiple chapters. Part I consists of the front matter, including the preface and introduction. Successively, highlights from the literature study report will be presented in Part II.

Part III will present the methodology, results, and conclusions drawn from verification, validation, and parametric studies on the virtual drop test of a fuselage section of the Fokker F-28 'Fellowship' airliner. Verification of the finite element model of the F-28 fuselage section consisted of a mesh sensitivity analysis. Validation, in turn, was achieved by comparing the average accelerations computed at predetermined locations, with those from a drop test performed by NASA, at the LandIR research center, in the early 2000s. This is shown in chapter 4. The parametric studies are in turn documented in chapter 5, and consisted of a sensitivity analysis of the crash characteristics of the F-28 fuselage section, on the floor beam height and fuselage eccentricity. More details about this will be given in the 'Research Objective' section of this chapter. The sensitivity analysis has been performed since, compared to conventional configurations, the FV aircraft presents a significant fuselage eccentricity, as well as a limited crumple zone below the passenger floor beam, thus, it was of interest to understand how these differences will affect the crash characteristics of the section.

In Part IV will document the conceptual study performed on the typical fuselage section of the FV aircraft. First, the finite element model set-up is presented in chapter 6. Successively, the conceptual design study, including all results and analysis will be shown in chapter 7. The crash concepts have

[1] A copy of the literature study report can be requested to the author via email: marcodesiderio21gmail.com.

been evaluated in terms of Dynamic Response Index and energy-absorption properties. The dynamics response index is a metric that gives an indication on the likelihood of spinal injury of the occupants, following a vertical acceleration impulse. Lastly, a sensitivity analysis has been performed on a set of geometric variables, with the main objective of investigating the effects of some assumptions and simplifications done, in order to speed up the research.

Part V includes conclusions, recommendations, and references, based on the results obtained in this research. Lastly, Part VI includes appendices.

Research Objective and Questions

The research objective of this project is to study the feasibility of the design of a crashworthy Flying-V typical section. The main research question, consequently, is the following: it is possible to design a crashworthy typical section of the FV aircraft? The crashworthiness requirements considered within this research are presented in chapter 2.

In order to answer this, it has been subdivided into multiple sub-questions:

- **Parametric studies on the fuselage section of the F-28 aircraft:** how are the crash properties of a typical fuselage section influenced by geometric eccentricity and vertical floor location? In particular, how will the mentioned parameters influence the mean acceleration and dynamic response index experienced by the occupants? How will the energy-absorption characteristics change?
- **Conceptual design study on a typical section of the FV aircraft:** what is the most-suitable crash concept for the FV aircraft? How are crash properties influenced by different floor structure designs? How are crash properties influenced by variations in the thicknesses of floor structures?

In the above, regarding crash properties, the two following metrics are considered: 1) dynamic response index, and 2) energy-absorption properties (absolute, and distribution by component).

II

Literature Study

This page intentionally left blank.

1

Relevance of the Research Topic

As evident from the title of this publication, the thesis will focus on the design and crashworthiness assessment of the Flying-V concept aircraft. A high-level overview of the Flying-V aircraft can be found on TU Delft's website[1]. Some of the most fundamental selling points of such innovative configuration, are the significant decrease in fuel consumption (≈20%) as compared to conventional tube-and-wing aircraft with similar mission requirements (i.e. Airbus A350-900) [1], and the possibility of relatively easily designing an aircraft family, as investigated by Oosterom [1], which is an economically attractive feature for airlines.

In order to introduce the reader to the relevance of this work, it is quintessential to firstly highlight the importance of aircraft crashworthiness, as well as the role that the Flying-V can have in the path towards sustainable aviation. These two points will be underlined in section 1.1 and section 1.2 respectively. Lastly, the research questions and objectives will be layed out in section 1.3.

1.1. Importance of Aircraft Crashworthiness for Passenger Safety

Aircraft crashworthiness is the ability of an airplane to protect its occupants in the event of a crash. The United States Federal Aviation Administration (FAA), requires four criteria to be addressed, when evaluating the crashworthiness of a fuselage: (1) guarantee of a survivable volume; (2) guarantee of acceptable acceleration and loads sustained by the occupants; (3) retention of items of mass; (4) preservation of occupants' egress paths. [2]. According to Boeing's 2020 statistical summary of commercial jet airplane accidents[2], within the analyzed timeframe (2011-2020), 54% of aircraft fatal crashes occurred during the final approach and landing phases, while 'only' accounting for 40% of total casualties. This can be visualized in Figure 1.1[3], where the rate of fatal crashes and casualties is distributed over the various flight phases.

This to highlight the importance of a crashworthy design: protecting the occupants during relatively low-speed impacts, will significantly decrease the risk of passenger injury, thereby saving human lives.

1.2. The Flying-V's Role in Sustainable Aviation

In 2015, civil aviation accounted for about 2.1% of global CO_2 emissions [3]. Still, the climate impact is not restricted to mere carbon emissions; more than half of the climate impact is due to water vapor and other greenhouse gasses being emitted by airliners. All included, civil aviation accounts for an estimated 4.9% of global warming, as researched by Lee et al. [4]. In addition, according to the Air Transport Action Group (ATAG), not only aviation is responsible for a staggering 12% of emission from all transport sources, but, also, about 80% of carbon emissions are generated from flights traveling

[1] https://www.tudelft.nl/en/ae/flying-v. Accessed on 05-Apr.-2022.
[2] https://www.boeing.com/resources/boeingdotcom/company/about_bca/pdf/statsum.pdf. Accessed on 24-Mar.-2022.
[3] ibid.

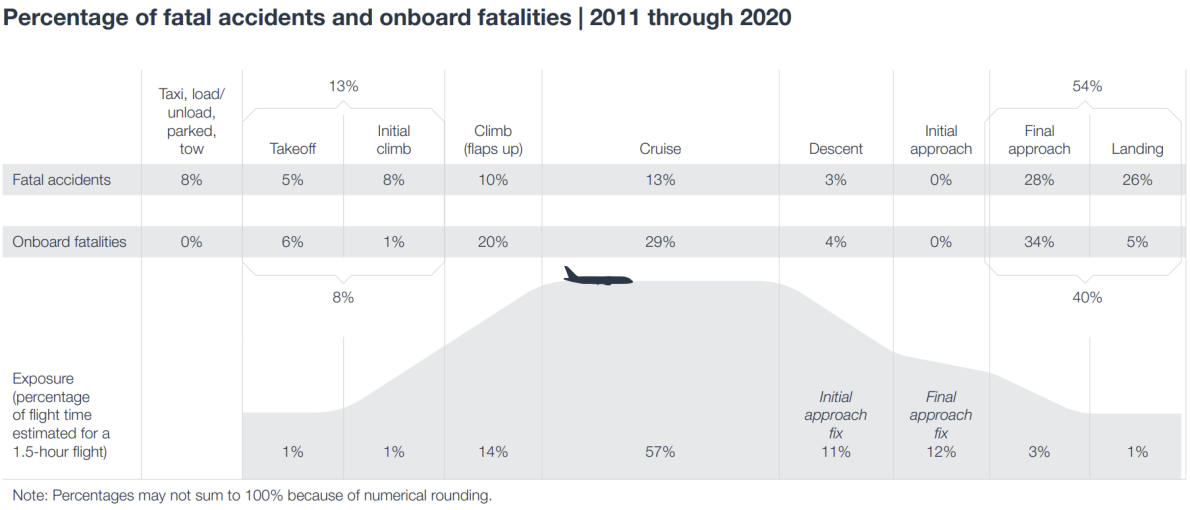

Figure 1.1: Distribution of aircraft fatal accidents and casualties over different flight phases.

longer than 1500 km, for which no feasible ground alternative is currently available[4]. Consequently, in order to meet the challenging goal of reducing aviation's carbon emission by 50%, by 2050 (as compared to 2005 levels), the deployment of unconventional, and more efficient aircraft configurations, can be a game-changer. As mentioned in the introduction paragraph of this chapter, the Flying-V is expected to be a replacement for the Airbus A350, a wide-body long range airliner, and is promised to lower fuel consumption by 20%.

1.3. Research Questions and Objective

As mentioned in section 1.1, crashworthiness is a fundamental design feature to ensure passenger safety. One of the main uncertainties of the Flying-V aicraft is the impact that this design aspect might have on the operating empty weight of the aircraft: the stating hypothesis of this research is that the crashworthiness behavior of the Flying-V will be different, compared to conventional cylindrical fuselage and wing aircraft configurations. Since the Flying-V has not yet been assessed in terms of crashworthiness, and considering that, in general, aircraft weight estimation methods are based on statistics (of existing aicraft), then the impact of crashworthiness aspect on fuel consumption is currently unknown. The objective of this research is thus to explore crashworthiness concepts to be utilized in the Flying-V aircraft, and, once a concept is selected, a typical, crashworthy, fuselage section will be designed and analyzed in order to, eventually, assess the impact that the crashworthiness aspect will have on the operational empty weight of the FV.

In order to achieve this, a thorough understanding of aircraft crashworthiness is to be gained in the first place, and, therefore, a multitude of research questions needs to be addressed.

To start with, a deep knowledge on the certification requirements, as amended by regulators (with FAA in the US, and the European Union Aviation Safety Agency, EASA, in the 'old continent', being the most influential), as well as crash injury criteria is to be gained, in order to set the requirements and be able to extract meaningful information from simulation results.

Secondly, one must familiarize with the topic, to gain an understanding of conventional aircraft crash dynamics. Within conventional aircraft crash dynamics, a neat distinction can be made between metal and composite fuselages, mainly due to (1) the relatively large plastic strains that can be achieved by metals as compared to fiber-reinforced plastic composites (FRP), which allows metal structures to be inherently able to absorb large amounts of energy, while deforming; and (2) there is a large variety of possible designs based on composite materials. The discussion herein presented is limited to the aforementioned FRP and fiber-metal laminates (FML).

[4] https://www.atag.org/facts-figures.html#:~:text=The%20global%20aviation%20industry%20produces,carbon%20dioxide%20(CO2)%20emissions.&text=Aviation%20is%20responsible%20for%2012,to%2074%25%20from%20road%20transport. Accessed on 05-Apr.-2022.

Thirdly, two possible skin and frame concepts are generally used in aviation, namely: (1) the 'conventional' concept where the skin is attached directly on the fuselage frames, which, in turn, have the so-called mouse hole cut-outs to allow for stiffeners continuity; (2) the floating frame concept that avoids the mouse hole cut-outs in the frames, which are in turn partially smaller in diameter than the stiffened skin, such that the load transfer is in turn carried out by structural elements usually referred to as shear clips or castellations that connect the frames to the stiffened skin panels. These two different structural concepts are likely to have different energy-absorption characteristics and, therefore, eventual similarities and differences are to be understood.

As stated by the research objective, it is of interest to explore and define a crashworthiness concept, before a more detailed design and analysis can be performed. In order to quickly iterate through multiple and different potential designs, ideally, an analytical model is employed. This allows to keep the problem computationally cheap and therefore fast to solve. A combined analytical-numerical approach has already been investigated by Poorte [5] to design a composite crash energy absorber for aircraft fuselage. While a maximum discrepancy of 25% is achieved in predicting the mean crushing load of corrugated beams (which Poorte considered to be acceptable given the fluctuating nature of the problem), the need to calibrate material properties also proved to be a limitation during the design phase of the absorber. Therefore, it is of interest to know if further research can be performed, toward the determination of more predictive analytical models, with corresponding validation. In general, as an anticipation, three main parameters are of particular interest when evaluating analytical approaches to model energy-absorbing crash components: peak load, mean crushing load, and total absorbed energy [6].

Fifthly, numerical crash simulations involve models that are generally hard to develop and validate (due to the non-linear and dynamic nature of the problem), yet quintessential in the 'modern' design process of aircraft structures: testing is expensive and time-consuming and, as a consequence of that, a general industry trend currently leans towards virtual testing, namely the replication of a traditional testing environment in a physical (finite element) simulation. As mentioned, a crashworthiness analysis is to be performed on the designed typical fuselage section. Researching and gaining a thorough understanding on what is the best numerical solver or modeling technique is outside the scope of this thesis. Still, obviously, a good enough approach has to be undertaken, in order to have reliable and validated results. It is therefore of interest to investigate what are the most common approaches used by researchers in the field; what are the advantages and disadvantages of each of the commonly used modeling techniques; what are some of the most innovative solutions; how are material models defined?

Last, but not least, recent developments in additive manufacturing (AM) techniques, as well as architectural design, have enabled engineers to create a new and wide range of metamaterials, mainly consisting of lattice structures, which are highly energy absorbing, are able to recover, for the most part, their original shape, and have excellent strength-to-weight ratio characteristics [7]. While such metamaterials will be surely finding widespread application within the aviation industry in the upcoming decades, and for decades to come, it is also argued that, currently, the development of such technologies is still at a rather larval stage. The engineering community is still far from finding solutions that enable the manufacturing of these metamaterials at industrial scale, therefore allowing for widespread application [8]. Such metamaterials are therefore discarded *a priori* from being a potential design solution for the crashworthiness of the Flying-V. Still, overlooking the importance of such future technology would not provide a complete picture of current and future developments on crashworthiness of civil aircraft. Consequently, a high-level overview of the current research status of high-energy absorbing metamaterials is to be obtained as well.

This page intentionally left blank.

2

Regulatory Requirements and Injury Criteria to Evaluate Aircraft Crashworthiness Performance

Air travel is the safest mode of transportation currently in existence[1], with the death rate per billion passenger miles being as low as 0.07 (as of 2009, in the United States of America); in prospective, it is two order of magnitudes lower than automobiles [9]. This is not by chance; over the past decades, air safety has improved dramatically thanks to extensive and up-to-date requirements that airliners need to comply with, and which are set in place by regulatory agencies. The United States' FAA and Europe's EASA are at the forefront in terms of certification specifications. The Flying-V falls under the category of 'part 25' and 'CS-25' in FAA's and EASA's regulatory requirements and means of compliance, both of which apply to 'turbine powered Large Aeroplanes' [10, 11]. Considering the similarities between both regulations, for the sake of simplicity, the discussion in this chapter will be, for the most part, limited to the requirements and acceptable means of compliance required by the European regulator. Nevertheless, if necessary, additional advisory circulars published by the FAA will be considered. As an example, prior to the extensive use of FRP in aircraft structures, crashworthiness regulations have evolved around the experience gained during actual aircraft operations, and fleet experience did not prove necessary the need for an aircraft level crashworthiness standard [2]. However, with the massive usage of FRP (and, in particular, Carbon Fibers Reinforced Plastics - CFRP), a similar level of protection, as compared to metallic fuselages, was no longer guaranteed. As a consequence, new crashworthiness requirements have been put forward by the FAA in the Advisory Circular (AC) 20–107B [2], as well as Special Conditions (SC) for both the Boeing 787-8 and the Airbus A350-900 (25-362-SC and 25-537-SC respectively) [12, 13]. Key takeaways from 25-362-SC and 25-537-SC are that FAA required the B787 and A350's crashworthiness characteristics to be such that a similar level of survivability would be guaranteed, as compared to similar-sized, full-metal fuselages (similarity principle), with the assessment of such characteristics to span a range of different speeds, up to 30 ft/s.

Considering the above clarifications that regulators have felt the urge to amend when the usage of CFRP for principal structural elements has substantially increased, given the novelty of the FV's aircraft configuration, and considering the FV's unusually large seat rotation with respect to a vertical plane containing its center line [1][2], then it is likely that, for certification purposes, crashworthiness requirements for the Flying-V will be more stringent that what is currently allowed. This would be due to (1) lack of operational history (novel aircraft concept) and (2) unconventional seating configuration. This very same concern is in fact also shared by the Transport Aircraft Crashworthiness and Ditching Working Group (TACDWG), whose work will be introduced later on in this chapter [14]. As such, in

[1] If one is to exclude elevators, reasonably, as they serve a different purpose.

[2] as it is instead found in conventional aircraft configurations - which is necessary for the FV, considering the flying wing configuration, yet still smaller than the maximum 18 deg allowed by CS25.785 for use of conventional belts

order to assess the crashworthiness properties of the Flying-V's typical section, the discussion herein presented is not limited to regulatory requirements, but also considers a series of injury criteria.

In order to thus lay down the Flying-V's crashworthiness requirements, this chapter has the following structure: firstly, a discussion on requirements from regulatory agencies is presented in section 2.1; successively, section 2.2 presents the most commonly used crash injury criteria. Lastly, section 2.3 provides an overview for the crashworthiness requirements that are assumed for the Flying-V aircraft.

2.1. Requirements from Regulatory Agencies

Requirements for aircraft crashworthiness, as well as acceptable means of compliance (AMC), are somewhat defined by EASA in the 'CS-25' regulation [11].

The general provision (CS-25.561) requires, vaguely, the structure to be designed such that occupants are given every reasonable chance of avoiding serious injuries in the event of a minor crash landing (assuming that proper use of seats, belts and all other safety provisions is followed). This is formalized by CS-25.561(b)(3), where the ultimate inertia forces to be experienced by the occupant are specified, for a retracted landing gear configuration:

- Upward - 3.0 g
- Forward - 9.0 g
- Sideward - 3.0 g on the airframe and 4.0 g on the seat and their attachments
- Downward - 9.0 g
- Backward - 1.5 g

It should be mentioned that, typically, the above applies to a typical fuselage section; due to other effects (e.g. section containing the central wing box; rigid body dynamics), the actual accelerations experienced by the passengers during a crash event will be different depending on the seat location. Furthermore, these load factors are to be applied in static analyses, and do not reflect the impact nature of crash impacts. Finally, rigid-body analyses of the aircraft under emergency landing conditions can render larger values for these load factors at specific regions of the aircraft, in which case the largest values are selected to evaluate the structures corresponding to these specific regions.

Going back to the discussion, CS-25.561 requires that seats, items of mass, and their supporting structure must not deform up to the above-specified loads in any way that would impede a rapid evacuation of the occupants. Although it is beyond the scope of this research, the potential use of energy-absorbing seats to enhance aircraft crashworthiness is of interest, as, in principle, aviation authorities would allow the use of some form of energy-absorbing seats in order to improve aircraft crashworthiness. While this has also historically allowed to certify seats independently of the aircraft's primary structure [15], it also implies that new interior configurations that affect survivable space and human impact criteria can and must be certified individually.

The above inertia loads are as experienced by the seated passenger, and are mainly to be used to design a structure able to withstand such loads. The dynamic landing environment used for seat specifications is further developed in CS-25.562 (and summarized here below for the sake of completeness):

- A change in vertical velocity of $10.7\,\mathrm{m\,s^{-1}}$, with the plane's longitudinal axis rotated 30 deg downwards, with leveled wings, with a peak acceleration no lower than 14 g, and occurring within 80 ms after the impact;
- A change in horizontal velocity no lower than $13.4\,\mathrm{m\,s^{-1}}$, with the plane yawing by 10 deg, in horizontal, leveled flight. The deceleration peak should not be lower than 16 g and should not occur later than 90 ms after the impact.

In accordance with the above-mentioned dynamic conditions, a series of performance parameters need to be satisfied, as specified in CS-25.562(c)(1) to CS-25.562(c)(5). Worthy to mention is the head injury criterion (HIC): when contact between the head of an occupant and surrounding structure could occur, then there should be sufficient protection such that the head impact does not exceed a HIC of

1000 points, with the HIC defined as [11]:

$$HIC = \left\{ (t_2 - t_1) \left[\frac{1}{(t_2 - t_1)} \int_{t_1}^{t_2} a(t) dt \right]^{2.5} \right\}_{\max} \tag{2.1}$$

with a_t acceleration response curve for the head impact, and t_1 and t_2 being the initial and final integration times, respectively.

The aircraft-level dynamic crash landing conditions are however left unspecified. This gap in regulation is also acknowledged by the TACDWG, a commission instituted by the Aviation Rulemaking Advisory Committee (ARAC), with the purpose of providing recommendations for new airframe-level crashworthiness and ditching standards to be included in the CS-25 and other relevant advisory material [14]. TACDWG members include both experts from the industry (Boeing, Airbus, Embraer, to mention some), and research institutes (NASA, the German Aerospace Center - DLR, among others). The final report was handed in to ARAC in October 2018, but, as of now, the recommendations are still to be implemented into CS-25 and similar.

As mentioned in section 1.1, the FAA, in AC 20-107B, requires four main criteria to be fulfilled: (1) guarantee of a survivable volume; (2) guarantee of acceptable acceleration and loads sustained by the occupants; (3) retention of items of mass; (4) preservation of occupants' egress paths.

Regarding loads sustained by the occupants, TACDWG's highlights the importance, in a crashworthy design, of establishing acceptable load levels such that an injured passenger would still be able to evacuate the vehicle. As such, the maximum allowable compressive load between the pelvis and the lumbar column should not exceed 1500 lbs (680 kg), as already specified under CS-25.562(c)(2). The main issue with this particular means of compliance, is the need to also include a model for the seat when performing a numerical simulation, as well as an anthropomorphic dummy, in order to obtain meaningful results. TACDWG recognizes this issue, and suggests that other crash injury criteria could still be used as acceptable means of compliance. One of these is the Dynamic Response Index (DRI). DRI is typically used in the aviation industry to show aircraft crashworthiness compliance [14]. It is a risk-based injury criterion [16], the value of which is determined considering the accelerations measured at the seat location (and, hence, no model for the ATD is to be implemented). More details about it will be provided in section 2.2. For now, it is important to keep in mind that, using historical data, a correlation has been established between the DRI value and probability of spinal injury. A DRI value of 16 corresponds to 1% probability of spinal injury; increasing the DRI to 18 will increase said probability to 5%. In short, DRI is already a well-established crash injury criterion, already used as alternative means of compliance for CS-25.562 (and anyway proposed by TACDWG as acceptable means of compliance for future aircraft crashworthiness regulations), and allows to exclude the passenger-seat model from numerical simulations. Consequently, this is probably the single, most important crash injury criterion to be discussed, and will be therefore presented, among others, in the subsequent section. In current designs, a DRI of 16 at most is accepted for certification purposes [14].

Once acceptable loads on passengers have been established, the question remains: what is an acceptable vertical impact velocity level? TACDWG's report addresses also this gap in legislation, by working with original equipment manufacturers (OEMs), in order to obtain estimates about the vertical impact capabilities of current aircraft. Almost all of the considered aircraft falling within the CS-25 legislation, is estimated to be able to protect passengers within a range of 20 to 30 ft/s vertical impact velocity, depending on the size of the aircraft itself [14]. A general trend is observed, where wide body aircraft, from the same manufacturer, are able to sustain higher speed impacts. This is likely due to larger crushing zone, which allows to reduce the loads being transmitted to the passengers. Subsequently, based on current OEMs' self-assessment, as well as accident studies, the vertical impact velocity requirement proposed by TACDWG is a function of the aircraft's maximum take-off weight (MTOW) and is shown in Figure 2.1. Oosterom, in his study on Flying-V family design, has estimated the MTOW of the Flying-V to range in between 207 ton ($456 \cdot 10^3$lbs), for the FV-800 variant, to 278 ton ($613 \cdot 10^3$lbs) for the FV-1000 one. This variation in MTOWs is highlighted in Figure 2.1 as well, as indicated by the red hatched pattern.

Of course, one of the main advantages of having a family of aircraft is the ability to be able to 'simply' stretch the fuselage, without the need to change geometry, for the most part. Subsequently, the typical

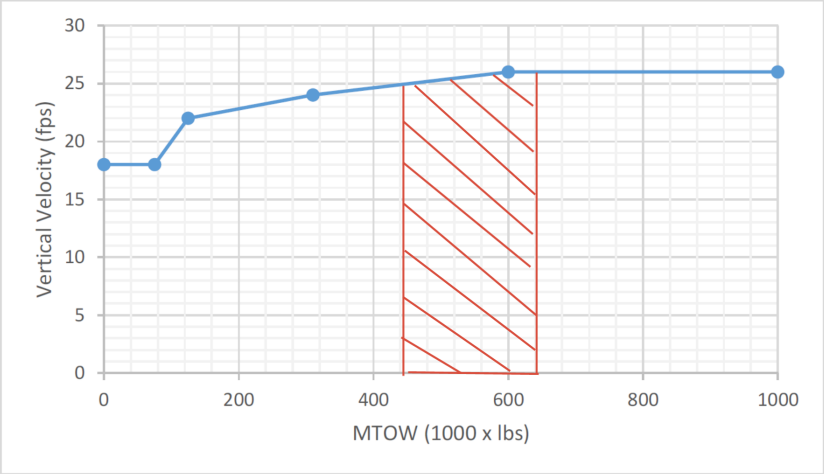

Figure 2.1: Vertical impact velocity requirement vs. MTOW, adapted from TACDWG [14]. The hatched pattern indicates the estimated range of MTOW for the Flying-V family, as determined by Oosterom [1].

section of the Flying-V will be required to be certified for the most stringent loading condition, which, in this specific case, corresponds to the FV-1000 configuration. For FV-1000's MTOW point, TACDWG suggest a vertical impact velocity of $26\,\mathrm{ft/s}$, or $7.9\,\mathrm{m\,s^{-1}}$ which, consequently, will be considered to be the vertical impact velocity requirement to be satisfied, in this research.

2.2. Crash Injury Criteria

In research performed by the US National Institute for Aviation Research, sponsored by the FAA, a myriad of crash injury criteria are identified, each specific for a loading condition or anyway region of the body [17].

In the current research, the objective is to obtain a preliminary - if not conceptual - design for crashworthiness of the Flying-V aircraft. As such, it would not be meaningful to consider, in the evaluation of passenger injury, any specific region of the body, while a final design of the cabin interior, seats and corresponding restraint system has not been achieved in the first place. As such, only the most commonly used and accepted injury criteria will be introduced and addressed in this section, and will be used to evaluate passenger injury in this research.

Four main injury criteria will therefore be introduced: Eiband diagrams, DRI, HIC and Lumbar Loads (LL). These will be discussed, respectively, in subsection 2.2.1, subsection 2.2.2, subsection 2.2.3 and subsection 2.2.4.

2.2.1. Eiband Diagrams

In literature, a commonly used crash injury criterion is the employment of Eiband Diagrams. In 1959, Eiband published a research on human tolerance to rapidly applied accelerations [18]. Of interest, in this research, is the tolerance to 'headward' acceleration, as defined by Eiband, which essentially is the vertical acceleration of a seated passenger, when the spinal cord gets compressed. These loads will generally cause spinal injury to the passengers. Eiband's research mainly involved the collection of empirical data of physical tolerance on acceleration, on humans, hogs and chimpanzee.

In the experiments, the subject was placed on a $50\,\mathrm{mm}$ Styrofoam cushion, with lap and shoulder straps, as well as a small back support. The results of the experiments are shown in Figure 2.2. Reasonably, a high-magnitude and short duration acceleration is well-tolerated by the human body. As acceleration pulses become longer in duration, the level of human tolerance to those will decrease (and the likelihood of injury will increase). This is logical, as a short-duration pulse will induce a transient response, while a long-duration acceleration will create a steady-state response.

It is worthy to note that, the above diagram, has been generated using lap and shoulder straps, only a lap strap would reasonably be used as passenger restraint system, for comfort. In most observed

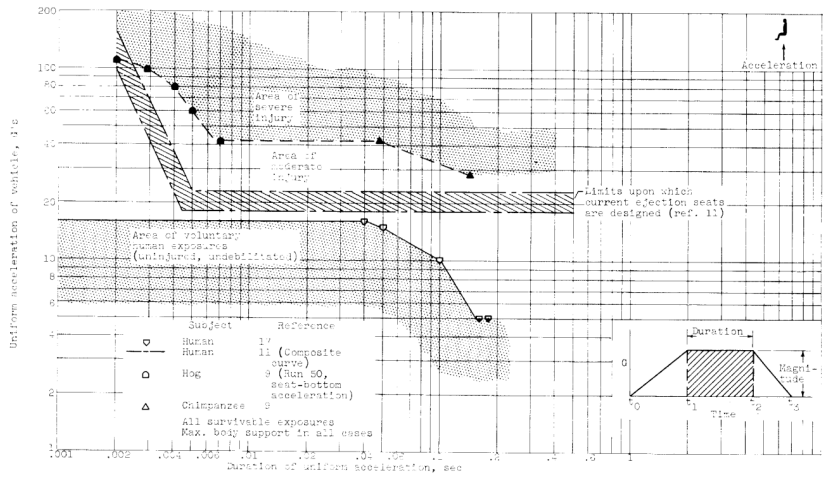

Figure 2.2: Injury envelope following headward acceleration as determined by Eiband [18].

literature on crashworthiness studies, which will be later on referenced in this research, from acceleration pulses at floor level (or even when seats are included and modeled), pulse magnitude vs. duration curves are obtained and compared to the results obtained by Eiband and shown in Figure 2.2. In the observed research, these is no mention of this subtle but fundamental difference between Eiband's and numerical simulation results. Before making use of such crash injury criterion, one should determine whether it would be conservative or not to compare numerical crash simulation results to the aforementioned ones.

Additionally, another limitation of the use of Eiband diagrams is that it is not sensitive to various and different acceleration pulse shapes. As an example, initially, ejection seats in military aircraft generated acceleration pulses up to $20g$, which falls within the 'moderate injury' category in Eiband diagram, yet spinal fractures were not an uncommon event [19]. In an attempt to mitigate this issue, a revised ejection seat program was initiated, during which the DRI was developed. This will be presented in the upcoming section.

2.2.2. Dynamic Response Index

The DRI is a method used since at least the 1970s, from the US Air Force (USAF), to determine the probability of spinal injuries in pilots subjected to the high-amplitude and short-duration accelerations induced by ejection seats [20]. In DRI, the total body mass acting upon the vertebrae is modeled as a point mass, thereby yielding the following differential equation [16]:

$$\frac{d^2\delta}{dt^2} + 2\zeta\omega_n\frac{d\delta}{dt} + \omega_n^2\delta = z \tag{2.2}$$

which is a typical equation for a single degree of freedom (SDOF) spring-dashpot model with external acceleration input, as shown in Figure 2.3[3]; with δ being the degree of freedom (denoted by x in Figure 2.3), ζ the damping ratio, ω_n the natural frequency (i.e. $\omega_n = \sqrt{\frac{k}{m}}$, where k is the spring stiffness constant and m the point mass), and z is the acceleration input.

The DRI is subsequently computed [20]:

$$DRI = \frac{\omega_n^2\delta_{\max}}{g} \tag{2.3}$$

Stech and Pain [21], considering the 50th percentile of USAF pilots of the time, found $\omega_n = 52.9$ rad/s and $\zeta = 0.224$. Using the aforementioned coefficients, and assuming a normal, random, uncorrelated

[3] https://en.wikipedia.org/wiki/Mass-spring-damper_model. Accessed on 18-Apr.-2022.

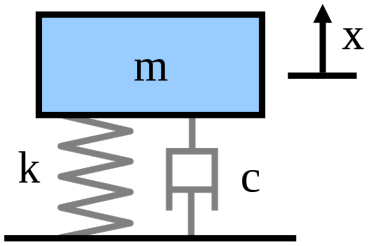

Figure 2.3: Single degree of freedom spring-dashpot system.

distribution for body weight and breaking strength, then the injury probability over a range of DRI values is determined and shown in [20]. As mentioned, DRI is an extremely simple criterion, computationally efficient, and for which the only required input is the acceleration profile at the airframe level, which is easily determined from crash impact simulations (or anyway fuselage drop tests).

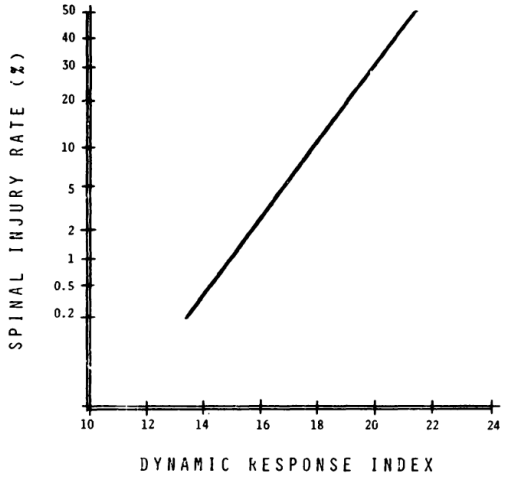

Figure 2.4: DRI vs. probability of spinal injury [20].

The main issue, that has not been addressed yet in literature, yet is worryingly relevant, is that currently used coefficients for DRI are indeed based on the 50th percentile of USAF pilots about 50 years ago. First of all, up until the 1970s, there was hardly any woman working in the USAF, let alone female combat pilots[4]. Additionally, it is reasonable to assume the anthropomorphic characteristics of the 'typical passenger' to be significantly different from those of fighter jet pilots. In synthesis, while in theory, the DRI provides an estimate of the likelihood of spinal injury in humans when subjected to acceleration, in practice, the accuracy of the actual correlation between DRI and spinal injury rate is disputable, for passenger aircraft. This is because the probability function has been derived in the 1970s, based on injury data from a sample that lacks diversification in terms of age, gender, and body type.

Still, a DRI lower than 16 is already accepted by regulators as acceptable means of compliance for crashworthiness. The DRI can be effectively considered to be an index that provides information regarding the severity of an acceleration event, and, thus, a baseline for comparison, rather than a probability function, and the experience gained to this day shows that such DRI (of 16 units) is sufficient. Further research in this direction would therefore not add any additional benefits for passenger safety. DRI is therefore still to be considered a very good indicator to assess the crashworthiness of civil aircraft, although the statistical correlation shown in Figure 2.4 (and outlined in TACDWG's report) will not

[4] https://www.nationalmuseum.af.mil/Visit/Museum-Exhibits/Fact-Sheets/Display/Article/2383446/women-in-the-air-force-displays-in-cold-war-gallery/. Accessed on 18-Apr.-2022.

be accurate, likely unconservative.

2.2.3. Head Injury Criterion

The current state-of-the-art methodology to assess head damage is the HIC. HIC was developed about 50 years ago by the US National Highway Traffic Safety Administration (NHTSA), on the basis of clinical reports and statistical data [22]. In 1985, test data obtained for human surrogates was analyzed by Prasad and Mertz, to determine the relation between HIC and skull and brain injuries [23]. The test data included 54 head impacts, with HIC in the range of 175 to 3400. The results are shown in Figure 2.5.

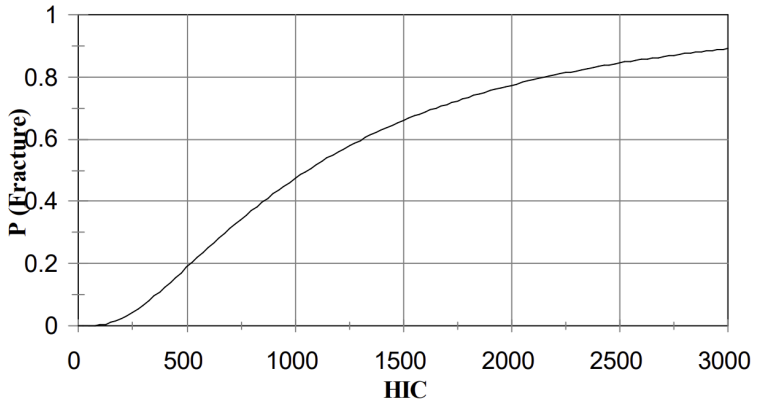

Figure 2.5: Head injury risk probability vs. HIC value [22].

CS-25.562(c)(5) requires HIC to have a value below 1000 units, if head contact with seats or other structures can occur.

2.2.4. Lumbar Loads Injury Criterion

As mentioned in subsection 2.2.2, the index was developed by correlating empirical data with the DRI value itself. This inherently will introduce a bias with respect to not only the anthropomorphic characteristics of the passengers considered in the study, but also seat design and restraint system. While DRI is still considered AMC for crashworthiness certification, the FAA, to address these shortcomings, has introduced a lumbar load tolerance criterion [19]. Using anthropomorphic test dummies (ATDs), the FAA has performed a series of dynamic tests in order to correlate DRI with lumbar loads, as shown in Figure 2.6.

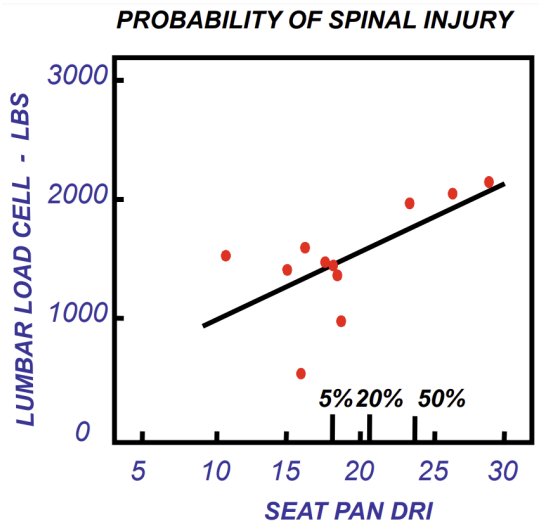

Figure 2.6: Correlation between ATD lumbar load and DRI [24]

Table 2.1: Maximum lumbar loads for injury, depending on gender, size and ATD type [19]

	Small Female Hybrid III Type ATD (103 to 118 lb)	Mid-Size Male Hybrid II Type ATD (170 lb)	Mid-Size Male Hybrid III Type ATD (170 lb)	Large Male Hybrid III Type ATD (200 to 245 lb)
Compression (lb)	933	1500	1395	1757

This resulted in a 1500 lbs load corresponding to a DRI of 19, which the FAA considered to be acceptable. Of course, the lumbar load risk of injury changes depending on the size and gender of the passenger. Additionally, the determined lumbar load also depends on the type of ATD use in the tests itself. This is shown in Table 2.1.

Furthermore, in TACDWG's report, a DRI of 16 is suggested as AMC for crashworthiness, which is more conservative than the determined 19. This is likely indeed due to the variations in spine column strength noted in Table 2.1 between different genders and ATD used, which call for a more conservative approach.

2.3. Flying-V Crashworthiness Requirements

After having reviewed current and potential future crashworthiness regulations from airworthiness authorities, a formal list of requirements that the outcome of this research needs to fulfill can be generated:

FV1000-CRASH-001: The crashworthiness properties of the typical section of Flying-V aircraft shall be evaluated by means of a drop test at a minimum vertical impact velocity of 26 ft/s, with the fuselage center line horizontal.

FV1000-CRASH-002: The Flying-V typical section shall be designed such that, following the dynamic conditions specified in **FV1000-CRASH-001**, an equivalent DRI not greater than 16 units is achieved.

FV1000-CRASH-003: The Flying-V typical section shall be designed such that, following the dynamic conditions specified in **FV1000-CRASH-001**, the compressive lumbar load of a mid-size, male, hybrid II type ATD shall not exceed 1500 lbs.

FV1000-CRASH-004: The Flying-V typical section shall be designed such that, following the dynamic conditions specified in **FV1000-CRASH-001**, the HIC of a mid-size, male, hybrid II type ATD shall not exceed 1000 units.

In the context of this research, cabin interior cannot and will not be considered. Additionally, **FV1000-CRASH-003** will not be possible to be verified. The initial intent was to develop a model which included ATDs; due to time constraints, this was not done. As such, only **FV1000-CRASH-001** and **FV1000-CRASH-002** will be considered.

Lastly, **FV1000-CRASH-002** refers to 'an *equivalent* DRI not greater than 16 units'. In essence, an equivalent DRI of 16 units can be considered to be a weighted average of DRIs for different seats, such that, overall, the likelihood of spinal injury is the same as if a DRI of 16 units was measured at each seat location.

3

Crashworthiness of Metal Conventional Aircraft

Energy absorption is generally considered to be an inherent property of metals (aluminum alloys, in this specific case), thanks to their ductile behavior. As such, the crashworthiness of metal fuselages of conventional aircraft has been taken for granted in previous decades by the regulators, such that there has been no need for a general crashworthiness standard [2]. This is likely also the reason for which most of the research on aircraft crashworthiness mainly focuses on composite fuselages, and little work as been done in the past to understand the crushing behavior of metal fuselages.

Xue et al. [25] in 2014 investigated the crashworthiness of a conventional metal aircraft, by performing a finite element simulation of a drop test of a typical fuselage session, using PAM-CRASH as the nonlinear explicit solver. Seats and passenger masses are modeled as solid blocks, while all the metallic structures used aluminum 2024 (likely -T6) and 7075 (again, likely -T6) alloys. It is not clear which alloy is used for which component, but, reasonably, the 2024-T6 was employed for the skin and stiffeners, considering its superior fatigue properties, whereas the precipitation-hardened 7075-T6, with higher yield strength, was used for frames and floor struts. One limitation of this study is that it employs a three-frame typical fuselage section, which does not align with the six-frame section typically used for certification purposes: having a sufficient number of frames will imply that the fuselage section has, on average, the same stiffness, strength and mass properties to represent the overall fuselage [26]. Having only three frames implies that the kinetic energy to be dissipated is that of the three frames and the two bays of stiffened skin in between the frames. Assuming that the frames are the structural elements that dissipate most of the energy[1], then each frame bears $\frac{2}{3}$ of each bay. If a longer typical fuselage section is used, e.g. six frames, then there will be five bays of stiffened skin between two adjacent frames, meaning that one frame bears $\frac{5}{6}$ of each bay. In essence, assuming that most of the kinetic energy is dissipated via plastic deformation of the frames, then having a too short typical fuselage section entails that each frame needs to dissipate a lower amount of kinetic energy, thereby making the analysis unconservative. The same discussion can be extended when passenger dummy masses are included. The virtual drop test is performed at $9\,\mathrm{m\,s^{-1}}$, which is in line with other published literature [27], but on the higher end of the spectrum [28, 26, 29]. The fuselage is modeled using 134,000 shell elements, while the ground is modeled as a fixed rigid board. The model proposed by Xue et al. is illustrated in Figure 3.1.

The results presented in Figure 3.2 show the common deformation achieved by the typical section following a drop test, where three plastic hinges develop. Generally, the first plastic hinge is created in the area below the cargo floor structure. Two other plastic hinges are in turn at the location of the cabin floor struts. Empirical results showing this deformation patterns can be seen in Figure 3.3, where a drop test of the typical section of the Airbus A320 has been performed. Xue et al. also investigated

[1] This assumption will be indeed proven to be correct later on.

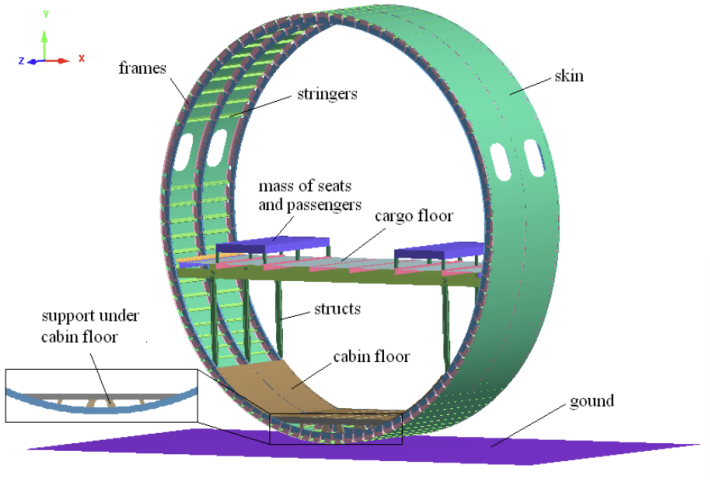

Figure 3.1: Numerical model developed by Xue et al. of the typical metal fuselage section [25].

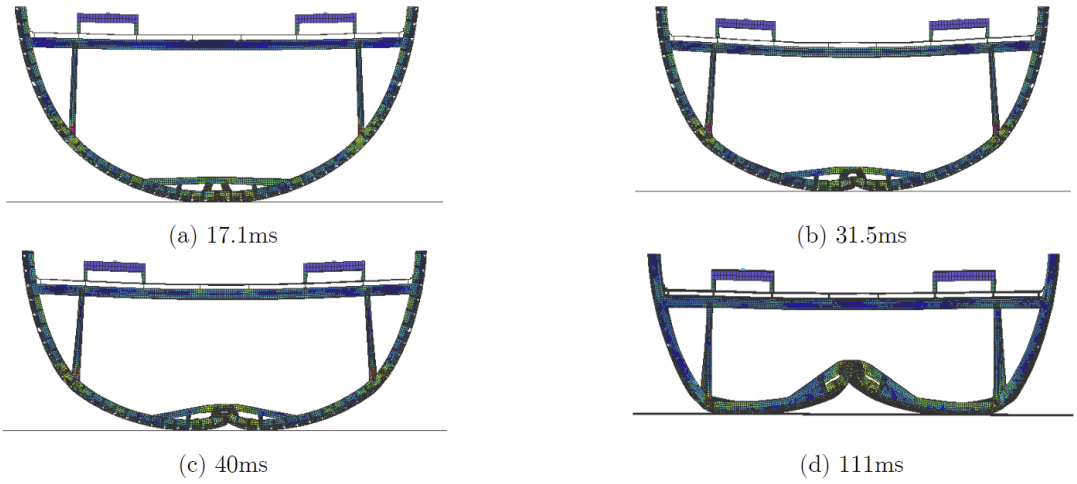

Figure 3.2: Results of the virtual drop test [25].

the contribution of various components to crash energy absorption. These are presented in Figure 3.4 and summarized in Table 3.1.

Not surprisingly, most of the energy is being absorbed by the frames, mainly due to the aforementioned plastic hinges. Another substantial portion of the energy is being absorbed by the structure underneath the cargo floor, followed by the skin and stringers themselves. Rightfully, the cabin floor itself has a marginal contribution to energy absorption, since it is required to remain intact after impact, in order to (1) maintain survivable space and (2) maintain occupants' egress paths. Considering the above distribution, one way to significantly increase the amount of kinetic energy dissipated by the fuselage could be to induce the generation of additional plastic hinges, since, currently, at each plastic hinge location, only one line of material parallel to the fuselage longitudinal direction is being plastically deformed. The benefits of increasing the number of such 'lines of material' would be clear: a more progressive crushing behavior that would thus decrease the acceleration peaks experienced by the occupants. Of course, such a design feature would likely come with a structural mass penalty. While this would not be attractive for (full metal) conventional aircraft configurations, it might be a potential solution for the Flying-V aircraft.

Going back to the original discussion on the crash properties of a generic fuselage section, Xue et al. have also explored other vertical impact velocities: 6 and $12\,\mathrm{m\,s^{-1}}$; the three simulated velocities are therefore compared. The results are shown in Figure 3.5.

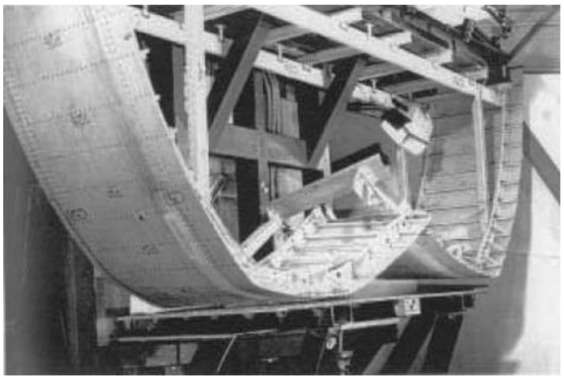

Figure 3.3: Drop test of A320 fuselage substructure [26].

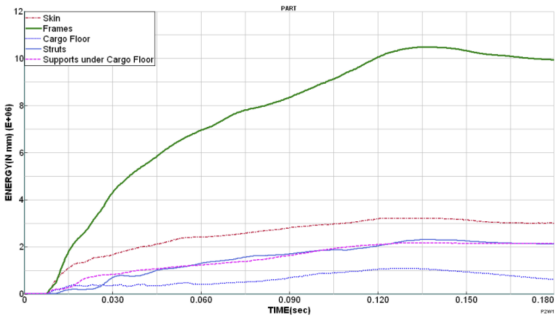

Figure 3.4: Energy vs. time for different structural components [25].

Table 3.1: Portion of crash energy absorbed by each component [25].

Part	Internal energy (kJ)	Percentage (%)
Frames	15.667	59.08
Skin and Stringers	3.607	13.59
Cabin floor	0.614	2.31
Struts	2.112	7.96
Cargo floor and its supports	4.332	16.33

From Figure 3.5, multiple observations can be made. By exclusively focusing on the acceleration time history, it is clear how at low velocities the first acceleration peak is larger in magnitude, whereas for higher impact velocities the second peak becomes larger. The reason for this is rather simple; the initial crushing behavior involves the structures underneath the cargo floor, with the formation of the first plastic hinge. If the impact velocity is lower, the deformation will be limited for the most part to the cargo bay area, and will not involve the cabin floor support struts. As the impact velocity increases, and therefore the overall deformation of the structure increases, the second peak will emerge, which corresponds to the moment when the cabin floor struts hit the rigid floor. To validate this or other theories, it would have been useful if Xue et al. had provided the energy absorption distribution by component as shown in Table 3.1 for all the three different vertical impact velocities, which is unfortunately not the case. As mentioned above, the structure underneath the cargo floor is able to absorb a substantial portion of the kinetic energy. As such, Xue et al. also investigated the effects of changes in thickness of the beams at that location, in order to improve the crashworthiness characteristics of the typical section, obtaining dubious results. The main issue is that only peak passenger acceleration loads and relative duration are being considered to qualitatively assess the energy-absorption performance, while an assessment on the mean acceleration is completely neglected. Still, despite these shortcomings, the aforementioned research provides a good initial glance with respect to the kinematics involved in energy absorption of conventional metal fuselages.

A similar study to that of Xue et al. was performed by Alderliesten et al. [26], where a finite element method was developed to compare metal and composite fuselage sections in drop testing. A validation attempt consists of comparing the magnitude and frequency of the obtained accelerations with those from literature, which includes actual acceleration data of the typical fuselage section of an Airbus A320. The failure modes and magnitude of acceleration pulses are different from those found in literature [29] (see Figure 3.3). The reasons for this are unknown, but could be related to: (1) differences in modeling passenger mass (both distribution and magnitude) and; (2) the fact that no rivets are allowed to fail in the drop test simulation from Alderliesten, while although undesired, the opposite is true in the physical world. Indeed, from Figure 3.3, one can notice how the cargo floor support structure has indeed separated from the frames, and is relatively straight, thereby indicating the possibility of fastener failure. The result of the A320 drop test simulation is shown in Figure 3.6.

The reason for Alderliesten et al. to perform a virtual drop test of only a two-frame fuselage section is simply for model validation purposes only. The simulation results can indeed be visually compared to

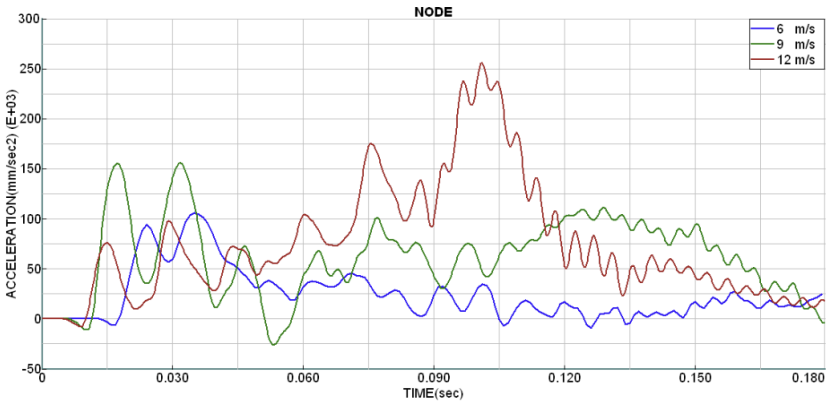

Figure 3.5: Time history of passenger accelerations for different vertical impact velocities [25].

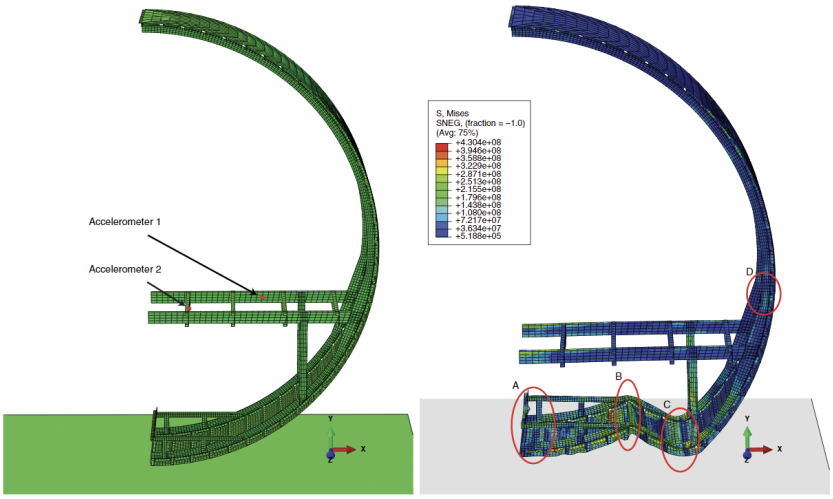

Figure 3.6: Before and after impact deformations in the virtual drop test of a two-frame A320 fuselage typical section [26].

the damaged structure in Figure 3.3. The main difference in the deformation pattern is the lack of a plastic hinge in the underfloor of the cargo compartment. Due to the failure of the rivets connecting the cargo floor structure to the fuselage frames; in Alderliesten's research, the cargo support struts do not buckle sufficiently, but connection failure does not occur, which causes the plastic hinge to occur at the root of the cargo bay floor (region B in Figure 3.6).

As also investigated by [25], the presence of this plastic hinge is mainly dictated by (1) the vertical impact velocity and (2) the stiffness of the underfloor area of the cargo bay itself. A low enough vertical impact velocity is not sufficient to introduce buckling in the cargo bay underfloor area, meaning that a plastic hinge will be created at the root of the cargo floor. The same effect is achieved, in turn, if the cargo floor struts are too stiff. On the other hand, if the support struts are too compliant, then they will not be able to absorb sufficient energy, and therefore damage must occur elsewhere. This will be a recurring theme further on in this research, where it will be highlighted that a good balance between rigidity and flexibility is required to achieve good crash properties for the FV's typical section.

In 2000, Abromowitz et al. [30] performed a drop test of a Boeing 737 fuselage typical section, with a conformable auxiliary fuel tank onboard ($2.3\,\mathrm{m}^3$ in volume) located in the cargo bay area. The objective of the research was to investigate the influence of the presence of such auxiliary fuel tank on the floor structure and airframe in general, under severe but survivable crash conditions. Pre and post-test images are shown in Figure 3.7 and Figure 3.8 respectively. The drop test was performed at a vertical impact velocity of about $9\,\mathrm{m\,s}^{-1}$. Additionally, the lumbar loads and accelerations as experienced by the anthropomorphic test dummies are presented in Table 3.2.

Figure 3.7: Boeing 737 typical fuselage section drop test setup [30].

Figure 3.8: Post-crash of Boeing 737 typical fuselage section, with an auxiliary fuel tank onboard [30].

Table 3.2: ATD data for Boeing 737 drop test [30].

ATD No.	Location	Lumber Load (lb)	Accelerometer Data	
			G_{peak} (g)	Pulse Duration (ms)
1	FS 427 LS	1804	17.4	49
2	FS 426 RS	906	17.3	48
3	FS 462 LS	1734	34	32
4	FS 462 RS	1269	21	55
5	FS 497 LS	1247	27	61
6	FS 498 RS	961	17	18

Firstly, it is worthy to note how, for the most part, the recorded lumbar loads recorded by the ATDs are within the limit required by CS-25.562(c)(2). It should be noted however, how, in this particular test, the auxiliary fuel tank introduced additional stiffness to the structure, and therefore inherently increased the passenger's lumbar loads. For certification purposes, this aspect is not required to be considered.

Differently form what was found by Xue and Alderliesten et al., in Abromowitz's case, the typical section shows a flattening deformation behavior, rather than the creation of a plastic hinge in the middle of the cargo underfloor area: this is caused by the presence of the auxiliary fuel tank, which prevents the upfolding of the frames. The same effect of the presence of cargo in the kinematic behavior of fuselage section upon vertical impact is observed by other drop tests performed by Abromowitz et al. [31] (which focuses on overhead storage bins, and with normal luggage stored in the cargo area), and confirmed by numerical simulations performed by Xianfei et al. [32], where the effect of luggage stored in the cargo area on crashworthiness is explicitly studied; the failure modes are shown in Figure 3.9 and Figure 3.10.

In Xianfei's research it is, counter-intuitively, discovered that the presence of luggage in the cargo bay area has in fact a positive effect on crashworthiness, in general. The cargo itself, absorbs a substantial

Figure 3.9: Boeing 737 typical fuselage section drop test, with luggage in the cargo bay [31].

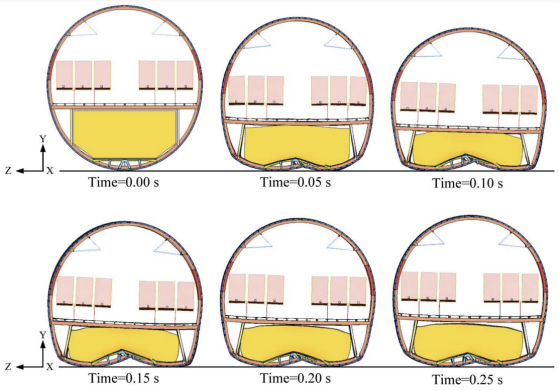

Figure 3.10: Effect of cargo in the failure behavior of a typical metal fuselage section [32].

amount of energy, as shown in Figure 3.11. Additionally, the luggage provides a significant 'dampening' effect: while the first acceleration peak is rather similar to the condition without cargo (logically, since the cargo only contributes once significant deformation has already occurred), subsequent acceleration peaks are smaller in magnitude and shorter in duration. This is also clearly shown in Figure 3.12.

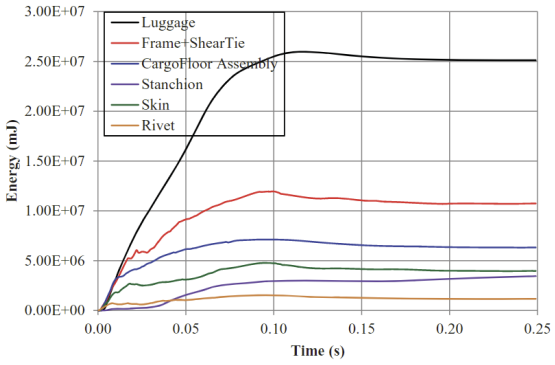

Figure 3.11: Energy absorption by component with luggage loading [32].

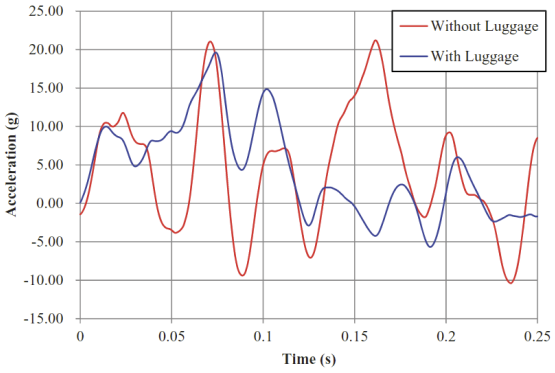

Figure 3.12: Comparison between passenger accelerations: with and without luggage [32].

Of course, accurately modeling the luggage located in the cargo area is difficult. In Xianfei's research, the luggage is modeled as a viscous foam. Simulations are performed for a wide range of stiffnesses and viscosities, so that a sensitivity analysis is performed. Nevertheless, the stiffness values used to model luggage, are in line with those empirically found by Fasanella et al. [33].

Considering the aforementioned results, it then does make instead perfect sense to perform drop tests for certifications purposes with an empty cargo bay area. First of all, of course, type and amount of luggage present in the cargo bay of an aircraft can differ significantly, depending on season, departure location and arrival destination, to mention a few factors. Secondly, the test will be conservative or unconservative, depending on how would a 'typical luggage' compare to actual cargo being carried by the aircraft. Then, it is logical to establish a common baseline which will be conservative in most occurrences, and be less unconservative in case of a crash-landing of an aicraft carrying less conventional passenger cargo.

As a final note to this section, Lützenburger [34] explored the possibility of adding an additional cabin in the aircraft's cargo compartment, so called lower deck seating (LDS). This study, although performed based on the assumption of a full metal fuselage, is tremendously relevant to the topic of this research, since it faces a similar challenge: absorbing energy with a limited crumple zone available. If Xianfei et al. demonstrated that luggage in the cargo bay has a net positive effect on crashworthiness, this is unfortunately not the case for the Flying-V aircraft, where all the cargo is stored in standard LD4 containers in the aft part of the fuselage [1].

Lützenburger, starting from two patented concepts from Airbus and Boeing, show in Figure 3.13, considering the unnecessary addition in weight and aerodynamic drag associated with the Airbus concept, focuses his research on Boeing's one.

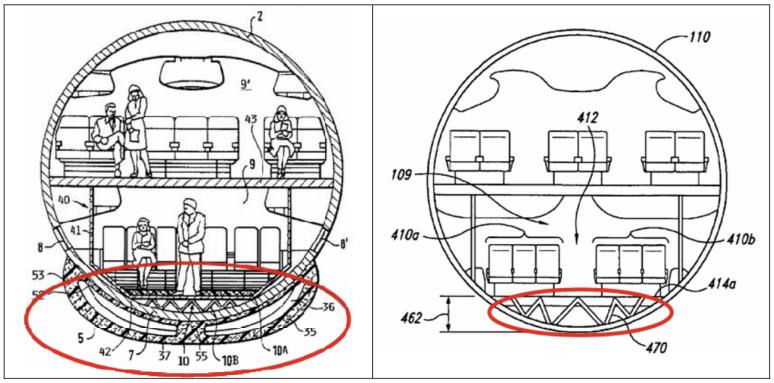

Figure 3.13: Concepts from Airbus (left) and Boeing (right) for passenger cabin located in the cargo hold of an aircraft [35, 36].

A large number of design concepts is evaluated using DRI-KRASH, a crash simulation solver which mainly employs masses, nodes, beams and spring elements, thereby being computationally efficient (which is, of course, traded at the expense of accuracy). In order to evaluate the different concepts, the BASE criterion is introduced. BASE stands for (1) overhead bins; (2) acceleration; (3) survival space; (4) escape route. These are a representation of the four criteria mandated by regulators and already mentioned multiple times throughout this report: retention of items of mass, etc.... Passenger injury following acceleration loads is measured by the employment of the Eiband diagram for vertical accelerations, already introduced in subsection 2.2.1. Eventually, the winning concept identified by Lützenburger is shown in Figure 3.14. As suggested by Boeing's patent, the energy is absorbed, for the most part, by the struts present in the underfloor of the lower deck cabin.

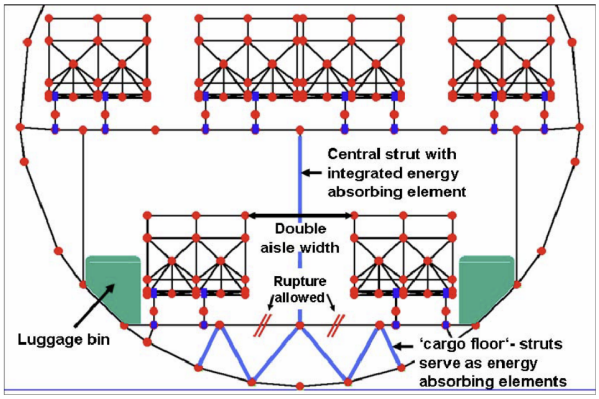

Figure 3.14: Final concept determined by Lützenburger for LDS [34].

From a structural prospective, the most evident design feature in the proposed concept is the presence of the central strut supporting the upper passenger floor beam. This is necessary, in order to avoid the collapse of the upper cabin on the LDS volume. The central strut stiffness properties need to be balanced in such a way that it is not excessively compliant (to indeed preserve survivable space), but neither too stiff, which would otherwise result in increase acceleration experienced by the passengers for both upper and lower deck seats. Lützenburger goes even further, by suggesting that energy absorption mechanisms should be an inherent design feature of the strut itself. This result is also consistent with the research performed by Xue et al., where, as mentioned, it is found that a substantial portion of kinetic energy is absorbed by the passenger floor struts [25]. Additionally, the lower deck floor beams, in the proposed configuration are allow to rupture (in tension). Again, this has to do with energy absorption. When exploring multiple concepts, if was found that not allowing those floor beams to break, would have caused a rebound of the fuselage, with subsequent increase in acceleration ex-

perienced by the passengers. Still, this design feature can potentially compromise escape routes for passengers, which are clearly of critical importance. Lützenburger does not address this specific issue in the research, although, as also shown in Figure 3.14, a double aisle width is recommended to indeed provide improvement of escape routes (considering indeed also the presence of the upper deck floor support struts placed in the middle of the aisle). Lastly, just for the sake of completeness, the luggage bins, in the lower deck, are not placed overhead, as in conventional configuration, but instead on the side of the seats, offering additional protection for the occupants by providing a better retention of items of mass, making it possible to achieve larger partial collapses of the upper floor without risking injury to occupants of the lower deck.

III

Studies on the F-28 Fuselage Section

This page intentionally left blank.

4

Crash Simulation of a Fokker F-28 'Fellowship' Typical Section

This chapter will provide an overview of the procedures used to set up, verify, and validate the non-linear, explicit-dynamic finite element model developed in the context of this research. Firstly, the verification and validation plan will be presented in section 4.1. Secondly, an overview of the test campaign performed by NASA in the early 2000s, from where validation data has been acquired will be given. This is section 4.2. Successively, a description of the finite element model will be provided in section 4.4. Lastly, conclusions will be made in section 4.5.

4.1. Verification and Validation Plan

In order to analyze the Flying-V (FV) aircraft's typical fuselage section crashworthiness characteristics, and, eventually, apport modifications to create necessary improvements, a validated numerical model is needed. The proposed cost- and time-effective way to do so, considering the time frame of the current research, is to create a model for a different aircraft, for which a drop test of the typical section has already been performed and the test results are available. Then, such a model can be validated, and the same modeling techniques subsequently be used to perform a virtual drop test of the FV's typical section. A wide variety of such physical tests have been performed in the past, and for which plenty of test data is readily available in the literature, as shown in Part II.

The main bottleneck, however, is the availability of detailed CAD models of such aircraft. Without reliable data on skin thicknesses and dimensions of cross-sections of the airframe's structural elements, it is not possible to develop a validated model. Luckily, the Faculty of Aerospace Engineering of TU Delft is in possession of a three-frames fuselage section of the Fokker F-28, herein also referred to as the 'Fellowship' aircraft. Consequently, it was possible to recreate a virtual replica of the fuselage section using the 3DEXPERIENCE platform, shown in Figure 4.1.

By visual comparison, the virtual replica closely matches the actual fuselage section, considering parameters such as passenger floor height, fuselage diameter, inclination and positioning of the floor support struts, frames pitch, and stiffeners positioning. Considering the accuracy of the measuring instruments used: measuring tape for large distances and a caliper for thicknesses. For large distances, all linear dimensions are expected to be accurate within a couple centimeters tolerance. Thicknesses, in turn, are expected to be accurate to the tenth of a millimeter. Such relatively small differences (expected to be within a few percent of the "original" section), although will clearly introduce some error, are not expected to significantly affect simulation results and thus validation of the model. Further simplifications which are not included in the model and are expected to introduce additional errors are:

- Lack of structural web cutouts (generally to lighten the structure while, simultaneously, providing additional resistance to buckling [38]);
- Window cutouts in the fuselage skin are not included. This is not expected to have any influence

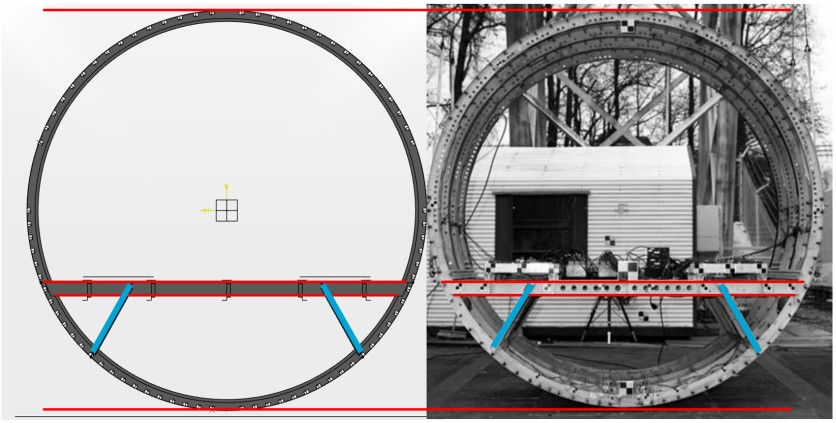

Figure 4.1: Comparison between virtual replica (left) and actual F-28 fuselage section (right). Adapted from [37].

on the results, as the region of window cutouts is distant from that of the plastic hinges);

- The number of stiffeners included in the model is accurate, while their spacing not necessarily (in CAD the spacing is constant, while in the physical model it is not);
- Other discontinuities in the frames or floor beams assembly (which usually are assembled using multiple elements and lap joints) are not present;
- As it will be further mentioned later on, fasteners are replaced by surface tie constraints.

In the early 2000s, NASA performed a drop test on an F-28 fuselage section, with limited available data for a detailed comparison of post-crash displacements and strains, but sufficient for validation purposes when considering the accelerations perceived by the passengers, as detailed in section 4.2. The finite element model of the F-28 is verified by means of a mesh convergence study and validated by comparison to the physical test and simulation performed by NASA. Subsequently, the same modeling techniques will be applied for the parametric studies and, ultimately, to assess the crashworthiness of the FV aircraft. The validation criterion will consist in comparing the average accelerations measured by accelerometers installed on the dummy masses with those probed in the simulation, during the first 110 ms after the impact [37].

4.2. The Fokker F-28 ‘Fellowship’ Test Campaign at NASA LandIR

The Fokker F-28 ‘Fellowship’ is a twin-engined jetliner, developed by the Dutch aircraft manufacturer Fokker in the 1960s, and introduced in 1969. It has a wingspan ranging between 23.6 m and 25.1 m, and a MTOW between $29\,480$ kg and $33\,110$ kg, depending on the variant. The fuselage outer diameter is about 3.3 m [37], with passengers sitting in a 2-3, single aisle configuration. A picture of the F-28 is shown in Figure 4.2[1].

In the late 1990s, NASA purchased a complete, retired F-28 aircraft, plus three additional fuselage sections; to test them as part of the ‘Systems Approach for Crashworthiness’ program [39]. Subsequently, in 2001, a vertical drop test of one of the three sections, the typical section, was performed. The drop test that took place at the NASA LandIR research facility was carried out in a ‘clean configuration’, meaning that no luggage was present in the test section, but only 20x34 kg (75 lb) dummy masses representing the passengers. The section impacted the ground, a concrete surface, at a vertical speed of $9.14\,\mathrm{m\,s^{-1}}$. The physical drop test was compared to an MSC.Dytran™ simulation that has been simultaneously developed, for validation purposes. The finite element model was developed by modifying an existing one of a similar aircraft, the Fokker 70 [37]; the model includes a four-frames section of the fuselage portion forward of the wings. Structural features, such as frames and shear clips are represented using a combination of shell and beam elements. The skin stiffeners are also represented by beam elements.

[1] https://www.airliners.net/photo/Piedmont-Airlines/Fokker-F-28-1000-Fellowship/0451713/L. Accessed on 03-Oct.-2022.

Figure 4.2: A Fokker F-28-1000 (registration N469US).

Figure 4.3: From left to right: pre-test, post-test, and simulation results from the F-28 drop test performed at NASA LandIR; adapted from [37, 39].

A comparison between the fuselage sections pre-test, post-test, and finite element simulation results can be found in Figure 4.3.

In order to investigate the effects of uncertainty when modeling nonlinear structural impact, a Monte Carlo simulation was performed, by running a multitude of FEA analyses with different input parameters (the ranges of which are shown in Table 4.1), in order to determine the upper and lower bounds in which physical tests result would have been expected.

The results are shown in Figure 4.5, whereas the accelerometers location and labeling are clarified in Figure 4.4. The results provided in the aforementioned figures will be used for validation purposes of the finite element simulation developed in the context of the current research.

Table 4.1: Description of input variables for the FE model (units: kg, s, mm). The term ‘castellations’ is used to refer to the shear clips; adopted from [37, 39].

Variables	Bounds			Nominal values	
No.	Physical quantity	Lower (b_L)	Upper (b_U)	Frame	Castellation
1	Yield stress	0.9	1.10	420.0	275.0
2	Hardening modulus	0.9	1.1	1245.0	1236.0
3	Castellation failure strain	0.5	1.0	-	0.17
4	Frame thickness	0.9	1.1	1.5,1.6,2.9,3.0	-
5	Castellation thickness	0.5	1.0	-	0.55,0.74
6	Frame failure strain	0.8	1.2	0.05	-

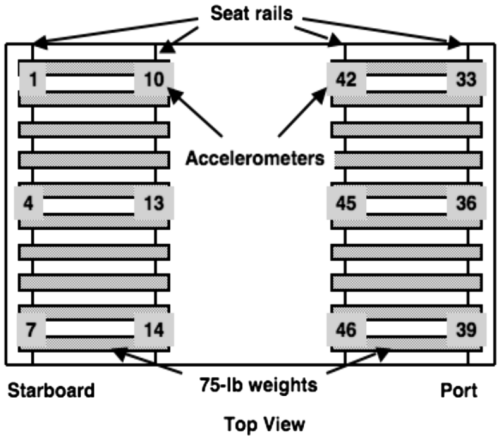

Figure 4.4: Schematic of fuselage section floor, and selected accelerometer locations and IDs [37].

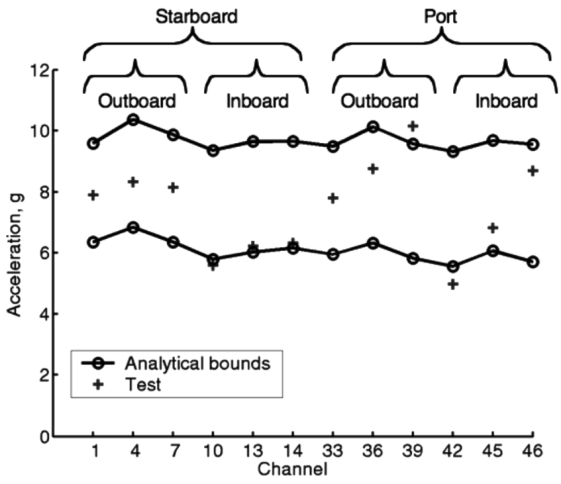

Figure 4.5: Comparison between probabilistic analysis bounds for the finite element analysis, and physical test results [37].

Table 4.2: Thicknesses of different structural components, F-28 typical fuselage section.

Item	Shell thickness [mm]	Item	Shell thickness [mm]
Skin	1.5	Stiffeners	2
Frames	1.8	Shear Clips	0.5
Floor struts	1.8	Floor transv. beams	1.8
Floor long. beams	1.8	Dummy masses	104.5

4.3. Finite Element Simulation Set-Up

4.3.1. CAD Model

3D views of the CAD model are shown in Figure 4.6. The full CAD model has been made open source, and can be accessed via the following link: `https://doi.org/10.5281/zenodo.7702918` [40].

The 3D model of the F-28 typical section includes frames and shear clips, skin, stiffeners, floor transverse beams (transverse to the direction of flight), and floor longitudinal beams (parallel to the direction of flight). It does not include seats, overhead storage, a passenger floor, and other cabin interior components. The payload is represented by dummy masses equivalent to those employed by NASA in their F-28 drop test.

4.3.2. Finite Element Model

The meshing of the F-28 typical section was performed using the 3DEXPERIENCE platform mesher, for convenience reasons: it provides seamless integration between the CAD and the finite element models. If changes to the geometry are performed, the FEM can update accordingly, reducing model building time significantly. Additionally, since the integrated solver in the 3DX platform is the same one used in Abaqus/Explicit, then a minimum of additional pre-processing was required before submitting the input file for analysis to the TU Delft computer cluster.

Section Assignment

The FEM was built using exclusively shell elements, considering that all the structural features of the fuselage section are made out of plates whose thickness is significantly smaller than the other two dimensions. The mesh is quad-dominated, using fully integrated, first-order elements (S4), which are well-suited for impact dynamics problems [41]. The assigned thicknesses for each structural component are shown in Table 4.2.

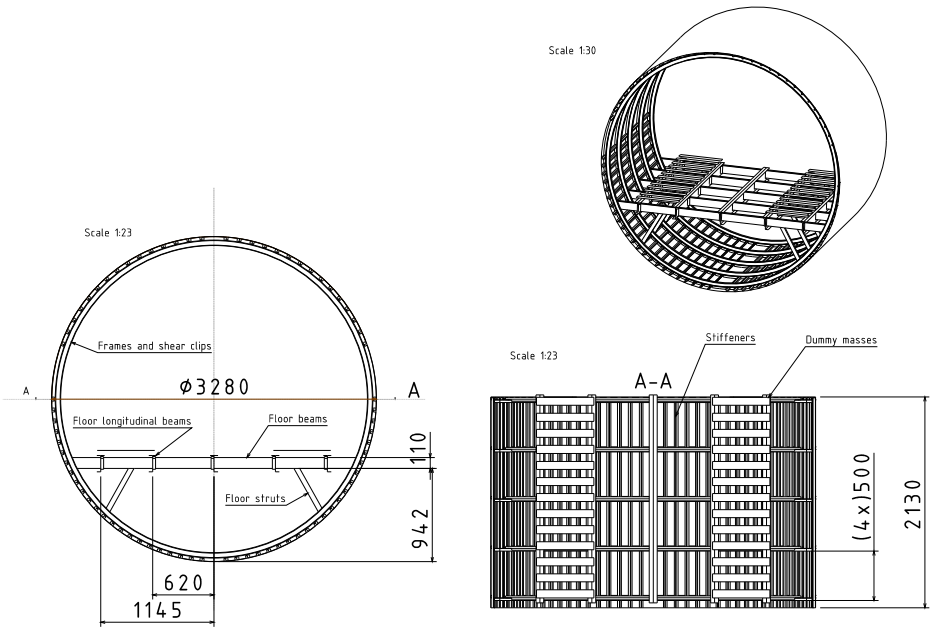

Figure 4.6: Views of the Fokker F-28 fuselage section virtual replica. Note that scaled dimensions are relative to the figure being printed in an A4 sheet (landscape).

Material Assignment

The Fokker F-28 Fellowship airframe is made, for the large part, of Aluminium 2024-T3 alloy [42]. The properties for such alloy, from literature, are presented in Table 4.3.

The chosen material model to be used in the simulation is the Johnson-Cook model (JC), an elastic-plastic model which can also include temperature and strain-rate dependencies. It is computationally efficient and widely used in industry for impact damage simulations [43].

In the JC model, the flow stress is defined by the following relation [43]:

$$\sigma_y = \left(A + B\bar{\varepsilon}^{p^n}\right)\left(1 + c\ln\dot{\varepsilon}^*\right)\left(1 - T*^m\right) \tag{4.1}$$

with A and B being the material yield strength and hardening modulus respectively, $\bar{\varepsilon}^p$ the plastic strain, n hardening parameter, $\dot{\varepsilon}^*$ the strain rate, c the strain-rate dependency parameter, T^* the dimensionless

Table 4.3: Parameters used for JC elastic-plastic model, including damage [43]. c, n, m, D_4 and D_5 have been set to zero considering the strain-rate insensitivity of AA2024-T3, and that all analyses are performed at room temperature. All units in kg, N and mm.

Variable	Value	Variable	Value
A	369	D_1	0.112
B	684	D_2	0.123
c	0	D_3	1.5
n	0.73	D_4	0
m	0	D_5	0

Table 4.4: General element sizes for different structural components, baseline configuration.

Item	Element size [mm]	Item	Element size [mm]
Skin	40	Stiffeners	15
Frames	15	Shear Clips	12.5
Floor struts	10	Floor transv. beams	15
Floor long. beams	20	Dummy masses	40

temperature ($T^* = \frac{T - T_{\text{room}}}{T_{\text{melt}} - T_{\text{room}}}$) and, lastly, m the temperature dependency parameter.

The employed failure model is a strain-based one [43]:

$$\varepsilon_{\text{failure}} = [D_1 + D_2 \exp(D_3 \sigma^*)\,[1 + D_4 \ln(\varepsilon^*)\,[1 + D_5 T^*] \tag{4.2}$$

with D_1 to D_5 being empirically-determined failure parameters. σ^* is the pressure-to-effective stress ratio:

$$\sigma^* = \frac{\text{pressure}}{\bar{\sigma}} \tag{4.3}$$

In the JC model, fracture occurs when the damage parameter $D > 1$. D is the ratio between the effective plastic strain and the failure strain determined using Equation 4.2:

$$D = \sum \frac{\Delta \bar{\varepsilon}^p}{\varepsilon_{\text{failure}}} \tag{4.4}$$

Interaction and Contact Properties
All riveted connections are modeled by means of tie constraints, in order to avoid failure at the joint: by design, failure of joins is undesired and, therefore, as shown experimentally [37, 39], in a crash scenario this is unlikely to happen. It was therefore decided to completely remove the possibility of this happening to start with.

In order to avoid element penetration (which physically would not be meaningful), a general contact interaction property was defined. The normal behavior is hard contact, while the tangential behavior is defined using a penalty friction formulation, by thus specifying the friction coefficient. The chosen coefficient is 0.5 (slip-rate independent)[2], which is a good estimate for both aluminum/aluminum and aluminum/asphalt contact interfaces.

4.4. Verification and Validation of the Finite Element Model

4.4.1. Verification: Mesh Convergence

For mesh convergence purposes, three different mesh sizes have been compared: baseline, refined and coarse. The mesh is refined or made coarser by multiplying the baseline general element size by a scaling factor, which for the coarse mesh is 2 generating elements that are twice as large as the baseline. For the refined mesh the adopted scaling factor is 0.75. The scaling factor does not apply to the skin, because it is assumed that the effect of the skin on the energy-absorption characteristics of the overall structure is considerably smaller than the other structural elements, and therefore it will not have a prominent effect on mesh convergence outcome. The general element size for each structural element, for the baseline configuration, is shown in Table 4.4.

The discussion on mesh convergence focuses on two key aspects: plastic energy dissipation and accelerations. The results are shown in Figure 4.7 thru Figure 4.11. The initial kinetic energy of the fuselage section, prior to impact, is of about 50 kJ.

[2] https://www.engineeringtoolbox.com/friction-coefficients-d_778.html. Accessed on 07-Nov.-2022.

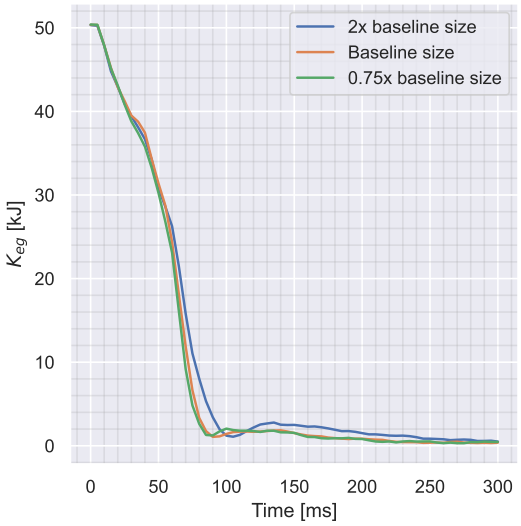

Figure 4.7: Kinetic energy time history of the models. The coarse mesh model exhibits stiffer behavior than the other two (longer impact time, and larger rebound). The baseline and refined mesh models show close to identical behavior.

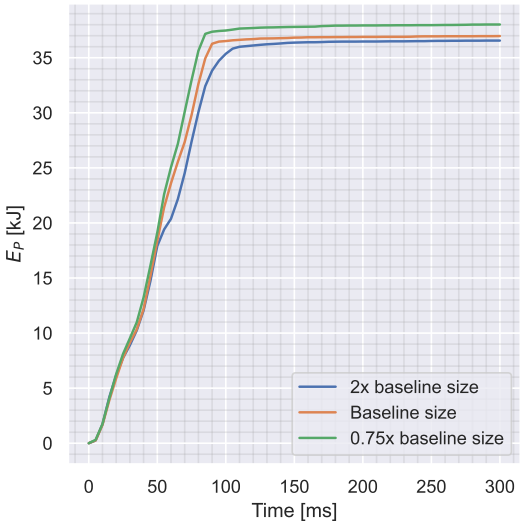

Figure 4.8: Energy dissipated by plastic deformation of frames and shear clips vs. time. Coarser mesh model underestimate the absorbed energy, as they are not able to capture crippling of the flanges in compression.

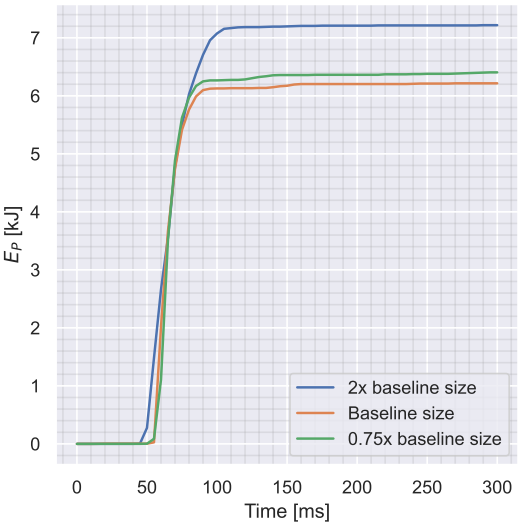

Figure 4.9: Energy dissipated by plastic deformation of floor struts vs. time. Good agreement between baseline mesh and refined mesh data.

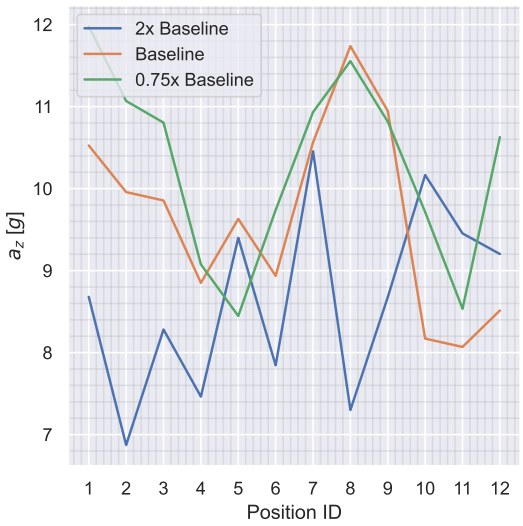

Figure 4.10: Mean acceleration determined at each accelerometer position. The position IDs 1 thru 12 correspond to those shown in Figure 4.4, in ascending order. Good agreement is found between the baseline and refined mesh cases, both in terms of trend and magnitude of the accelerations.

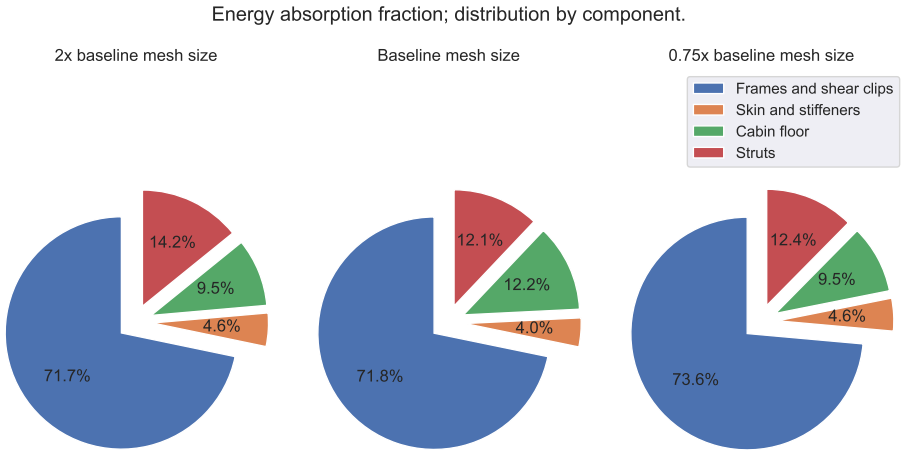

Figure 4.11: Energy fraction absorbed by each component, for the three different global element sizes. No significant differences are present.

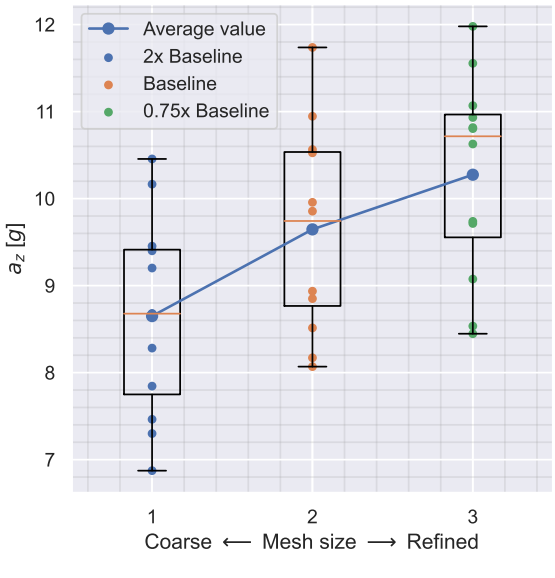

Figure 4.12: Box plot of acceleration determined for the three different global element sizes. Each dot represents the mean accelerations determined at a given floor location (as shown in Figure 4.10). A 6% difference is present between the 0.75x refined mesh model and the baseline one.

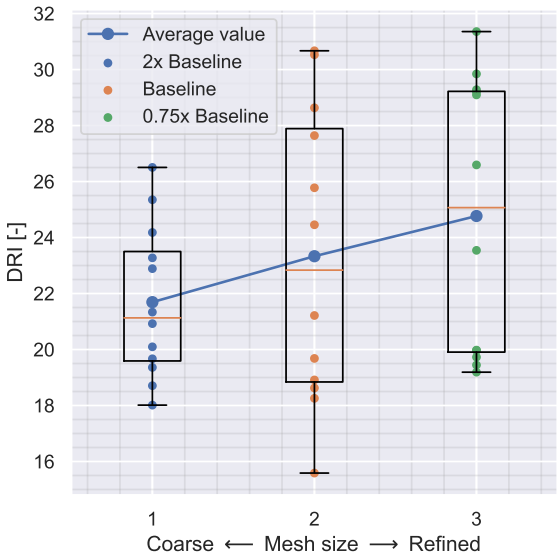

Figure 4.13: DRIs for the three different global element sizes. The change in DRI is consistent with the mean accelerations trend observed in Figure 4.12.

Considering the energy absorbed, starting from Figure 4.7, where the kinetic energy of the system versus time is plotted, the 'baseline' model shows an almost identical behavior to the one with a refined mesh. The most evident difference with the coarse mesh model is the maximum deformation point, i.e. the point at which the kinetic energy is minimum. This occurs at $t = 85$ ms for the refined mesh, $t = 90$ ms for the baseline, and $t = 105$ ms for the coarser mesh. The previous observations are consistent with what is expected: generally, finite element analyses with a coarser mesh exhibit a stiffer behavior than those with a more refined mesh; as a consequence, the collapse of the floor struts, and the subsequent impact of the frames on the floor beams, which have been observed to be the most critical failure modes leading to the maximum deformation state of the crash section, are delayed, and so is the minimum kinetic energy point. Lastly, the difference in crash time duration between the baseline and the refined mesh is approximately 6%.

Moving on to the energy absorbed by the frames and shear clips, shown in Figure 4.8, the total plastic energy absorbed is of 36.6 kJ, 37.0 kJ, and 38 kJ for the coarse, baseline and refined mesh configurations, respectively; that is, the energy absorbed by the frames and shear clips in the baseline configuration is within 3% of that absorbed in the more refined mesh case, which is a positive result, in terms of mesh convergence. The same can be observed when comparing the energy absorbed by the floor support struts, plotted vs. time in Figure 4.9. The struts absorb a total of 7.2 kJ in the coarse mesh analysis. In contrast, in the baseline and refined mesh ones, the plastic energy absorbed by the floor struts is of 6.2 kJ and 6.4 kJ respectively, a 2.8% difference.

Lastly, to conclude the discussion on crash energy absorbed, it is worth noticing that no significant difference is present between the fraction of energy absorbed by different structural components. The most significant differences are the decrease in energy fraction absorbed by the floor struts from 14.2% to 12.4%, and, only for the baseline mesh model, the increase of the fraction of energy absorbed by the cabin floor beams from 9.5% to 12.2%. Regarding the former, this is due to finite element models being overly stiff for coarser meshes. The struts will thus require a larger force to buckle, and, thus, more energy. On the other hand, a more refined mesh will also allow to better capture the crippling of structural components. As in the baseline mesh, compared to the coarse one the struts lose part of the ability to absorb energy, the up-folding of the frames will occur at a faster rate (the test section carries more kinetic energy); thus, they will also carry more momentum when impacting with the floor structure. This causes an increase in the fraction of energy absorbed by the floor structure. For a more refined mesh, however, the model is able to better capture the crippling of the frames at the locations of the plastic hinges, and, thus, the frames and shear clips themselves will absorb more energy, as observed in Figure 4.16.

Regarding data on acceleration response and computed DRI at floor location, to start with, considering Figure 4.10, it is clear how, both in terms of absolute value and overall trend, very good agreement is found between the baseline and refined meshes. In Figure 4.10, the position IDs 1 thru 12 correspond to those shown in Figure 4.4, in ascending order, and have been renumbered simply for the sake of clarity. The average of the all the measured mean acceleration values for the refined mesh case is of approximately 10.2 g, while for the baseline model is of 9.6 g, a 6% difference. The same holds for the computed DRIs. This is expected, considering that the DRI is a function of the input acceleration. This result is thus also used as a verification method for the tool used to determine the DRI from the accelerometer data.

Given all the above data, the following conclusions are drawn:

- The numerical model, as well as the DRI calculation tool, can be considered to be verified;
- The baseline mesh has been determined to be refined enough to consider the results to be accurate. Although it is not guaranteed that convergence has been achieved, it is important to highlight that: 1) the overall error between the baseline mesh and the refined case is low; 2) good agreement is found between the developed model, the model from NASA and the physical test. Thus, in all the subsequent studies, the baseline global element size will be used, which, once again, is tabulated in Table 4.4.

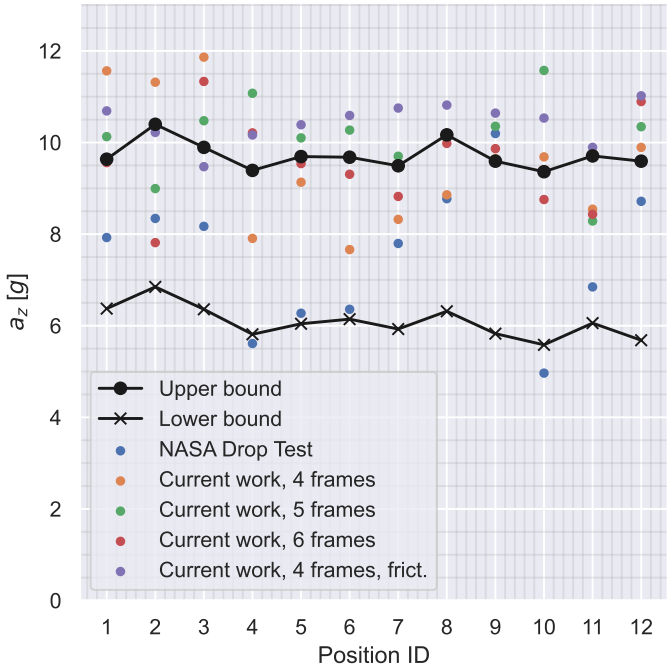

Figure 4.14: Comparison of mean acceleration values between NASA's F-28 drop test and simulation results [37, 44], and current work. The position IDs 1 thru 12 correspond to those shown in Figure 4.4, in ascending order. The following observations can be made: 1) the measured accelerations for the 4 frames section are in line with those expected from NASA's study; 2) The introduction of friction reduces scatter in measured accelerations; 3) no fundamental differences can be observed between sections with different number of frames.

4.4.2. Model Validation and Minimum Model Size

This section will cover two fundamental aspects on the crash simulations performed in the current research. Firstly, the developed numerical model needs to be validated using experimental data. Secondly, for the parametric studies to be performed, it is of interest to determine what is the minimum model size that can be used while still having accurate results. Namely, in general, for certification purposes, a six-frame typical fuselage section is used, since, on average, it has the same stiffness and mass properties of a larger fuselage [26]. However, if it can be demonstrated that a section that includes a fewer number of frames can still provide accurate enough results for the purpose of this research, then this would be advantageous since it would reduce the computational cost, as well as the overall amount of data that is generated as a result.

Model Validation

As mentioned in section 4.1, the FE simulations will be validated by comparison with the mean accelerations at accelerometers locations reported in Figure 4.5. The results are shown in Figure 4.14, where the data from Figure 4.5 has been digitized for the sake of clarity. For model validation, the mean acceleration at each accelerometer location for the 4 frames, friction model (in purple) is compared with NASA's drop test and simulation (upper and lower bound) results.

There is good agreement is found between both the physical drop test and simulation results. The mean acceleration levels determined in the current work are on the higher end of the spectrum, as compared to the numerical upper bound determined by NASA's simulation. The main reason for this is likely that, since the structural components' dimensions, in particular thicknesses, have been determined by measuring the actual dimensions of the fuselage section in possession of TU Delft, then it is not physically possible to underestimate the thicknesses; thus, all measured thicknesses are accurate at best, and likely overestimated, thus resulting in an overall increase in stiffness of the fuselage section. Lastly, Figure 4.15 compares the after-impact state of the fuselage section with that of NASA's physical drop test and simulation. Once again, good agreement is found between the three deformed shapes, in particular when comparing the two simulations.

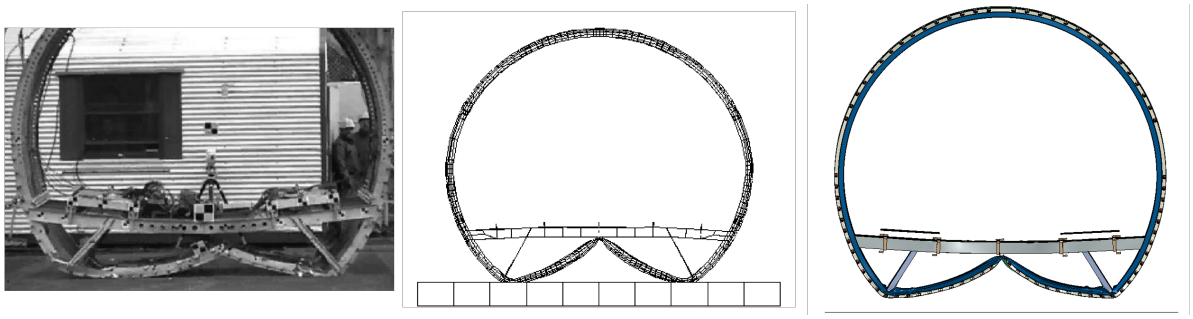

Figure 4.15: Side-to-side comparison between NASA drop test and simulations (left and middle), and current work (right). Adapted from [37].

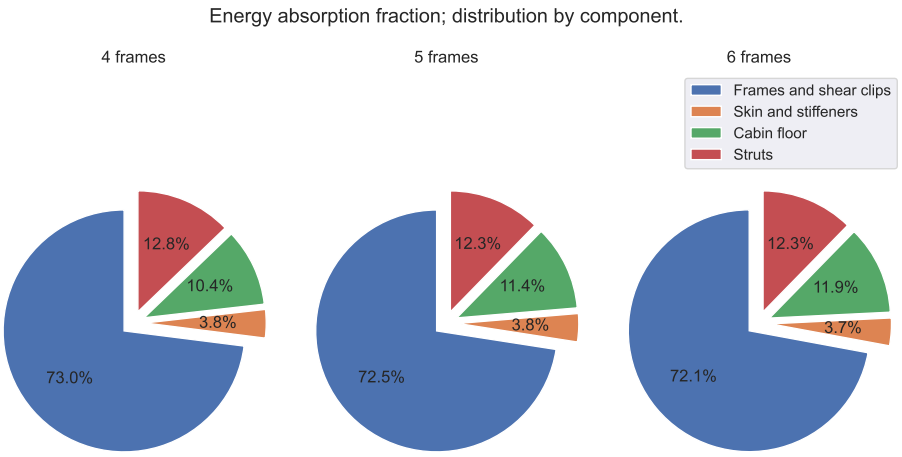

Figure 4.16: Energy fraction absorbed by each component, for a different number of frames sections.

Considering all of the above, the numerical model is validated.

Minimum Fuselage Section Size for Modeling

The final step towards the development of a validated FEA model to assess the crashworthiness of the FV, is the definition of the minimum fuselage section size that needs to be analyzed. As mentioned, in general, for certification purposes, a six-frame section is used. Subsequently, it was decided to investigate if in fact a shorter section could be analyzed, in order to reduce the model size and thus the computational cost.

The data is presented in Figure 4.16.

Clearly, the difference between the three different sections is negligible. From visual inspection of the results, a reduction in the coupling between the crushing and twisting behavior of the fuselage section was noticed. The twisting motion originates from the up-folding frames hitting the central floor longitudinal beam. Due to the asymmetrical cross-section of such a beam, the frames are deflected sideways, and this deflection gives origin to the crushing-twisting motion. Longer sections show to have increased stability against the crushing-twisting mode and, therefore, the frames are constrained to remain in the center. The result is a harder impact of the frames with the floor beams, causing the former to deform less and the latter to deform more.

All in all, however, the difference in behavior between the three tested sections is small, and, thus, it is concluded that a five-frame section will be used to assess the crashworthiness of the FV. The main

reason is that, from visual inspection of the results, although this is not captured by the data presented in Figure 4.5 and Figure 4.16, the crushing-twisting motion observed in the four-frame section was significantly larger than for the other two.

4.5. Conclusion

This chapter has provided an overview of the modeling techniques used to develop a non-linear, dynamic, finite element analysis model for a fuselage section drop test. The same model will be used to perform parametric studies on the fuselage section eccentricity and vertical floor height location, using the F-28 fuselage section. In addition, the same modeling techniques will be employed to assess the crashworthiness of the FV. The model is built using the 3DEXPERIENCE platform mesher and solved using Abaqus/Explicit.

The modeling techniques are verified by means of mesh sensitivity analysis and validated by comparing the crash analysis of the fuselage section of a Fokker F-28 aircraft with a physical drop test of the same section, performed by NASA at the LandIR research lab, in the early 2000s. Good agreement has been found between experimental and simulation data.

Additionally, in order to reduce the computational cost of future simulations, the minimum required fuselage section size has been identified. It has been found that five-frame sections will be sufficient to achieve accurate results, and, that, in fact, data shows little difference in the crashing behavior of four, five, and six-frame fuselage sections.

5

Parametric Studies on the Typical Section of the Fokker F-28 Aircraft

In general, during a crash event, a circular fuselage undergoes an ovalization process and tension forces are induced in the passenger floor beam (which is exploited by Waimer [45, 46] for the implementation of a tensile energy absorber concept). Unfortunately, due to the nature of the aircraft configuration, the fuselage of the Flying-V aircraft is already oval in shape. In addition to this, the vertical location of the passenger floor beam on crash kinematics, for both circular and eccentric fuselage is also not fully understood. As such, two parametric studies have been performed and will be documented in this chapter: one on the effects of fuselage ovalization, and one on the effects of vertical floor location.

In particular, the research question addressed is: how will fuselage eccentricity and vertical floor location influence the energy-absorbing capabilities, crash kinematics, and loads experienced by the occupants, during a drop test of a typical fuselage section?

Thus, section 5.1 and section 5.2 will give a brief summary of the research plan in order to address the aforementioned question, while the results will be presented an analyzed in section 5.3.

5.1. Fuselage Ovalization

Compared to conventional aircraft configurations, the most significant geometric difference between the FV section and conventional fuselages is the high eccentricity ($e \approx 0.75$, with e being the eccentricity parameter of an ellipse that approximates the shape of the FV typical section). The original concept for the FV included a tubular pressurized fuselage structure, in a horizontal double-bubble configuration [47]; more recent iterations have, in turn, converged towards an oval shape, in order to maximize the space available in the cabin for the occupants. As such, it has been deemed of interest to understand the effect that such an oval shape would have on the crash properties of a general aircraft's typical section.

In order to achieve so, the CAD model of the F-28 aircraft developed for validation purposes has been modified in order to allow the fuselage section to achieve an elliptical shape. Then, the ellipse's eccentricity parameter has been varied in order to correlate the crashing behavior with the fuselage section eccentricity.

As the section is modified to become more eccentric, the vertical space inside the cabin will subsequently. In order to still be able to fit an equal amount of passengers compared to the F-28, the cabin width is also increased, and the floor height decreased. This approach, unavoidably, will result in reduced, if not missing at all, volume for cargo below the passenger floor. While this is a significant difference, a few considerations here need to be made. First and foremost, as already mentioned in chapter 3, in general, cargo has a dampening and therefore overall positive effect on aircraft crashworthiness. Thus, the lack of cargo below the passenger floor is to be seen as an overall negative effect,

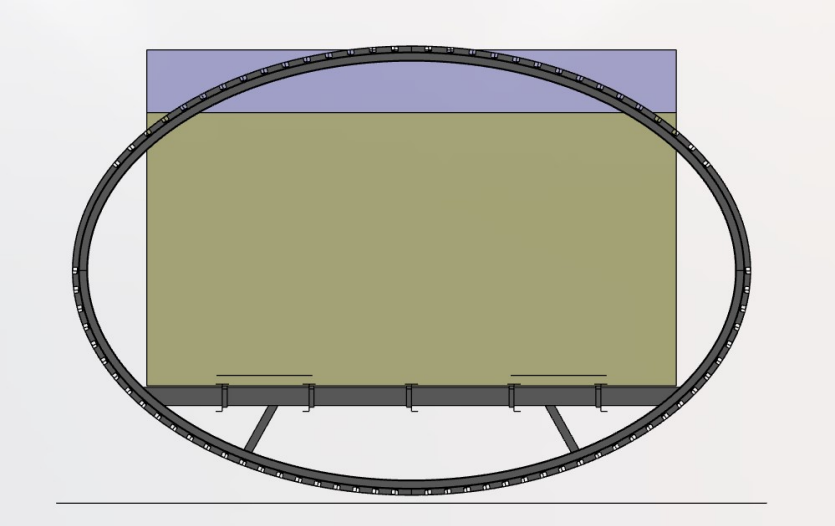

Figure 5.1: Screenshot from the ovalized F28 fuselage section, depicting the cabin headroom (yellow) and aisle height (blue) envelopes, as recommended by Raymer [48].

thus a conservative approach. Secondly, this is more similar to the case of the FV aircraft in the first place.

The conservation of passenger living space has been performed considering the initially available space for the F-28 aircraft, as well as the passenger envelope recommended by Raymer, for preliminary aircraft design [48], and then selecting the most critical case of the two, to account for the geometry differences between the F-28 circular section, and an oval one, as shown in Figure 5.1.

A comparison between the original, circular, and highly eccentric fuselage sections layout is presented in Figure 5.2, 1A thru 6A. The results of the parametric study will, in turn, be presented in subsection 5.3.2. The original F-28 section will be compared to other five similar ones, with different levels of geometric eccentricity: $e = [0.2, 0.4, 0.6, 0.7, 0.75]$.

5.2. Vertical Floor Location

Compared to conventional aircraft configurations, and as already discussed in and section 5.1, due to the accentuated geometric eccentricity of the fuselage section, the FV fuselage will also present a reduced crumple zone below the passenger floor beams. For crashworthiness purposes, this is highly undesired: by reducing the space available for energy dissipation, inherently, passengers will experience larger accelerations and, thus, the probability of spinal injury will increase. Thus, a sensitivity analysis on the dependence of the crushing response with respect to the vertical floor location has been performed. The objective is to understand what is the impact of changing the floor height as little as 50 mm, when the fuselage section has a highly oval shape: the floor beam height will be one of the design variables during the design phase of the FV section.

Thus, four different oval fuselage sections will be compared ($e = 0.75$), with different floor heights, as measured from the bottom-most point of the fuselage: $h = [500, 550, 600, 650]$mm. Once again, the results will be presented and discussed in subsection 5.3.3. A comparison between the four layouts is shown in Figure 5.7, 1A thru 4A.

5.3. Results and Discussion

The current section will address results obtained from the parametric studies on the F-28 fuselage section. The key metrics used will be first presented in subsection 5.3.1. Successively, subsection 5.3.2 and subsection 5.3.3 will give an overview of the results. Lastly, section 5.4, will provide a final discussion on the results of the parametric studies.

5.3.1. Evaluation Criteria

The key metrics on which the bulk of the upcoming discussion will be based are the following:

- Visual inspection of the crash section, in its final state;
- Kinetic dissipation over time;
- Mean accelerations and DRI;
- Component energy absorption distribution.

The reasons for the selection of those criteria will be provided in the remainder of this subsection. Overall, however, all the aforementioned criteria cannot be considered singularly, to examine the crash characteristics of the section; rather, they, together, will provide a clear and consistent picture on the similarities and differences of the crash events.

Visual Inspection of the Crash Sections

From a visual inspection of the crash section, first and foremost, it is possible to verify if the crash simulation is behaving as expected: are the tie constraints working? Are the interaction and contact properties able to avoid element penetration? Secondly, it will be possible to identify the energy-absorbing mechanisms, and, thus correlate those with the collected data, for data validation.

Kinetic Energy Time History

The kinetic energy time history plots are meaningful in multiple ways. First and foremost, the slope of the K_{eg} vs. time curve, $\dot{K}_{eg}$, is the rate at which the kinetic energy of the fuselage section, and of the occupants, is converted to elastic and plastic energy (with the latter being favorable over the former). A higher rate of dissipation will imply harder contact with the ground, and, consequently, larger acceleration pulses felt by the occupants. This is followed by the point of maximum deformation, meaning the moment in time in which the kinetic energy is at a minimum, and most of the kinetic energy has been absorbed by the structure. Generally, counter-intuitively, the kinetic energy does not become null at this point: although it is generally minimized, as the velocity of components (including dummy masses), tends to zero, there will still be residual kinetic energy, due to different nodes reaching a zero-velocity point at different points in time. Additionally, due to storage constraints, the energy history output has only been exported every 5 ms; at the actual minimum point, the kinetic energy has in fact been observed to be of 600J, for the $e = 0.0$ configuration.

Third, the rebound phase occurs. All elastic energy stored in the structure is released and converted, once again, in kinetic energy (or dissipated by means of vibrations, in case of material failure), and, thus the fuselage section bounces up. Generally speaking, rebounds are undesired, as they will effectively prolong the duration of the acceleration pulse experienced by the occupants. As highlighted in chapter 2, humans are able to relatively well tolerate high-magnitude, low-duration acceleration pulses. The longer the duration of the pulse, the lower the acceleration magnitude can be tolerated, without increasing the risk of injuries.

Mean Accelerations and DRIs

An obvious key metric, when evaluating the crash characteristics of the test section, is to measure and compare the acceleration pulses felt by the occupants, and their relative response (DRI). As explained in subsection 2.2.2, while the DRI might be inaccurate to measure the actual spinal injury rate of occupants, it will still provide a good baseline for comparison of the crash characteristics between different configurations of the F-28 and FV sections.

Energy Absorption Distribution by Component

The energy absorption distribution by component (absolute value and normalized[1]) is yet another important metric to evaluate the crash characteristics of the section, for a series of reasons.

Firstly, the overall energy absorption characteristics of the section need to be monitored: if less energy is dissipated thru friction and plastic deformation, then, the difference will be stored as elastic energy,

[1] i.e. dissipated energy by component over total dissipated energy

which will favor a rebound. As mentioned earlier, rebounds are undesirable, as they prolong the duration of the acceleration pulses. Secondly, absolute energy absorption values, by components, can be correlated with visual observations, in order to corroborate or disprove theories on the involved energy-absorbing mechanisms, and vice versa: visual observations cannot, alone, provide a full picture of the crash event, and vice-versa.

Thirdly, and lastly, the normalized energy absorption distribution provides a clear and simple metric to identify the structural components that are most critical to dissipate crash energy. The variation of the normalized absorbed energy across different configurations will grant insights into how the relative importance of each component varies, for different geometric parameters.

5.3.2. Fuselage Ovalization

The discussion on the finite element analysis results of the study on fuselage ovalization study will be provided in this subsection. As mentioned in subsection 5.3.1, four different criteria are used for comparison: visual inspection, kinetic energy, accelerations, and energy absorption distribution, by component.

Visual Inspection of the Crash Sections

A visual comparison of the six analyzed crash sections is provided in Figure 5.2.

The first significant difference for increasing fuselage eccentricity is the reduced resultant up-folding of the frames, due to the initial flatter geometry of the fuselage keel. Additionally, the floor beams also create a physical barrier that limits the possible up-folding of the frames, which will further reduce the allowable deformation for increased eccentricity, as the distance between the keel and the floor beams is reduced. Secondly, as a result of the decreased ability of the frames to absorb energy, the floor struts will experience an increase in load, and, thus, buckle. Another result of the loss of the energy-absorbing ability of the frame is the increase in the bending load of the floor beams, whose web, subsequently, buckles. This is particularly pronounced in sections with $e = [0.6, 0.7, 0.75]$.

Kinetic Energy Time History

The kinetic energy time history plot is provided in Figure 5.3. First and foremost, although the geometry of the different sections varies, the initial kinetic energy is approximately constant (less than 0.5% variation, as also shown in Table 5.1), which indicated that the mass of all tested sections is approximately constant, and, any variation, is not expected to have any significant effect on the results.

It is clear how, for increased fuselage geometric eccentricity, $\dot{K}_{eg}$ increases. This is the direct result of the reduced distance between the passenger floor beams, and the fuselage keel (thus, a decrease in crushable volume), as the majority of the kinetic energy to be dissipated is stored in moving mass located above the passenger floor beams.

This is also reflected by the progressively decreasing time at which the maximum deformation point occurs: the crash event, due to a reduction in crushable length, needs to occur in a shorter time-frame (resulting in an overall increase in loads and accelerations), in order to dissipate a comparable amount of energy.

Lastly, for more eccentric fuselage sections, a larger rebound is present. The reduction in crushable length results in an overall decrease in the material available for energy absorption. Consequently, since the resultant K_{eg} at the maximum deformation point is approximately comparable for all curves, then, more energy is stored elsewhere by means of elastic energy. The total resultant kinetic energy once the rebound has occurred (local maximum after the point of maximum deformation) will consequently be higher for highly eccentric questions.

Mean Accelerations and DRIs

The mean accelerations measured during the impact (from $t = 0$s up until the maximum deformation point), and the DRIs, at different floor locations, are presented in Figure 5.4 and Figure 5.5 respectively. Mean accelerations and DRIs are closely correlated with each other, being the DRI computed directly from the nodal acceleration time history. The difference, however, is that DRI is also dependent on the acceleration pulses frequency: for the same mean acceleration computed during the crash event,

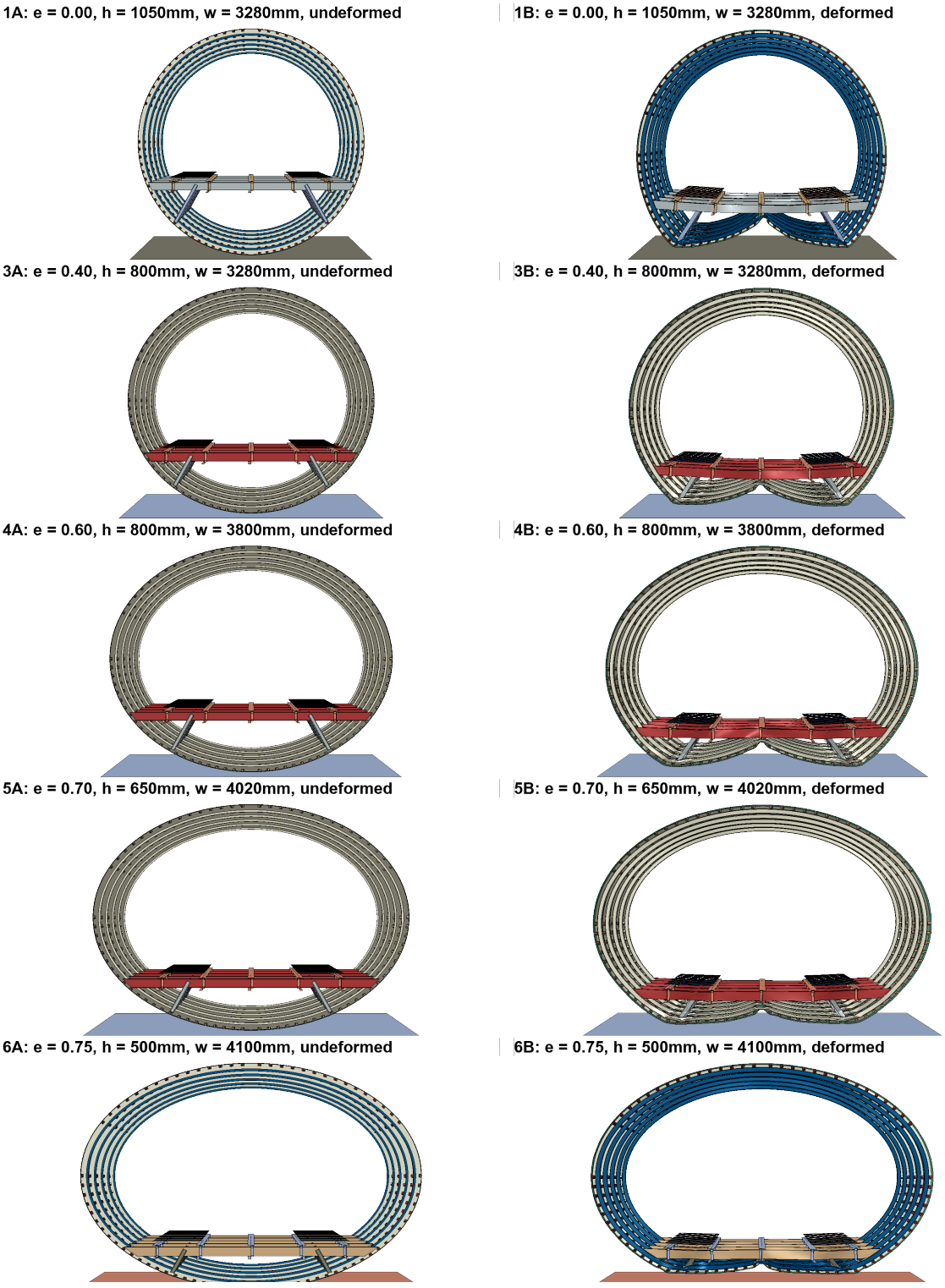

Figure 5.2: Comparison between the deformed F28 crash sections for different fuselage geometry eccentricity levels ($e = [0.0, 0.40, 0.60, 0.70, 0.75]$). Vertical floor height, h, and fuselage width, w, also change with changing of the eccentricity parameter, as the overall cabin space is required to be maintained. Figures 2A and 2B ($e = 0.20$) have been omitted due to the similarity with the $e = 0.0$ model. For more eccentric configurations, frame unfolding is constrained by the presence of the floor structure. $e = 0.75$, an unfolding of the frames is present, due to the collision with the floor structure. Also, floor struts experience higher compression for more eccentric configurations.

if the acceleration pulses have the same frequency of the human model described in chapter 2, then

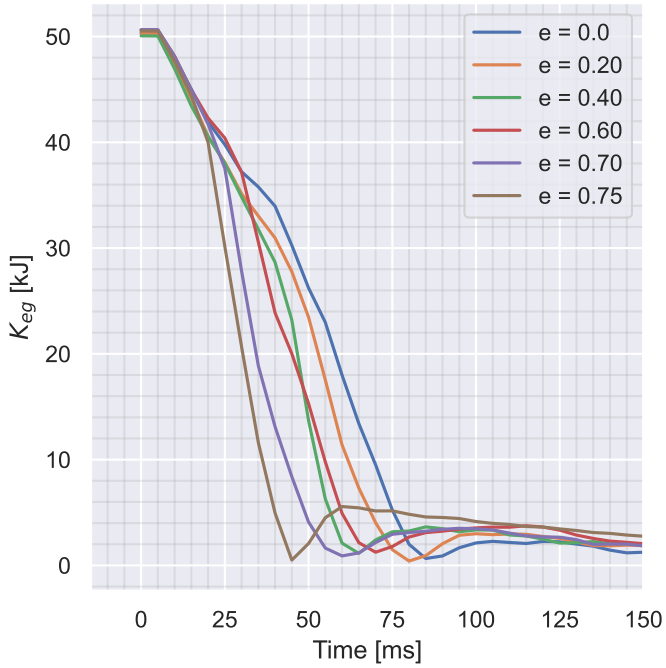

Figure 5.3: Model kinetic energy vs. time; different lines indicate different fuselage section geometric eccentricity.

resonance will occur, and the likelihood of spinal injury increase. This is likely the case between the configuration $e = 0.0$ and $e = 0.2$, where there is no noticeable difference in both mean acceleration and deformation of the crash section; the DRI, however, increases by over one unit, on average. The fuselage's slight geometry eccentricity likely decreased the section's stiffness enough to cause resonance. A fast-Fourier transform was performed on the acceleration pulses, in order to identify any obvious resonance occurring. This, however, did not yield any meaningful results.

Considering the overall trend, as expected, mean accelerations and DRI increase for increasing fuselage section eccentricity. While the main driver for the increase of the mean acceleration is the shortening of the time at which the maximum deformation point occurs, this is not just the case for the DRI. As observed, a larger rebound occurs for highly eccentric fuselage sections. This implies that, in practice, the acceleration pulse felt by the occupants is not limited to the time frame between the beginning of the crash event and the maximum deformation point, but it gets extended up until the point where the kinetic energy hits a local maximum, as the release of elastic energy throws the fuselage section back up. A larger spring back will create a further acceleration pulse, which will thus increase the measured DRI.

Additionally, the section for which $e = 0.4$ seems to be an outlier, with significantly higher mean accelerations, DRI, and shorter maximum deformation time (as shown in Figure 5.3), compared to neighboring configurations ($e = 0.0$ and $e = 0.2$). This was an unexpected, yet logical result. As mentioned, for larger fuselage eccentricity values, the distance between the floor keel beams decreases, and so will the length of the floor struts. A shorter floor strut will, however, have a higher Euler buckling load [49]:

$$P_{\mathrm{CR}} = \frac{n^2 \pi^2 EI}{\ell^2} \tag{5.1}$$

where n is the number of half-waves of the buckled shape that depends on the geometry and enforced boundary conditions; E and I are respectively the material's elastic modulus and the section's second moment of area; and ℓ the strut length.

As long as the strut deformation is fully elastic, the kinetic energy has to be absorbed elsewhere, and the crushable length is effectively decreased. For $e < 0.4$ no Euler buckling of the floor struts is present (at

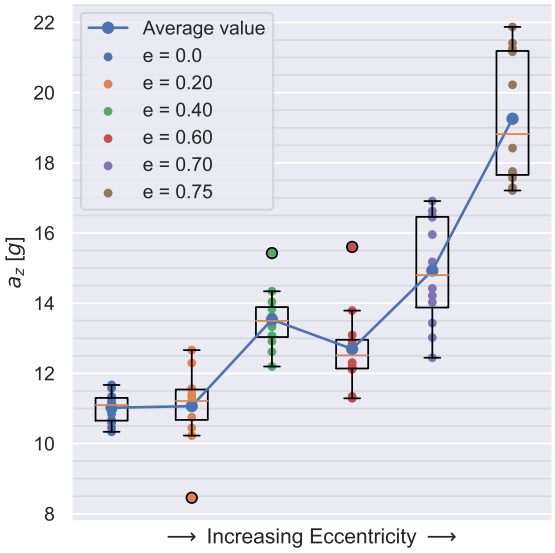

Figure 5.4: Mean acceleration determined for different fuselage section geometric eccentricity.

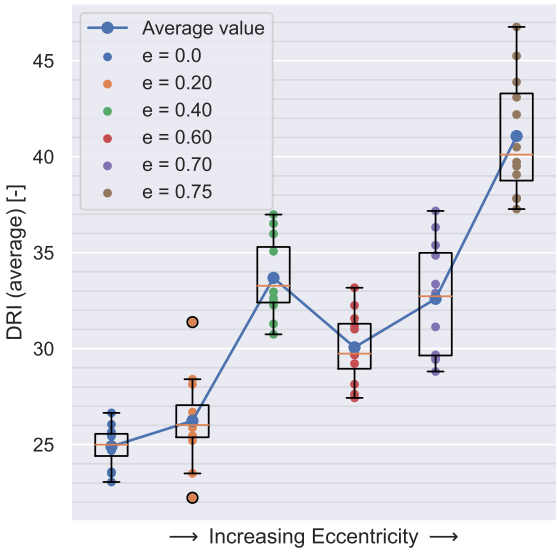

Figure 5.5: DRIs for different fuselage section geometric eccentricity.

most, local buckling due to the deforming frames pulling on the connection between the frames and the floor struts), and, thus, the crushing of the fuselage section is less progressive. For $e = [0.6, 0.7, 0.75]$; finally, the floor struts buckle and are able to also act as energy absorbers, while in configurations $e = [0.0, 0.2, 0.4]$ the main role is the triggering of the frames' plastic hinges.

An important consideration to be made is that, for increasing fuselage eccentricity, there will be a larger difference between accelerations and DRIs measured inboard and outboard. For increasing eccentricities, inboard occupants seating in the considered fuselage section will experience higher acceleration pulses than the outboard ones. This is likely due to the up-folding frames clashing with the floor structure, inducing a sudden stop that is more greatly felt by the occupants sitting closer to the collision.

Lastly, note that the average DRI for the non-eccentric original F-28 section is 25 units, which is significantly above what a certification authority would deem acceptable. There are two main reasons for the high DRI herein observed: 1) the accelerations are measured at floor level, while in a real scenario the seat compliance attenuates the impact loads; 2) the vertical impact velocity used was of $9.14\,\mathrm{m\,s^{-1}}$, which is considerably above what aircraft of similar MTOW would be able to withstand, as shown by Figure 2.1. Regarding seat attenuation, for the FV typical section design this will be solved, as also explained later on, by treating passenger and seat mass as a single $100\,\mathrm{kg}$ point mass, coupled using a flexible tie to the floor structure (seat model). Considering the above, then the results obtained are reasonable and expected.

Energy Absorption Distribution by Component

The plastic energy absorption fraction, by component, is shown in Figure 5.6. The total energies are, in turn, tabulated in Table 5.1.

First and foremost, it is clear how more eccentric sections are less able to absorb energy: 12.9% fewer energy is dissipated by configuration with $e = 0.75$, compared to $e = 0.0$.

Secondly, due to the oval shape, the rotation of the plastic hinge present in the frames will be reduced and, thus, the energy absorbed by the frames and shear clips will decrease (- 19.7% for $e = 0.75$, compared to the baseline, $e = 0.0$, in absolute terms). In turn, more load is transferred to the floor struts, which, consequently, buckle and are able to absorb a significantly larger amount of energy (+61%).

Thirdly, energy dissipated thru friction force also decreases. One large source of friction dissipation

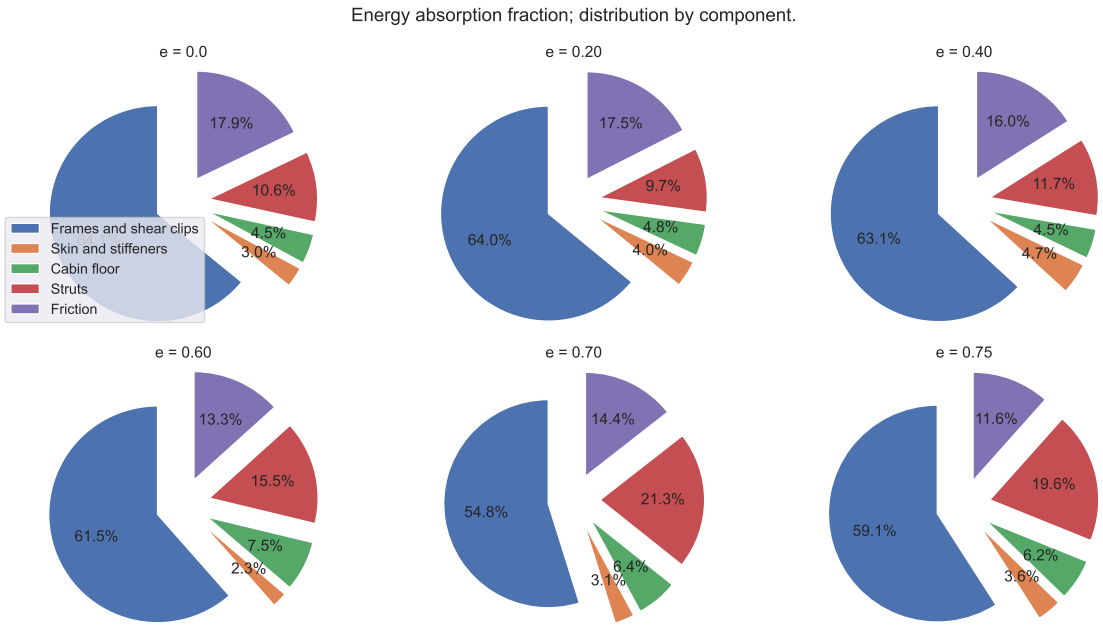

Figure 5.6: Energy fraction absorbed by each component, for different fuselage section geometric eccentricity.

Table 5.1: Energy dissipated, by component, for different geometric fuselage eccentricities. Note, the values of the components might not add up to the total energy dissipated, due to rounding errors.

Energy dissipated	$e = 0.0$	$e = 0.2$	$e = 0.4$	$e = 0.6$	$e = 0.7$	$e = 0.75$
Initial K_{eg} [kJ]	50.35	50.27	50.06	50.6	50.65	50.53
Plastic energy dissipated [kJ]	41.91	40.37	39.95	41.41	40.34	39.32
- Frames [kJ]	19.60	17.87	16.91	16.74	14.57	14.01
- Shear clips [kJ]	13.11	13.46	13.13	12.61	11.27	12.26
- Floor struts [kJ]	5.39	4.73	5.57	7.40	10.05	8.70
- Cabin floor [kJ]	2.27	2.37	2.12	3.58	3.01	2.74
- Skin and stiffeners [kJ]	1.54	1.94	2.22	1.08	1.44	1.62
Friction [kJ]	9.12	8.56	7.61	6.34	6.80	5.14

is the sliding of the fuselage skin on the ground, during the creation of the plastic hinge. For more eccentric sections, the rotation of the plastic hinge is limited, and thus less energy will be dissipated by friction forces.

Lastly, some minor variations are observed with respect to the energy absorbed by skin, stiffeners, and cabin floor, which together account for approximately 8-10% of the total absorbed energy. One reason for the increase in energy absorbed by the cabin floor is the impact of the up-folding frames against the floor beams, which is more significant when the distance between the floor beams and the keel is reduced. In turn, the variations in skin and stiffener energy absorption during up-folding are due to whether or not the stiffener flanges get crushed by the deforming frames and shear clips. This effect is however depended on small positional variations of the stiffeners when the fuselage geometry changes, thus not directly predictable, but also marginal, and therefore will not be further analyzed.

5.3.3. Vertical Floor Location

This subsection discusses the results of the parametric study on the floor beams' vertical placement. As mentioned in subsection 5.3.1, four different criteria are used for comparison: visual inspection, kinetic energy, accelerations, and energy absorption distribution, by component.

Visual Inspection of the Crash Sections

A visual comparison of the four analyzed crash sections is provided in Figure 5.7.

From visual inspection it is clear that for very low floor beam configurations the crushable volume is not sufficient to fully absorb the impact. One of the driving energy-absorbing mechanisms is the collision between the up-folding frames and the above passenger floor structure. Once the frames run out of space to deform, the floor struts get compressed and buckle, entering a post-buckled state. Yet, this is not enough to fully absorb the impact. Thus, the up-folded frames are compressed between the solid ground and the passenger floor structure, causing a flattening behavior. The frames thus absorb the remaining energy in this flattening deformation mode. Since the shear clips are more compliant with respect to the frames, during the flattening phase, they will be absorbing the energy. For increased floor beam heights, the overall frame up-folding also increases, up until the frames, once again, collide against the floor structure.

Kinetic Energy Time History

The kinetic energy time history plot is provided in Figure 5.8.

As expected, for lower floor configurations, $\dot{K}_{eg}$ increases, as a result of the reduction in the crushable length. Regarding the maximum deformation point, two considerations need to be made. Firstly, for the lower floor beam configurations, the time at which the maximum deformation occurs is reduced. Secondly, the residual kinetic energy during maximum deformation is considerably smaller than for $h = 600$mm and $h = 650$mm. The reason for this is the collision of the up-folding frames against the passenger floor structure: while in high-floor configurations, the floor beams are allowed to bend downwards, thus the dummy masses will still have a small residual velocity, also during the maximum deformation point, this is no longer true for low-floor configurations, as the floor structure is essentially being stopped by the rigid ground below the frames.

Lastly, it is clear how low-floor configurations will have a larger rebound, which is expected: due to the decrease in crushable volume, more energy is stored as elastic energy within the deforming structural components; this energy is then released as kinetic energy during rebound.

Mean Accelerations and DRIs

The mean accelerations measured during the impact (from $t = 0$s up until the maximum deformation point), and the DRIs, at different floor locations, are presented in Figure 5.9 and Figure 5.10 respectively.

As expected, data shows a close correlation between the measured acceleration pulses and the vertical floor beams location. For more extreme configurations ($h = [500, 550, 600]$mm, the reduction in occupants loads is more significant, when the floor beam is raised. Once again, a difference in response can be observed between the determined mean accelerations and the corresponding DRIs. Considering the extremely short duration of the crash event (between 45 ms and between 60 ms), it

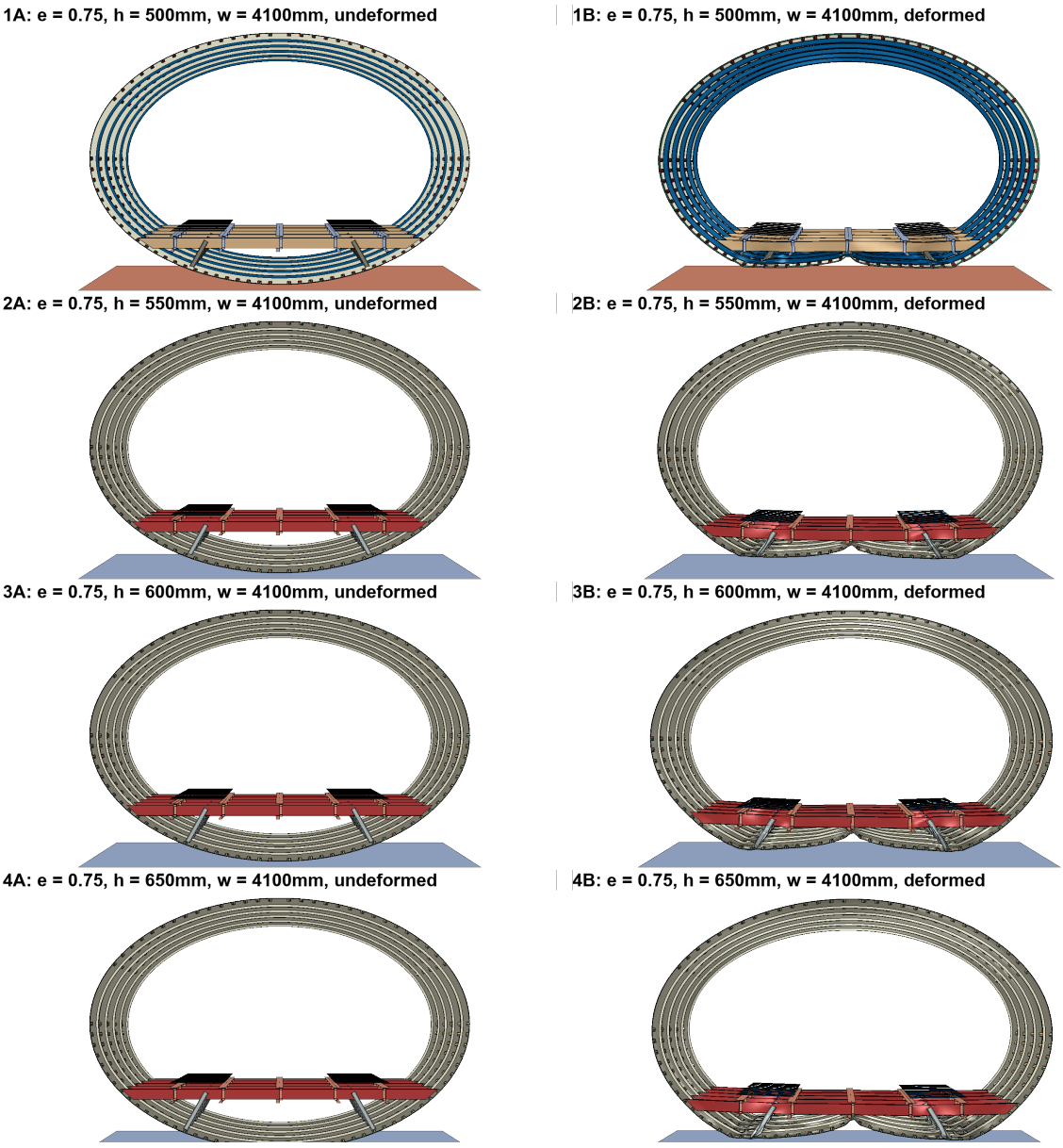

Figure 5.7: Comparison between the deformed F28 crash sections for different floor beam heights, as measured from the bottom-most point of the keel. From image number 1 to 4, respectively, $h = [500, 550, 650, 650]$mm.

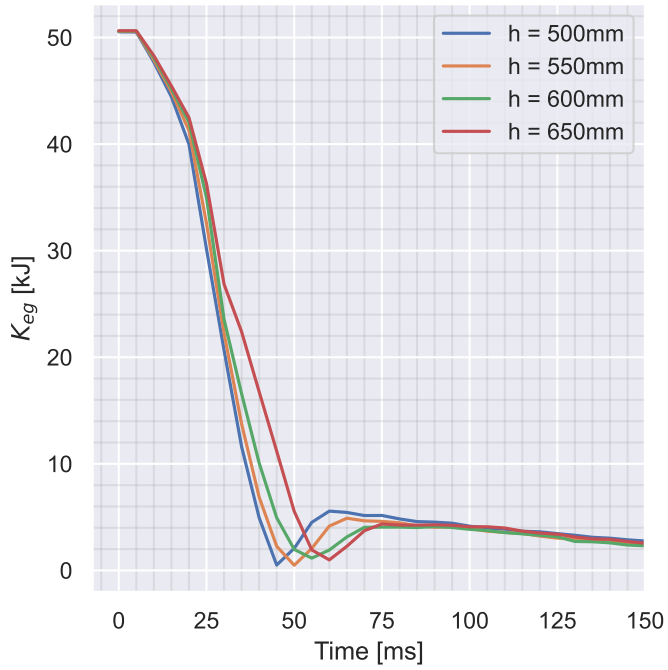

Figure 5.8: Model kinetic energy vs. time; different lines indicate different floor beam heights.

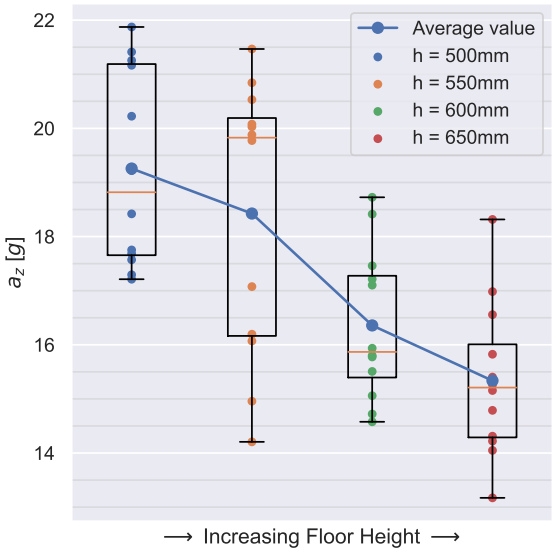

Figure 5.9: Mean acceleration determined for different floor beam heights.

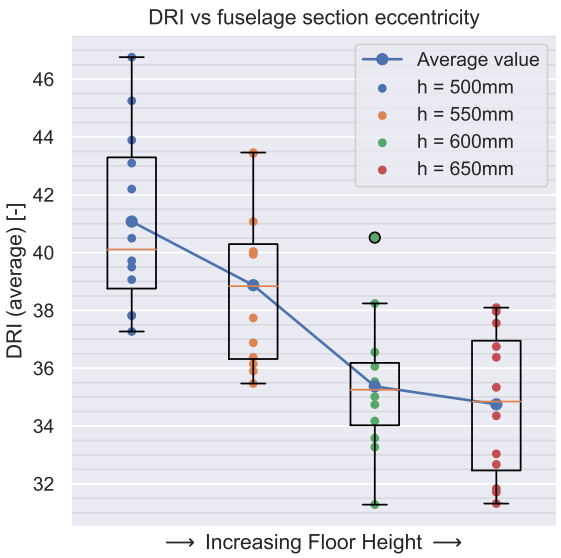

Figure 5.10: DRIs for different floor beam heights.

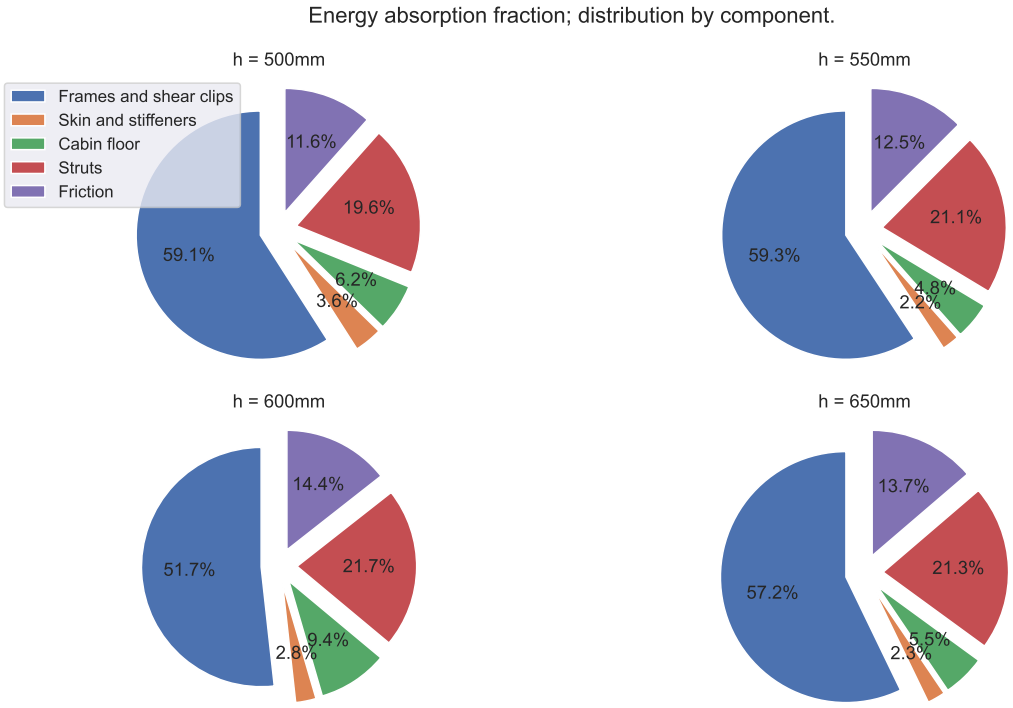

Figure 5.11: Energy fraction absorbed by each component, for different floor beam heights.

Table 5.2: The energy dissipated, by component, for different passenger floor beam heights. Note, the values of the components might not add up to the total energy dissipated, due to rounding errors.

Energy dissipated	$h = 500$mm	$h = 550$mm	$h = 600$mm	$h = 650$mm
Initial K_{eg} [kJ]	50.53	50.57	50.60	50.63
Plastic energy dissipated [kJ]	39.32	39.57	39.29	39.61
- Frames [kJ]	14.01	15.23	13.37	14.71
- Shear clips [kJ]	12.26	11.58	10.39	11.54
- Floor struts [kJ]	8.70	9.55	9.94	9.78
- Passenger floor [kJ]	2.74	2.19	4.33	2.52
- Skin and stiffeners [kJ]	1.62	1.03	1.27	1.06
Friction [kJ]	5.14	5.65	6.61	6.30

is likely that the larger acceleration pulse lacks the time to in fact cause an equally large response in the spring-damper-mass system representing the occupants. Once again, accelerations and DRIs are measured considering the nodal accelerations of the dummy masses, and, thus, are real occupant loads are overestimated.

Energy Absorption Distribution by Component

The plastic energy absorption fraction, by component, is shown in Figure 5.11. The total energies are, in turn, tabulated in Table 5.2.

The table indicates that, overall, the amount of energy dissipated is approximately constant throughout the four sections, with a few small variations depending on where, overall, the energy is lost.

First of all, for increasing floor beam heights, frictional energy dissipation increases; in general, energy is dissipated via friction, mainly, thru the scrubbing of the fuselage skin on the ground during frame up-folding. For lower floor configurations, as mentioned earlier in this subsection, up-folding motion is restricted and, therefore, so will frictional energy dissipation. In turn, however, more energy is absorbed by the floor structure itself, due to the harder impact of the frames on the floor itself.

Second, and lastly, configuration $h = 600$mm is an outlier regarding the amount of energy absorbed from frames and shear clips. Likely, this floor height is a transition zone between the previous configuration $h = 550$mm, where a part of the energy absorbed by the frames is due to the flattening after up-folding, and the successive one, $h = 650$mm, where, in turn, the plastic hinge located below the floor struts is allowed to rotate more, and, thus, absorb more energy. As a consequence, in configuration $h = 500$mm and $h = 600$mm, when the up-folding frames impact the floor structure, they do not carry enough momentum to cause significant damage, and, thus the successive flattening is the energy-absorbing driving mechanism. On the contrary, in configuration $h = 600$mm, when the impact between the frames and the floor structure occurs, significant plastic deformation is created on the latter and, thus, more energy is absorbed by the floor structure. This is evident in Table 5.2 and Figure 5.11.

5.4. Discussion on the Results

The results of the simulations show a large sensitivity of the fuselage section crash characteristics with respect to both eccentricity and vertical floor location. Fuselage sections with large eccentricities will limit the rotation of the plastic hinge created at the intersection between the floor struts and the frames, thus, causing the frames to absorb less energy. For the same reason, also less energy will be dissipated thru friction, since, most of the frictional energy derives from the scrubbing of the skin against the ground. With the limited rotation of the frames, less scrubbing will be present and, subsequently, less energy losses due to friction. These losses are thus compensated by the floor struts, as, at the time they impact the ground, the fuselage section has decelerated less and is thus carrying more momentum. Considering the above, with regards to the FV fuselage section, it is advisable to have a shallow angle between the floor struts and the frames, with the reason being that, once the floor struts hit the ground, it is likely that the fuselage section will still have a relatively large vertical velocity. With floor struts kept vertically the loads will be directly transferred to the passengers, thus increasing the likelihood of spinal injury. If the angle is instead kept shallow, the load introduced in the floor struts will be mainly transferred to the floor beams, horizontally, while energy is still dissipated, thus reducing the accelerations experienced by the passengers. Furthermore, it is advised to explore the possibility of having a flexible floor beam: the section eccentricity of the FV aircraft is an already fixed parameter. However, the impact time can be increased if a flexible floor beam is used. This will lower the accelerations experienced by the occupants.

Regarding the floor beam vertical placement, data from the sensitivity analysis shows that even increments as little as 50 mm will make a difference by significantly reducing the DRI determined. Based on this, the FV design recommendation is to increment the floor height as much as possible, which would be beneficial for two reasons: 1) the impact time duration is incremented, and, thus, average accelerations experienced by passengers are reduced in magnitude; 2) the crushable volume is increased, enhancing the energy-absorbing capabilities and, thus, reduce the post-crash rebound.

This page intentionally left blank.

IV

Flying-V Typical Section

This page intentionally left blank.

6

Flying-V Typical Section Model Set-Up

This chapter provides an overview of the modeling methodology, assumptions, and simplifications employed to generate a non-linear, dynamic explicit finite element model of the FV aircraft. First, in section 6.1, an overview of the current design status of the FV's wing-fuselage typical section is given. Secondly, section 6.2, documents the simplifications and modeling assumptions that have been applied to the existing typical section, to get to the model used in this research. Lastly, section 6.3 provides a detailed description of the developed finite element model.

6.1. Existing Design of the FV Fuselage Section

Over the past few years, a significant research effort has undergone in preliminary, high-level design of the FV aircraft[1]. From an airframe perspective, the most relevant and up-to-date work is from Dotman [50], where a structural sizing methodology for wing-fuselage of the FV is developed, and applied for two structural concepts: an oval cabin concept, shown in Figure 6.1a, and a no-leading edge spar concept (NLES), depicted in Figure 6.1b.The NLES concept is the chosen one for the FV aircraft, with one of the reasons being the increase in cabin space compared to the two-spar (oval cabin) one.

In Dotman's research, all structural members depicted in Figure 6.1b have been sized. For each member, a cross-section shape has first been defined and, successively, the thickness and beam cross-section height (referred to as frames height by Dotman) were treated as design variables. The distributions are shown in Figure 6.2 and Figure 6.3, respectively. Most importantly, the driving load case for the sizing of the frames was seen to be fuselage pressurization, due to the oval shape of the wing-fuselage, which, due to the pressurization, tends to become circular, and the frames need to be sufficiently stiff and strong such that the shape is preserved (Dotman's work focused on strength and did not consider compliance).

Additionally, the figures show how, following Dotman's sizing, all the dimensions of the structural members have been fixed, thus, in principle, leaving little to no space to design for crashworthiness. Ideally,

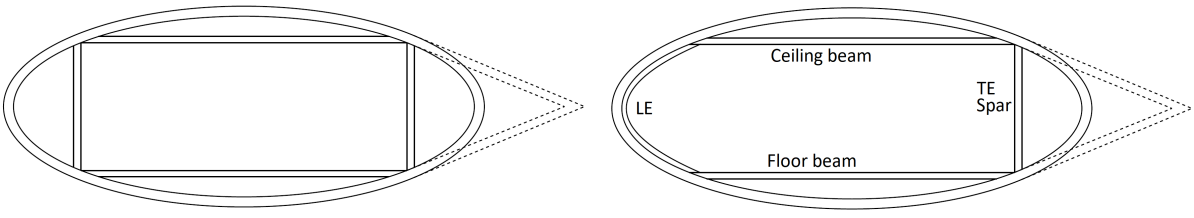

(a) Oval cabin structural concept [50].

(b) NLES structural concept, adapted from [50].

Figure 6.1: Structural concepts for the FV aircraft wing-fuselage.

[1] https://repository.tudelft.nl/islandora/search/Flying-V?collection=education&f%5B0%5D=mods_subject_topic_ss%3A%22Flying%5C%20V%22. Accessed on 27-Dec.2022.

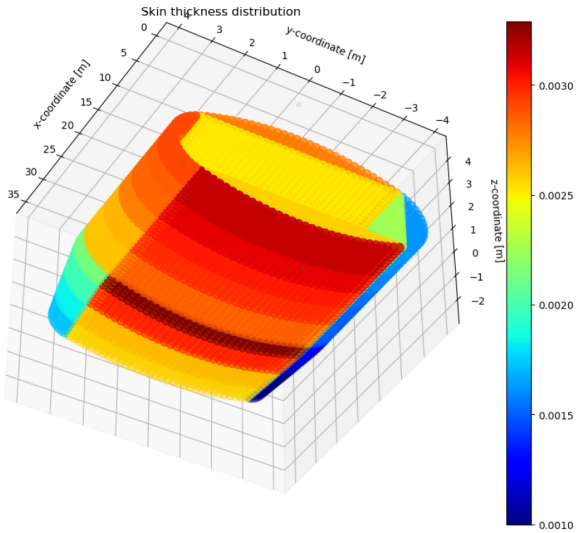

Figure 6.2: NLES concept, skin thickness distribution [50].

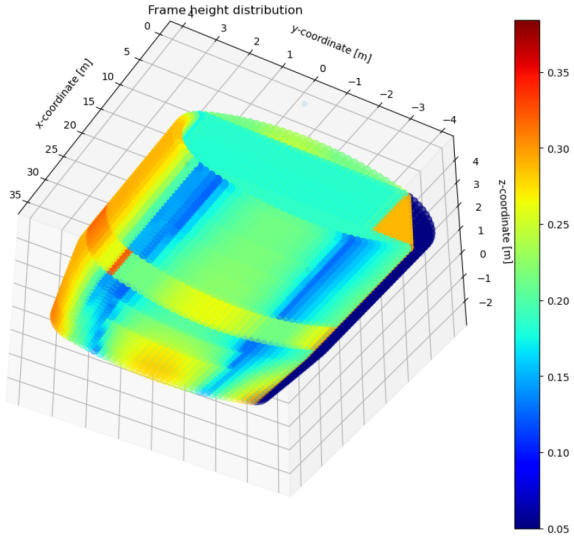

Figure 6.3: NLES concept, beams cross-section height distribution [50].

airframe sizing and crash analysis would be coupled within a single analysis, in order to generate a design able to optimally fulfill both requirements. However, this would require a significant effort, the time for which was not available. As such, in the context of this research, it has been decided to relax the constraints relative to the floor vertical location and beam sizing, which, among others, are going to be design variables. The impact of this relaxation on the overall airframe stiffness and strength is however unknown. Overall, however, an increase in frames stiffness is hypothesized to be required (with the former being more likely than the latter): Dotman has observed that pressurization induces a compressive load in the floor beams, thus, an increase in frames height or thickness would be required to compensate for the loss of the floor beams' stiffness. This last statement is written with the after-thought that, as it will be shown later, a more flexible floor beam is beneficial for crashworthiness.

6.2. Fuselage Typical Section Representation

As evident from section 6.1, Dotman's work aims to highly optimize the FV airframe. While fuselage skin panels are kept at a constant thickness across different bays, the same is not true for beam thicknesses, where a constant ratio of 33 units is maintained between the cross-section height and thickness [50]. As shown in Figure 6.3, the beams cross-section height is a design variable; this results in variable-thickness frames.

The conventional approach for the manufacturing of fuselage frames for typical cross-sections is by means of sheet metal forming (as can be observed, for instance, in the F28 aircraft), which, consequently, would require constant-thickness frames. For the FV, likely, a similar approach would be optimal: for serial production, sheet metal forming is typically significantly cheaper than machining. This choice would be further justified if one considers that the frames constituting the airframe of the typical section will be a repeatedly used component. The FV aircraft is designed to fulfill the same mission as the Airbus A350 and Boeing 787 airliners. To this day, cumulative orders and deliveries of such aircraft are in the order of $4,000$ units and counting[2,3]. Using this number as a baseline, and considering that the length of the FV's wing-fuselage constant section ranges between 18 m and 28 m, depending on the variant, as found by Oosterom [1], and assuming a constant frames pitch of 0.65 m [50], then, the total number of repeated fuselage frames to be manufactured can be estimated in the range of $100,000$ to $170,000$, for half-wing, although this number is likely an overestimate since commonality would also come with a weight penalty (thus, a compromise would need to be reached). Considering the above, the choice to opt for sheet metal forming rather than machining would be fully justified. Thus,

[2] `https://www.airbus.com/en/products-services/commercial-aircraft/market/orders-and-deliveries`. Accessed on 27-Dec.2022.
[3] `https://www.boeing.com/commercial/#/orders-deliveries`. Accessed on 27-Dec.-2022.

in the context of this research, all components of the airframe will be modeled with constant thickness sections.

Another significant simplification in this research, which is also a consequence of frames' sheet metal forming production process, will be to keep the frame height constant. This simplification has been made with a conservative strategy in mind. The defined frames height, of 200 mm, is a value that is slightly lower than the maximum defined frame height at the keel of the wing-fuselage, ≈ 225 mm, as shown in Figure 6.3, but higher than the minimum value achieved, which occurs at the outer part of the keel, and is equal to approximately 150 mm.

Additionally, the ceiling beam has not been included in the analysis, in an attempt to limit the model size, as its effect on the crash behavior has been deemed negligible. This would be generally true for conventional fuselages, where all deformations occur in the lower half of the fuselage section, and the same is expected to happen for the FV aircraft. This starting assumption will be shown to be correct, as little deformation will take place in the upper half of the fuselage section.

Lastly, passenger seats and masses will be represented by point inertia coupled to the passenger floor structure.

6.3. Finite Element Model

The FEM for the FV aircraft has been built using the 3DX platform, in order to couple CAD and FE models. The analysis is solved using Abaqus/Explicit, using TU Delft's cluster computer. The workflow used to pre-process, execute, and post-process all the simulations is shown in Figure 6.4.

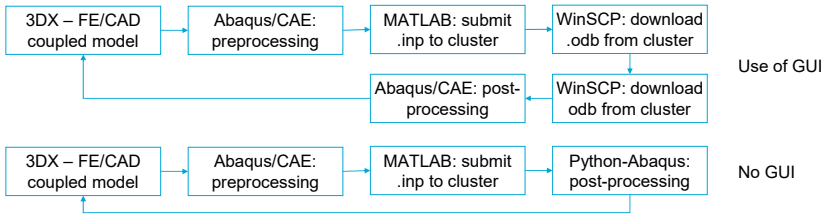

Figure 6.4: Flow chart indicating the steps followed to pre-process, execute and post-process the crash simulations.

In general, for validation purposes, as already mentioned in chapter 4, the modeling techniques employed in this analysis will be identical to those used for the F-28 fuselage section. The main and only difference between the two will be regarding passengers' dummy weights representation: while in the F-28 section they are represented by means of steel bars tied to the floor structure, in this case, passenger and seat mass are modeled by means of point inertia connected to the floor structure using a flexible coupling; this will avoid overly conservative estimates of the DRI.

A general view of the finite element model (HB-5 concept) is presented in Figure 6.5.

6.3.1. CAD Model

3D views of the CAD model of the FV fuselage section are shown in Figure 6.5. The CAD model includes frames, wing spar, skin, floor beams, and floor supporting structures. To limit the finite element model size, the following simplifications have been made:

- The stiffeners are excluded from the analysis, since, as also shown in chapter 4, they are not expected to significantly affect the crash characteristics of the FV in the first place. The mouse holes in the frames are however included;
- The analyzed section is a five-frame one: as shown in chapter 4, there is little to no difference between a five and six-frames section, which is generally used for certification purposes;

Lastly, it is worth noting that the structural concept for the trailing edge spar structure has changed since Dotman's research, and currently consists of a single, machined, orthogrid structure, the sizing of which has not yet been performed. Consequently, in the current research, orthogrid stiffener spacing, height, and thickness, as well as the orthogrid skin thickness values have been assumed such that little to no

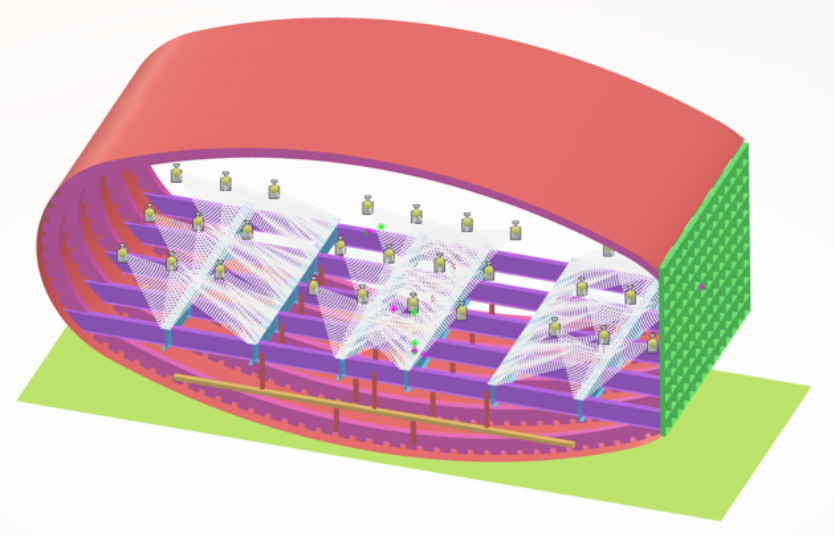

Figure 6.5: View of the FEM of the FV aircraft; HB-5 concept. Different colors are qualitatively representative of different section assignments.

plastic deformation will occur in the wing spar. This has resulted in orthogrid skin thickness of 3 mm, a stiffener spacing of 200mm, and stiffener height and thickness of 30mm and 3mm, respectively.

6.3.2. Section Assignment & Element Size

Similarly to the FEM of the F-28 section, the mesh is quad-dominated and makes use of S4 elements (first order shell); thickness assignments and global general element sizes are shown in Table 6.1. The components nomenclature is further clarified in Figure 7.1b to Figure 7.3.

Table 6.1: General element sizes for different structural components. The notation 'var' indicates that the thickness assignment is a design variable.

Item	Elem. size [mm]	Thick. [mm]	Item	Elem. size [mm]	Thick. [mm]
Skin	60	2	Ground	200	3
Frames	20	5.7	Floor beams	30	var
Floor long. beams	20	2	Floor struts	10	var
Spar skin	20	3	Horiz. beams	10	var
Spar stiffeners	20	3	Vert. struts	10	var

The floor beam is modeled as an I-beam. The beam height is of 230 mm, which is higher than Dotman's estimate (≈180 mm) [50]. In Dotman's work, however, passenger mass is linearly distributed along the floor beam, which would, in fact, underestimate the internal bending moment. Furthermore, crash loads are likely to be decisive when it comes to floor beam sizing. Thus, it has been decided to increase the beam height. The thickness is treated as a variable anyway, thus, the flexural rigidity can be changed accordingly. Lastly, the web height-to-flange width ratio has been set to 3, as it is a typical ratio for standard I-beam profiles[4].

6.3.3. Material Assignment

The material assignment, consists of 2024-T3 aluminum alloy; material selection for the FV airframe has already been performed by Dotman [50], and, thus, is outside the scope of this research.

The material model employed is the elastic-plastic JC damage, which is thoroughly described in subsection 4.3.2. Similarly, the used material properties are presented in Table 4.3.

[4] https://amesweb.info/Profiles/Standard-Steel-I-Beam-Sizes-Chart.aspx. Accessed on 08-Jan.2023.

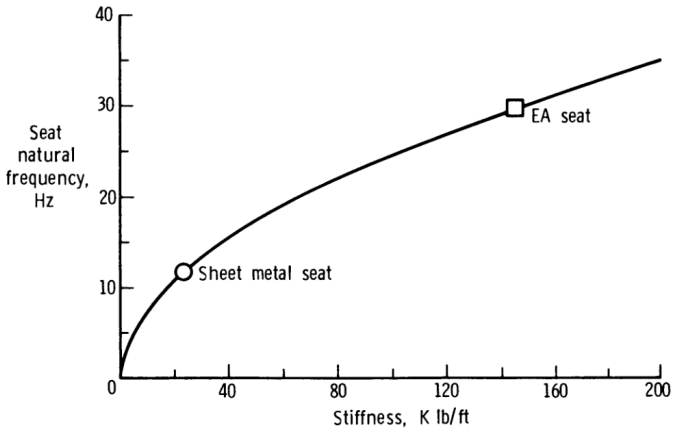

Figure 6.6: General aviation aircraft seat stiffness versus natural frequency [52].

6.3.4. Interactions and Contact Properties

The chosen interaction and contact properties are the same as for the F-28 fuselage:

- All joints represented by means of tie constraints;
- General contact interaction property to avoid element penetration: normal behavior is hard contact, tangential behavior uses a penalty friction formulation, with $k_f = 0.5$, with k_f being the friction coefficient.

6.3.5. Passenger and Seat Model

The assumed mass of a single passenger is of the 95th percentile male, equal to approximately 90 kg [51]. Additionally, further 10 kg have been allocated to account for the seat mass[5]. The total mass of the passenger and seat system is thus of 100 kg, and, in the FEA, has been modeled as a point inertia.

As mentioned, the seat is modeled by means of a flexible coupling with the floor structure, as shown in Figure 6.5. Reference values in the literature on the stiffness of airliner seats were not readily available; the opposite is true for general aviation (GA) ones. According to Alfaro-Bou et al. [52], as shown in Figure 6.6, GA aircraft typical seats have a stiffness of approximately 365 N/mm. Alfaro-Bou et al. then proceeded to prototype an energy-absorbing (EA) seat, which resulted in an associated stiffness increase up to 2200 N/mm. The reason for this is the requirement, for a crashworthy seat, to have constant crushing force. Consequently, the overall stiffness of the seat needs to be higher in order to reach the predetermined crushing force quickly.

GA aviation seats are expected to be more compliant than commercial aviation (CA) ones, considering the larger vertical speeds and thus accelerations that occur during the landing phase of CA aircraft. Consequently, the chosen spring constant in the FEM used to model the seat has been of 3924 N/mm, which is approximately a factor of 11 stiffer than GA sheet-metal seats. The associated seat deformation if a male, adult passenger was to sit on such a seat, would be a fraction of a millimeter. Thus, overall, this estimate is reasonable. The vertical distance between the point mass and the floor beams has been set to approximately coincide with the location of the lumbar region of a seated passenger.

Lastly, it is worth noticing that, opposite to what had been hypothesized, later in this report, data will show that the effect of implementation of a flexible coupling to model the stiffness of the seat, will have a small effect on the DRI. The reason for this is that no damping factor is included in such a model; as a consequence, all the energy stored in the spring will be restituted back to the passenger. Effectively, the spring has been seen to be acting as a filter, removing high-frequency, high-amplitude acceleration components, in favor of low-frequency, low-magnitude ones. In fact, DRIs measured with the seat being modeled as a flexible coupling are slightly higher than those when the seat is infinitely stiff, at times. The reason for this is that, with infinite seat stiffness, no elastic energy can be stored by the seat

[5] `https://www.recaro-as.com/en/aircraft-seats/economy-class/sl3510.html`. Accessed on 28-Dec.-2022.

model; as a consequence, more plastic energy is absorbed by the structure, and, thus, restituted to the passenger during the rebound phase. This is clearly shown by Figure 7.6, where the DRI is plotted versus the total dissipated energy for the 4S concept configurations. The only difference between 4S-4 and 4S-5 is the inclusion, in 4S-5, of compliance in the coupling between the point mass and the floor structure.

7

Flying-V Typical Section Conceptual Design

This chapter provides an overview of the conceptual design process used to develop a crash concept for the FV aircraft. Firstly, the crash concepts herein developed are presented in section 7.1. Secondly, during the design phase, each of the concepts presented in the aforementioned phase are revisited successive attempts to achieve acceptable DRI values. The geometric variables considered for each concept are outlined in section 7.2. Thirdly, the evolution of the concepts following the variation of the geometric variables are presented in section 7.3. Subsequently, a high-level comparison of the performance of all the analyzed sections are given in section 7.4, followed by an in-depth analysis of each crash concept given in subsection 7.5.1 to subsection 7.5.4. It is worth noting that, for each crash concept, only the best version in terms of DRI is analyzed. Lastly, a discussion on the results follows in section 7.6.

7.1. Concepts Definition

As shown in Figure 4.3, in conventional aircraft configurations, fuselage floor beams are supported by floor struts that connect the beams themselves to the fuselage keel. During nominal operations, these struts stiffen the floor structure; during a crash, instead, the floor struts buckle and plastically deform, in addition to inducing the creation of plastic hinges nearby their attachment point on the frames.

In the first two defined concepts, the floor structure is supported in a similar manner. The difference between the two concepts consists on the number of floor struts present: six and four, as it is not clear whether it would be beneficial to have a larger number of more flexible floor struts or a smaller number of stiffer ones. For the sake of convenience, these two concepts hereinafter will be referred to as ‘6S’ and ‘4S’, and are depicted in Figure 7.1a and Figure 7.1b, respectively.

The third concept consists of the addition of a horizontal beam below the floor structure, and replacement with some, or all oblique floor struts with multiple, more compliant, vertical ones, with a closed rectangular cross-section. Hereinafter, this concept will be referred to as ‘HB’; a generic section is in turn shown in Figure 7.2

The reason for the selection of this concept is an attempt to lower the peak load, which occurs during the initial stage of crushing. By using the horizontal beam, during the initial stages of the impact, part of the load is carried by the bending of the horizontal beam. Further on during the impact, as the horizontal beam deforms more, the loading mode is hypothesized to transition from bending to tension, which will result in an increase of the beam’s stiffness, thus causing a progressive increase of the crushing force.

This concept has been successively evolved in a two-layers hierarchical structure, as shown in Figure 7.3, herein referred to as the ‘HBH’ configuration.

The hypothesis behind the HBH configuration is that, when observing the results from the HB configu-

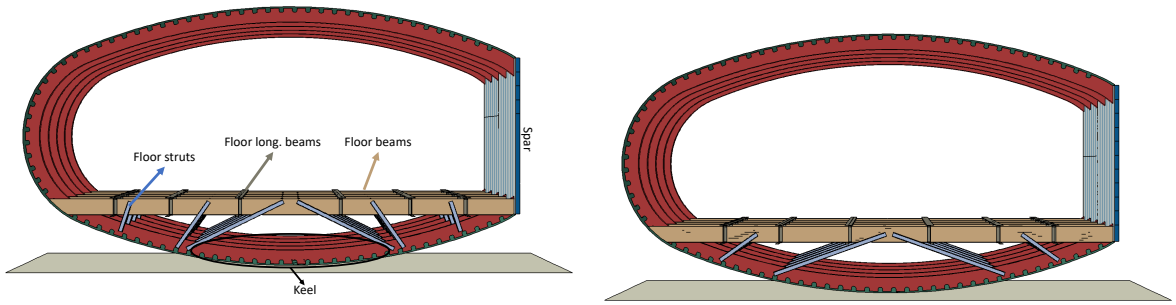

(a) Floor struts concept for a generic 6S configuration, including components nomenclature. Skin and frames have been left unlabeled for the sake of clarity.

(b) Floor struts concept for a generic 4S configuration.

Figure 7.1: Fuselage sections depicting 6S (left) and 4S (right) floor struts concepts. Across different concepts of the same family, the floor strut positioning (rotation and translation) is a design variable. Different colors are qualitatively indicative of different section assignments. Black striations in the image are due to rendering errors of Abaqus.

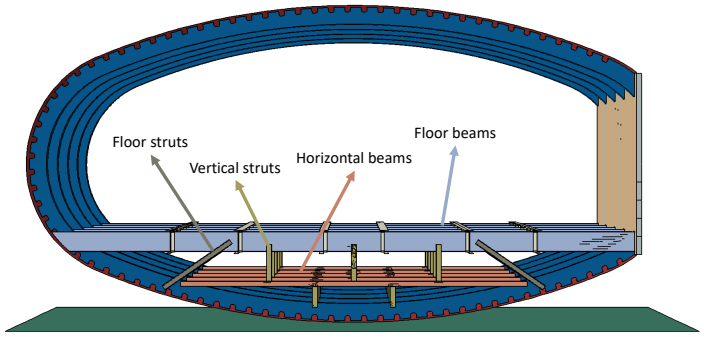

Figure 7.2: Fuselage section depicting the HB crash concept configuration, including components nomenclature. Vertical struts thickness and positioning, as well as the horizontal beam thickness and cross-section have been varied across variations of this concept. Different colors are qualitatively indicative of different section assignments. Black striations in the image are due to rendering errors from Abaqus.

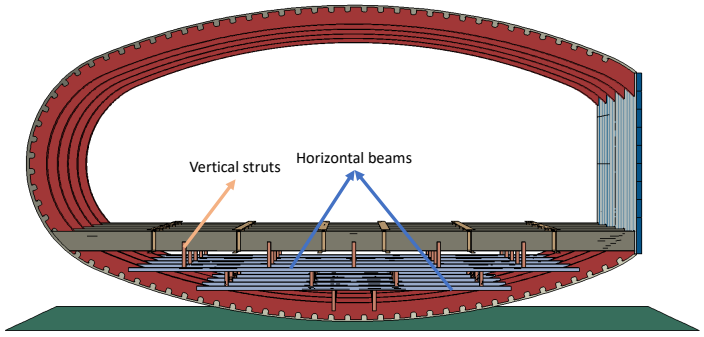

Figure 7.3: HBH concept configuration. The thickness and positioning of the vertical struts, as well we the cross-section and thickness of the horizontal beams have been treated as geometric variables. The nomenclature of all unlabeled components is similar to that of other crash concepts. Different colors are qualitatively indicative of different sections assignment. Black striations in the image are due to rendering errors from Abaqus.

ration, it was noted that the vertical struts, instead of being crushed, mainly failed due to Euler buckling instability; although the subsequent folding of the rectangular cross-section was still able to guarantee energy absorption, this was not the objective of the rectangular cross-section design. To solve this issue, it was decided to divide the vertical struts into two sections, in order to reduce their nominal length and, thus, increase the buckling load.

Additionally, from observation of the deformation of the 6S, 4S, and HB concepts, it became clear that achieving a plastic hinge on the frames to be challenging, with part of the reason for this also being the simplification of the structure to constant-height frames; consequently, it was decided to avoid trying to create the plastic hinges at all, but, rather, exploit the elastic deflection of the passenger floor beam as a mean to absorb the energy, by crushing the floor beam supporting structure.

7.2. Geometric Variables

This section provides an overview of the geometric variables used to get different variants for each of the crash concepts presented above. subsection 7.2.1 presents the geometric variables used in concepts 6S and 4S, followed by subsection 7.2.2 where the variables used in concepts HB and HBH are outlined.

Lastly, it is worth noting that the aim of the current work was not to solve an optimization problem; meaning that, all the geometric parameters have been manually modified following visual and numerical observations of the results. The development of a fully automated coupled CAD-FEM-solver model was deemed to be an extensive programming challenge, likely unfeasible within the considered time frame. This is however encouraged and part of the recommendations for future work, as it would allow for a structural optimization considering simultaneously airworthiness and crashworthiness requirements.

7.2.1. 6S and 4S Concepts

Regarding the 6S and 4S concepts, the geometric variables used to try to reach a working design have been the orientation and horizontal positioning for the floor struts, their thickness, and the floor beam thickness. The floor beam height has been increased as much as possible, while still preserving sufficient cabin volume, with additional margin, as shown in Figure 7.4.

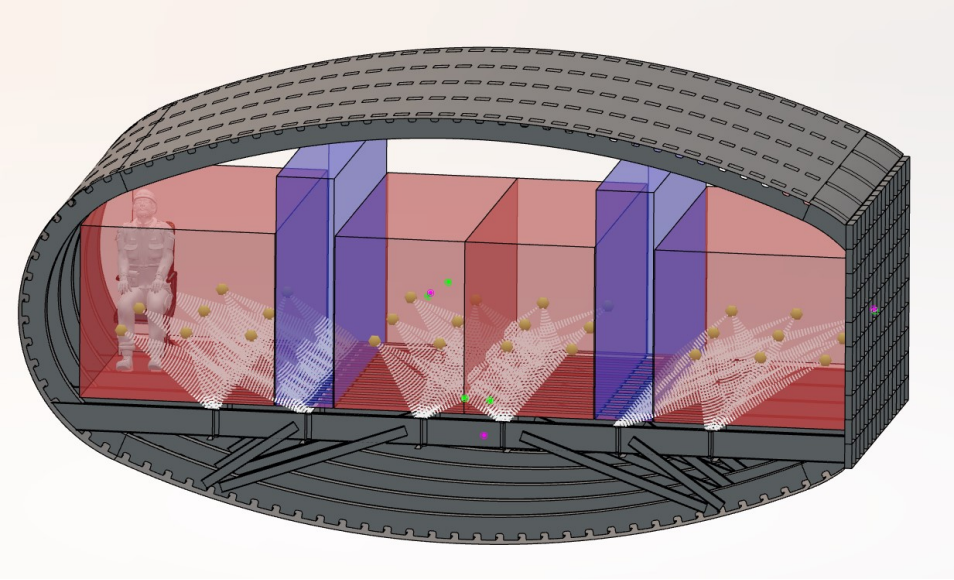

Figure 7.4: 3D view of the FV CAD model, including bounding boxes representing cabin space for passengers. Red boxes represent passenger seats, while the blue ones represent aisle space.

The floor struts cross-section is a C-section, with a web height of 60 mm, a flange-to-web ratio of $\frac{1}{2}$, and 5 mm double corners to improve crippling resistance. Thicknesses have been varied in increments of 0.5 mm, generally in the range of 1.5 mm to 3.0 mm. Floor beam thicknesses have also been varied in with 0.5 mm increments, in the range of 1.0 mm to 2.0 mm.

7.2.2. HB and HBH Concepts

The geometric variables for the HB and HBH concepts are the same, due to the similarity between the two, and consisted of the vertical struts' thickness and their positioning, and the thickness of the horizontal beams. The horizontal beam cross-section has also been tuned in an attempt to minimize out-of-plane bending, thus maximizing the crushing behavior. Regarding the oblique struts (when present), and floor beams, their thickness has been set to 1.5 mm, which, in 4S and 6S configurations, was consistently observed to be giving the best results. Thicknesses for the vertical struts have been tested for values of 0.5 mm and 0.75 mm, while those for the horizontal beam have assigned a value of 1.0 mm and 1.5 mm; the reason being that thinner wall for vertical struts will lower the peak crushing load.

7.3. Concepts Evolution

Once concepts have been defined, and the geometric variables established, each concept has been modified a number of times, in an attempt to minimize the DRI. The aim of this section is to thus document the evolution of each of the proposed concepts. Subsection 7.3.1 to subsection 7.3.4 will present the evolution of concepts 6S, 4S, HB and HBH, respectively.

7.3.1. 6S Concept

The 6S concept has been abandoned rather quickly in the initial stages of the design. The reason for this is evident from Figure 7.5. Overall, even if sufficient deformation of the passenger beam occurs, as well as some plastic deformation of the frames (as it will be also observed later on for the other concepts, the creation of the plastic hinge on the frames is hardly happening, across all configurations), the structure in the neighborhood of the frames, is already stiff by itself. Having additional stiffening elements there is not beneficial to reduce the acceleration loads of passenger seating on the outboard seats of the 3-4-3 seating configuration of the FV.

This is further confirmed from Figure 7.12 where, clearly, even if 6S configurations are able to absorb a decent amount of energy, the computed equivalent DRI is significantly larger than all other tested concepts.

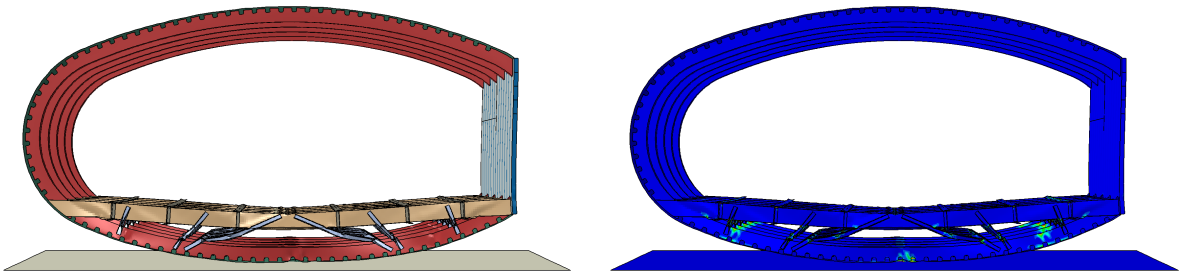

(a) 6S concept section, deformed.

(b) 6S concept section, equivalent plastic strain.

Figure 7.5: 6S section, post-crash. Both floor beam and struts thickness is of 1.5 mm. The outboard floor beam is hardly deforming, compared to the central part, due to the stiff triangular region composed by the outboard floor strut, the frame, and the floor beam.

Thus, concept 6S has been discarded in favor of 4S, where, additionally, the floor struts attachment on the frames can be brought closer together, in order to (attempt to) favor the creation of the aforementioned plastic hinge on the frames.

7.3.2. 4S Concept

The evolution of the 4S concept is shown in Figure 7.7 and Figure 7.8, where both the undeformed and deformed sections, for the best-performing variant for each concept (that with the lowest DRI), are represented.

Starting with 4S-1, which is the first evolution of the 4S concept, the main observations that can be

made from visual inspection of the post-crash section, in Figure 7.7, are that: 1) a plastic hinge is hardly achieved, and 2) the passenger floor beam is subjected to bending instability. The objective of the second iteration of this concept was thus to localize the load on the frames, favor the creation of the plastic hinge, and reduce the internal load of the passenger floor beam. This was meant to be achieved by bringing the floor struts closer together.

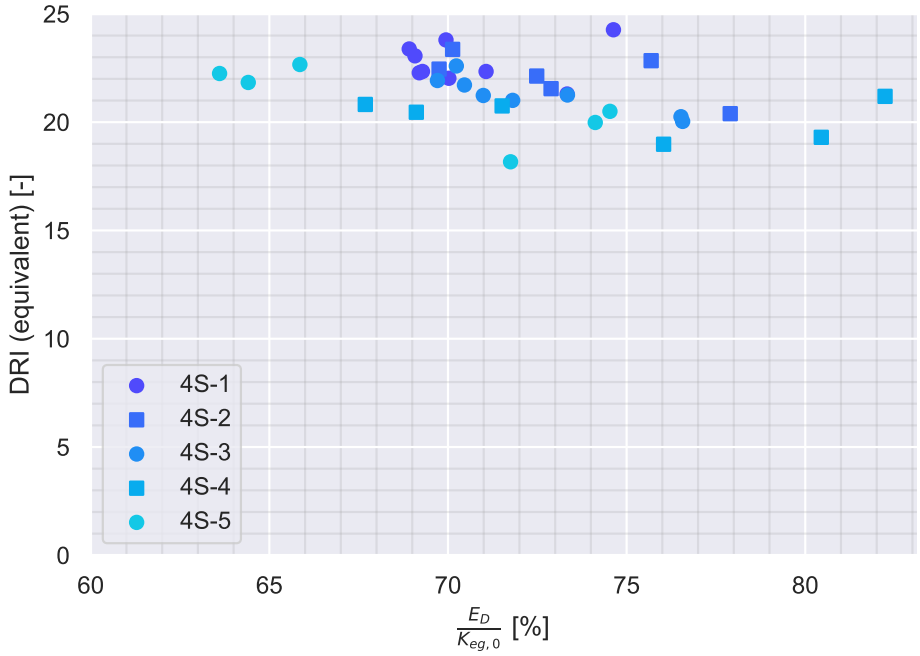

Figure 7.6: Equivalent DRI versus the dissipated energy normalized by the pre-impact kinetic energy, for all variants of the 4S concept. From the figure, it is clear that 4S-5 is the best-performing concept, in terms of DRI; additionally, in general, concepts that are able to absorb more energy, do also show a decrease in DRI.

The struts orientation has been successively made more shallow and centralized (4S-3), in order to further increase the load in the floor struts, and, thus, once again, increase the bending load in the frames. The difference between 4S-3 and 4S-4 is the raising of the floor structure by $100\,\text{mm}$. The expected effect of this was to 1) increase the floor beam length, and, thus, allowable deformation; 2) increase the length of the portion of the frame under the floor structure. This was expected to result in a further increase in energy absorption and a decrease in DRI. As shown from Figure 7.6, this indeed resulted to be the case.

Lastly, the coupling between point inertia and floor structure was made flexible, in order to model seat compliance as well. This is the only difference between 4S-4 and 4S-5. As clear from the data, this has a net effect of shifting the DRI vs. $\frac{E_D}{K_{eg,0}}$ to the left: the compliant coupling decreases the overall peak loads, however, it does not dissipate any additional energy (as expected, since it is fully elastic). On the contrary, the coupling momentarily stores energy, which, thus, will not be dissipated by means of plastic deformation.

7.3.3. HB Concept

As mentioned, the initial idea of the HB concept was to introduce a horizontal beam in order to achieve progressive crushing behavior. In the first iteration, other than the two oblique struts, a single, vertical strut was placed, connecting the center of the horizontal beam with the center of the floor structure. as shown by Figure 7.9, it became quickly evident that an unsupported horizontal beam would not be able to function as intended. The main observed drawback was the tendency of the horizontal beam to move toward the frame, as a result of the compression-induced secondary bending. Consequently, it

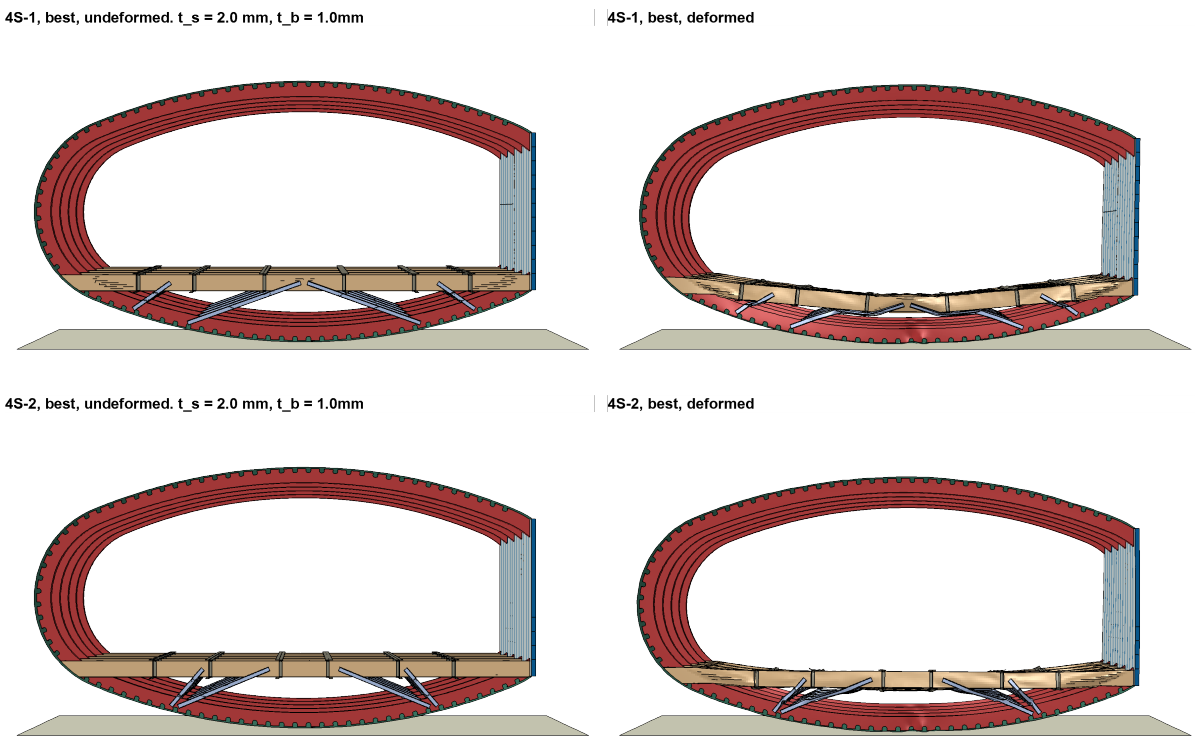

Figure 7.7: Undeformed and deformed FV crash sections, 4S concept (4S-1 and 4S-2), best configurations. Different colors are indicative of different section assignments. t_s and t_b indicate the shell thickness of the floor struts and the floor beams, respectively. Fuselage frames, due to their high bending stiffness, do not deform significantly, and, thus, the impact is dissipated thru the buckling of the floor beam and floor struts.

was decided to add central support and replace the single, vertical strut with three, thinner ones. This is concept HB-2, and it is visible in Figure 7.9. In HB-2, the horizontal beam supports and the three vertical struts share the same cross-section and thickness, to reduce simplify the model. This, however, resulted in the buckling of the horizontal beam supports, rather than the vertical struts. Thus, it was decided initially to reduce the cross-section of both struts (HB-3), with the reason being that the lower struts are shorter in length and, thus, their critical buckling load will be higher compared to the vertical ones. As shown by Figure 7.10, this eventually worked, with both upper and lower struts buckling. One more attempt was subsequently made to explore the possibility of more compliant horizontal beam supports. The reason for this was to further lower the acceleration peaks. This is configuration HB-4, where the horizontal beam supports have a smaller cross-section than the vertical struts.

Lastly, it was decided to test a configuration where the oblique struts have been removed completely. This is HB-5. In order to account for the loss in stiffness and strength of the oblique struts, the size of the cross-section of the vertical struts was increased once again.

7.3.4. HBH Concept

Initially, the HBH concept seemed to be a promising one, with many crushable elements, and, thus, the potential for high energy absorption. The design philosophy was to not achieve, by design, the creation of the frames' plastic hinge but, rather, to absorb energy by exploiting the elastic-plastic bending of the floor beam. The main issue observed with this concept, as mentioned, was the high propensity to structural instability, as the vertical struts have been observed to rotate almost rigidly about the horizontal beams. This is shown in Figure 7.11. As a consequence, the three design iterations for the HBH concept have aimed to mitigate this issue, by stiffening the horizontal beams (HBH-2), and reducing the bending stiffness of the middle vertical struts (those in between the two horizontal beams), in order to favor buckling of the struts, rather than the instability of the structure as a whole (HBH-3). Unfortunately, both attempts were unsuccessful, and, thus, this concept was abandoned.

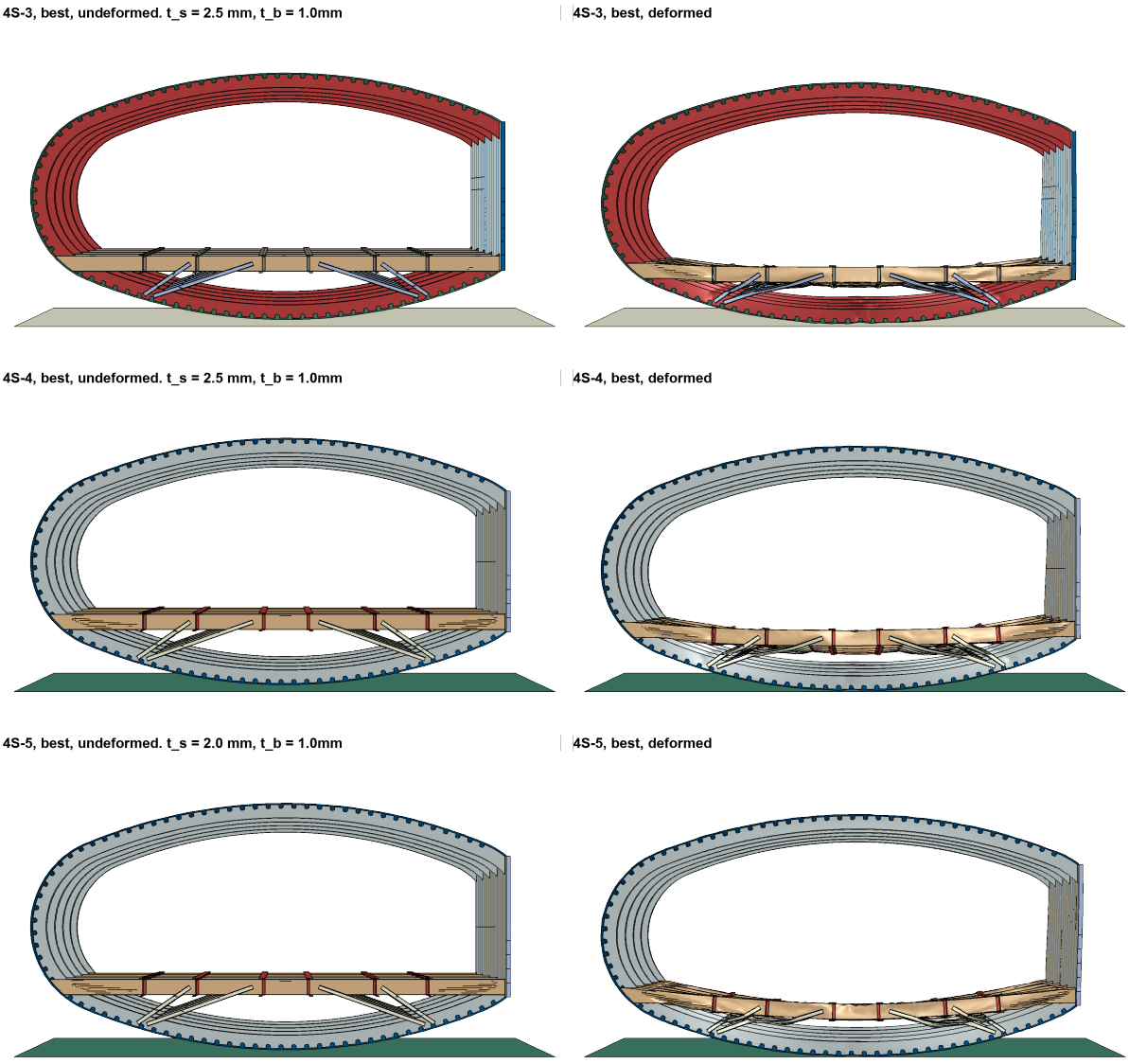

Figure 7.8: Undeformed and deformed FV crash sections, 4S concept (4S-3 to 4S-5), best configurations. Different colors are indicative of different section assignments. t_s and t_b indicate the shell thickness of the floor struts and the floor beams, respectively. Fuselage frames, due to their high bending stiffness, do not deform significantly, and, thus, the impact is dissipated thru the buckling of the floor beam and floor struts.

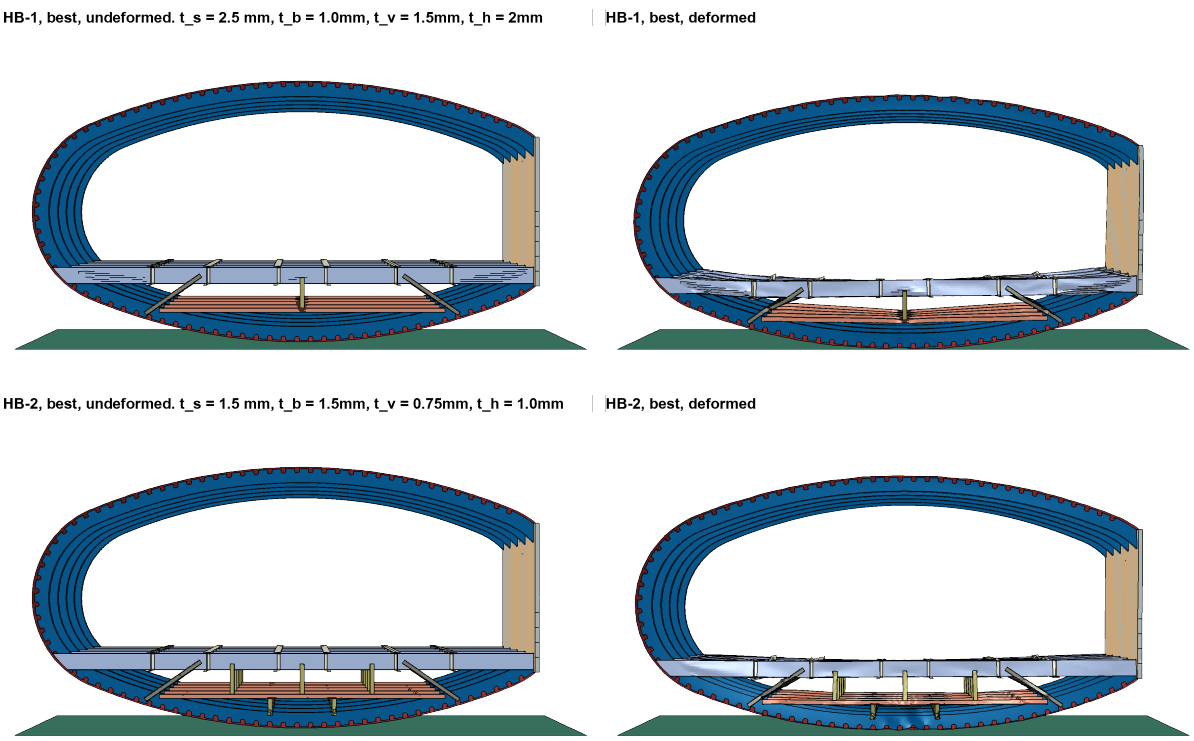

Figure 7.9: Undeformed and deformed FV crash sections, HB concept (HB-1 and HB-2), best configurations. Different colors are indicative of different section assignments. t_s and t_b indicate the shell thickness of the (oblique) floor struts and the floor beams, while t_v and t_h those of the vertical struts and horizontal beam, respectively. HB-1: limited plastic deformation of both the horizontal beam and the vertical strut. HB-2: good crushing of the vertical struts below the horizontal beam, but poor plastic deformation of those above.

HB-3, best, undeformed. t_s = 2.5 mm, t_b = 1.0mm, t_v = 0.5mm, t_h = 1.5mm | HB-3, best, deformed

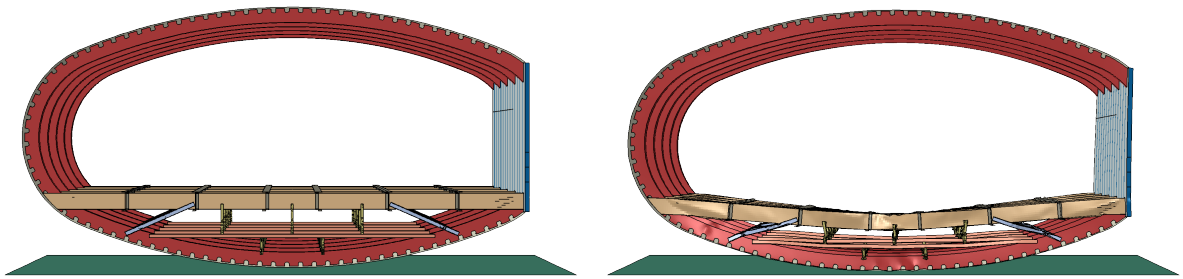

HB-4, best, undeformed. t_s = 1.5 mm, t_b = 1.5mm, t_v = 0.5mm, t_h = 0.5mm | HB-4, best, deformed

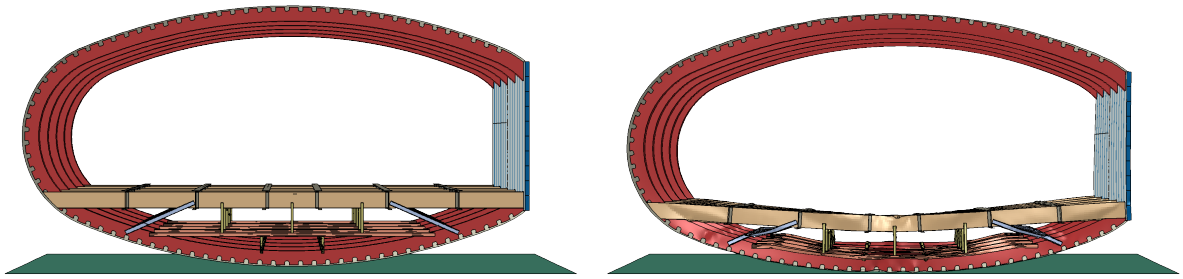

HB-5, best, undeformed. t_v = 0.75mm, t_h = 0.75mm | HB-5, best, deformed

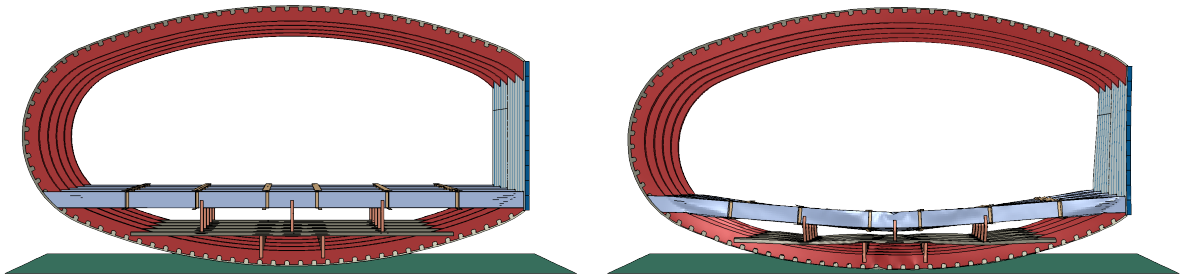

Figure 7.10: Undeformed and deformed FV crash sections, HB concept (HB-3 to HB-5), best configurations. Different colors are indicative of different section assignments. t_s and t_b indicate the shell thickness of the (oblique) floor struts and the floor beams, while t_v and t_h those of the vertical struts and horizontal beam, respectively. HB-3: all elements are plastically deforming and thus contributing to dissipate energy. HB-4: the cross-section of the horizontal beam has been reduced and, thus, it collapses due to bending instability. HB-5: crash concept without oblique struts. Energy is absorbed thru Euler buckling of the vertical struts.

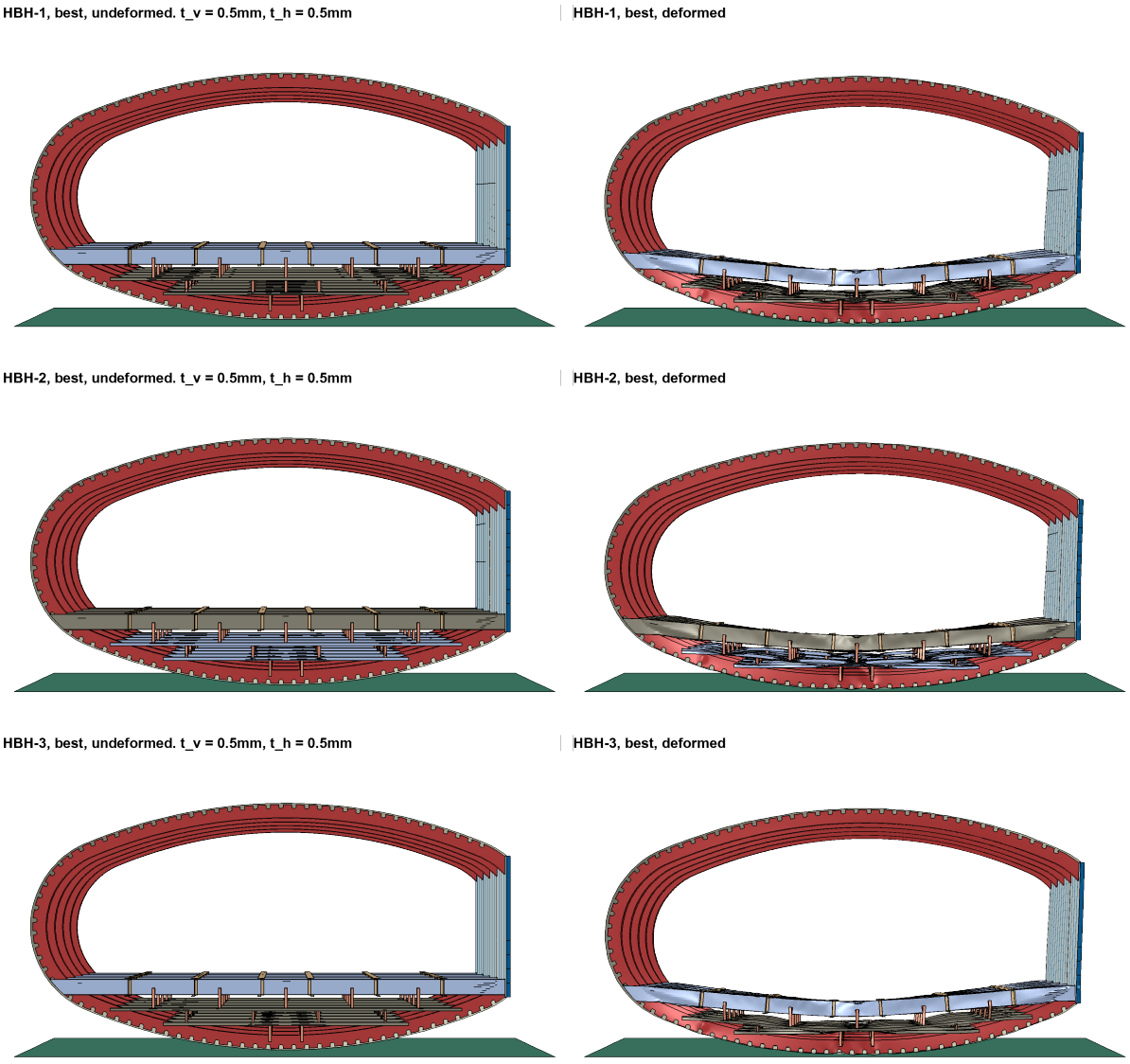

Figure 7.11: Undeformed and deformed FV crash sections, HBH concept (HBH-1 to HBH-3), best configurations. Different colors are indicative of different section assignments. t_v and t_h indicate the shell thickness of the vertical struts and horizontal beams, respectively. All configurations perform poorly as their are affected by structural instability (torsion about the horizontal beams).

7.4. Concepts Comparison

This aim of this section is to provide a high-level comparison across all the tested concepts, in terms of DRI, specific energy absorption (SEA, kJ/kg), and fraction of kinetic energy dissipated. The aforementioned data is provided in Figure 7.12 and Figure 7.13. Furthermore, the results are tabulated for the best performing configurations (those with the lowest DRI) in Table 7.1.

First of all, as evident from Table 7.1, for all concepts, the mass fraction of the crushable structure, compared to the mass of the entire section, ranges between ≈1.2% and ≈2%. On average, all sections had a mass of 3900 kg, distributed in the following manner:

- 3000 kg for passenger and seats mass;
- 83 kg for the (aft) spar mass; the accuracy of such value is unknown due to the lack of sizing data in this regard;
- 262 kg for the skin. This value overestimates the actual skin mass, as the assumed skin thickness is the largest one computed by Dotman, as shown in Figure 6.2;
- 443 kg for the frames;
- 44 kg for the floor longitudinal beams
- The crushable mass (variable).

The total mass of the sections, therefore, ranges between 3878 kg (4S-2) to 3907 kg (HB-3), with the crushable mass ranging between 47.3 kg to 76.8 kg (4S-2 and HB-3, respectively).

Secondly, it is clear that concept 6S, although it is approximately able to absorb the same energy fraction of some of the 4S concepts, the equivalent DRI is still significantly higher. The reason for this, as mentioned in subsection 7.3.1, is that the section of concept 6S is significantly stiffer than 4S, due to also the presence of the struts at the corner created by the frames and floor beams, resulting in overall higher accelerations.

Thirdly, regarding concept 4S, the one able to absorb most of the energy is 4S-2. As evident from Figure 7.7, in 4S-2, compared to 4S-5, other than the floor beams having been raised, the floor struts are also less shallow, meaning that, overall, the 4S-2 concept is stiffer. This resulted in a higher DRI. From the above, it is clear that a good balance is needed, between rigidity and flexibility: a very compliant structure, especially one which would easily buckle, might not be able to dissipate sufficient energy and, thus, at the end of the impact, the elastic energy is converted back into kinetic energy, thereby making the crushable structure ineffective. On the other hand, an excessively stiff structure, although might create large plastic deformations elsewhere, will also increase the loads felt by the occupants, consequently increasing the probability of injury.

Table 7.1: DRI, fraction of initial kinetic energy dissipated, SEA and crushable mass as a fraction of the total section mass, for the best configuration of each concept.

Version	DRI [-]	$\frac{E_D}{K_{EG}}$ [%]	SEA [kJ/kg]	$\frac{m_{crush}}{m_{tot}}$ [%]	Version	DRI [-]	$\frac{E_D}{K_{EG}}$ [%]	SEA [kJ/kg]	$\frac{m_{crush}}{m_{tot}}$ [%]
6S-1	23.5	72	1.35	1.64	HB-2	23.9	71	1.07	2.05
4S-1	23.1	73	1.84	1.24	HB-3	24.5	70	1.11	1.97
4S-2	20.4	78	1.99	1.22	HB-4	23.4	70	1.26	1.74
4S-3	20.0	77	1.74	1.37	HB-5	24.6	64	1.15	1.75
4S-4	18.9	76	1.51	1.60	HBH-1	24.9	66	1.19	1.74
4S-5	18.2	72	1.47	1.60	HBH-2	24.4	68	1.19	1.78
HB-1	22.2	69	1.27	1.76	HBH-3	24.8	67	1.19	1.75

Regarding concepts HB and HBH, data clearly shows that they are not able to as much energy as 4S and 6S. Still, it is worth noticing that concepts HB and HBH are significantly more complex that 6S and 4S, with a larger number of design variables involved. Consequently, it is not possible, in the current research, to exactly determine whether they are, in fact, better or worse concepts than the others. On the other hand, Figure 7.14 does show a correlation between having a lower DRI and absorbing more energy via plastic dissipation of the frames. While concepts 6S and 4S aim to dissipate a significant

portion of energy by plastic deformation of the frames, HB and HBH completely disregarded this, and focused on exploiting the floor beams deformation. As such, it is argued that the performance of a crash concept which does not exploit the deformation of the frames will likely be always worse than that of one that does do so. The main bottleneck is the maximum allowable floor beam deformation: some of the aspects to consider for crashworthiness are the cabin environment and post-crash factors [53]. Excessive floor beam deformation might cause seats and other interior items attached to the floor to move excessively, and, thus, potentially hit and injure occupants. Additionally, a partially collapsed cabin floor will render cabin egress more difficult.

The overall best-performing concept, in terms of DRI, is 4S-5, with an equivalent DRI of 18.2. Although, at first glance, this number might seem to be very close to the required DRI of 16 units (about 14% larger), in fact, the *theoretical* associated risk of injury, as shown in Figure 2.4, would be four times larger. Thus, more work will be required in order to lower this number to acceptable levels.

Considering Figure 7.12 and Figure 7.13, a correlation is shown between SEA, the fraction of initial kinetic energy dissipated, and DRI; this is consistent with the above discussion: 1) if more energy is dissipated by plastic deformation and friction, then, during the rebound phase, less energy will be restituted to the passengers; 2) a good balance between flexibility and rigidity is required.

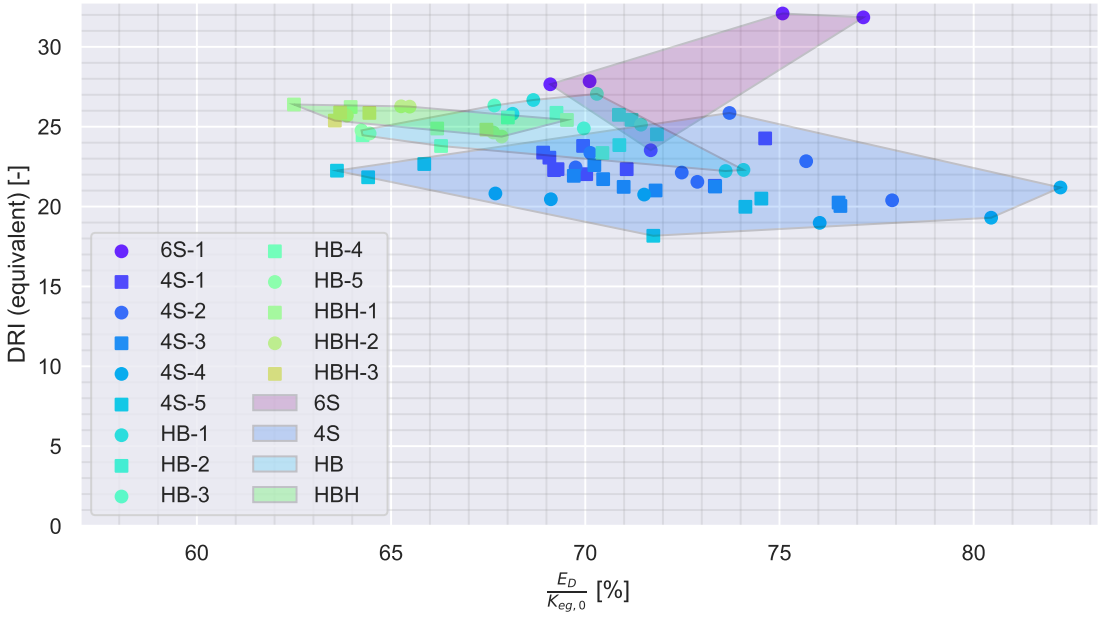

Figure 7.12: Equivalent DRI versus the dissipated energy normalized by the pre-impact kinetic energy, for all the tested variants. In general, in configurations that are able to dissipate more energy, a lower DRI is measured. This is not the case for the 6S concept, due to the high stiffness provided by the two additional struts, compared to concept 4S.

In conclusion, overall, all the different versions of concept 4S are not only the lightest ones, but are also able to dissipate the greatest amount of energy, and have the lowest DRI, since all structural elements are contributing to absorb the impact. Concept HB is somewhat more in the middle, with a DRI in the range of 21-24, about 70% of kinetic energy being dissipated, although the crushable structure does come with a larger weight penalty, compared to the 4S configuration. Lastly, as observed, the HBH concept was highly susceptible to structural instability. As such, the overall kinetic energy dissipated is the lowest for all the explored concepts, while the DRI is the highest. 6S is the worst-performing one, in terms of DRI, being the most rigid one.

7.5. Concepts Analysis

The aim of this section is to provide an analysis of the energy-absorption characteristics of the tested concepts. Three different metrics will be used for this comparison: SEA, energy dissipated by each

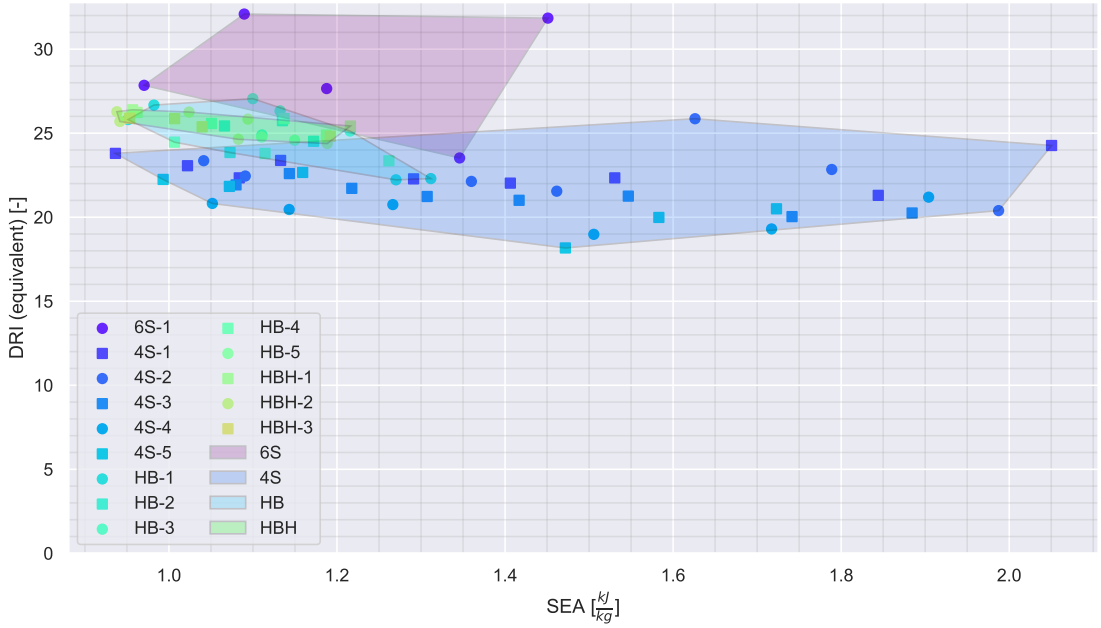

Figure 7.13: DRI versus the specific energy absorption of floor beams and crash structure (SEA). It can be observed that configurations with higher SEA will also have a lower DRI, since the crushable structure is more effective.

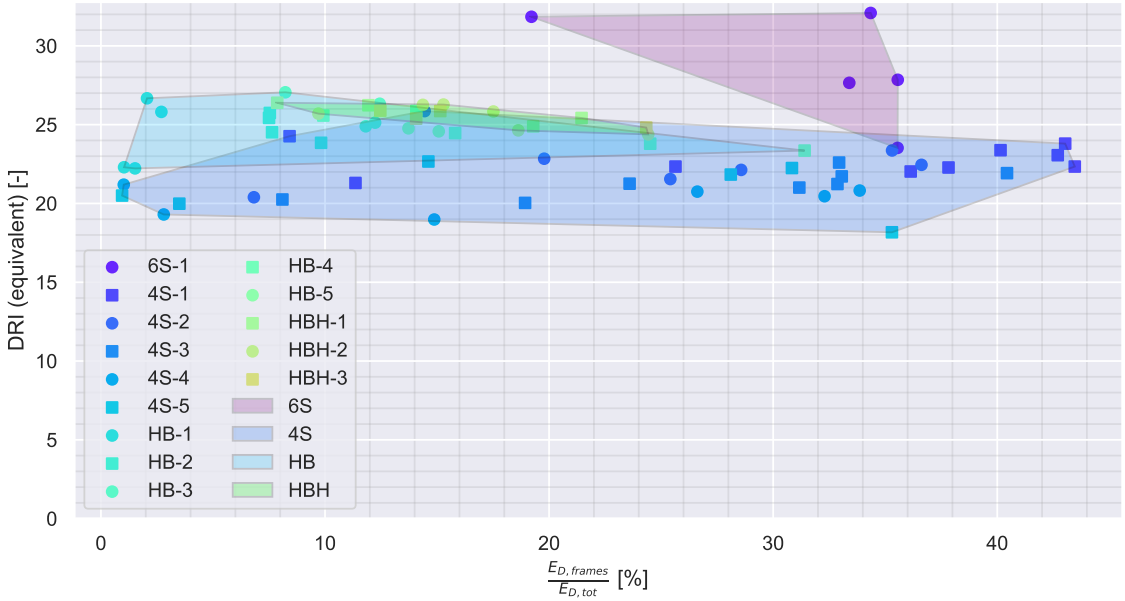

Figure 7.14: Dynamic Response Index versus the energy absorbed by the frames, normalized by the total absorbed energy. Data shows that having larger portions of energy absorbed by the frames, in general, is beneficial for crashworthiness.

component normalized by the total energy dissipated, and energy dissipated by each component normalized by the initial kinetic energy. It is worth noting that, for each concept, only the best-performing version will be analyzed: 6S-1, 4S-5, HB-1, and HBH-2. The results are provided in subsection 7.5.1 to subsection 7.5.4 respectively. For each version, a comparison across all variants will be provided.

7.5.1. 6S Analysis

Regarding concept 6S, starting off with the SEA, data shows two clear trends. The first one is that the configurations with a more flexible floor beam (smaller thickness) will have a higher specific energy absorption. In light of what has been stated previously in this chapter, this is totally logical and consistent. Looking at the distributions presented in Figure 7.16, the increase in the fraction of energy absorbed by the floor beam when the thickness becomes of 1 mm is truly impressive. Another contributing factor to the increase of SEA for thinner floor beams configurations is the actual decrease of crushable mass associated with a reduced thickness. SEA is the ratio of energy absorbed to crushable mass, thus, even if the former remains constant, if the crushable mass decreases, SEA will increase. Besides that, in general, configurations with a thinner floor beam, are able to absorb an equal or greater amount of energy. In configurations with thicker floor beams, the load is mainly transferred from the passengers to the floor beams, through the floor struts, and to the frames. When the floor beam thickness decreases, one structural instability mode is in turn triggered: lateral torsional buckling (LTB). The result of the structural instability will be out-of-plane displacement of the bending beam. Besides providing attachment points for the seats, one of the key roles of the floor longitudinal beams is to delay LTB by providing additional support. Consequently, when LTB is triggered, the load carried by the floor struts will decrease, and it will be directly transferred through the floor structure, to the frames, which will cause the floor structure to absorb more energy, as shown by the data.

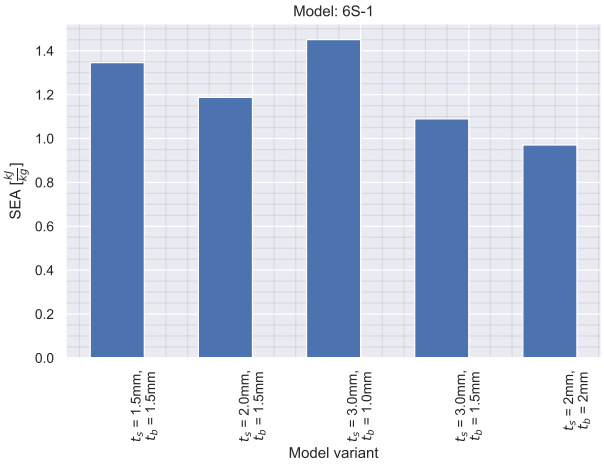

Figure 7.15: SEA for the 6S-1 concept. SEA trends depending on the floor struts and beam thicknesses.

Additionally, Figure 7.16 also does show how, for increased floor struts thickness, the fraction of energy absorbed by the frames will increase. Thicker floor struts will have a higher buckling and crippling load; as mentioned above, during the crash, the load is transferred through the floor struts to the frames, whenever LTB is not triggered. Consequently, a higher load will be transferred through the struts, when the thickness is increased, which will, in turn, result in an increase in the frames' plastic deformation.

7.5.2. 4S Analysis

As mentioned, and evident from Table 7.1, the best performing configuration for the 4S concept, in terms of DRI, is 4S-5. This is also the concept with the lowest DRI, across all the analyzed sections. SEA for the different variants of the 4S-5 configuration is thus shown in Figure 7.17, while the normalized energy dissipation distributions, by component, are shown in Figure 7.18.

Once again, two general trends are present, both in terms of SEA, and dissipated energy distribution. Starting with SEA, as visible from Figure 7.17, configurations with thinner floor beams show to have a higher SEA. Again, besides the slight increase in total absorbed energy shown in Figure 7.18b, this is mainly due to the decrease in structural mass associated with a decrease in thickness. The opposite is true, considering the thickness of the floor struts. Thicker struts, SEA-wise, perform worse, for the same reasons: Figure 7.18b shows a slight decrease in absorbed energy and, simultaneously, the struts become heavier.

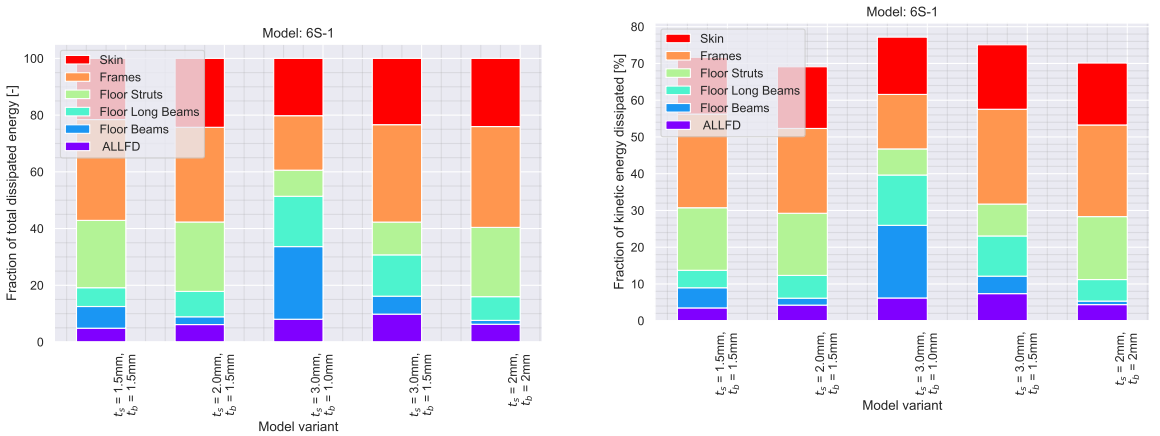

(a) Component energy absorption distribution, 6S-1 concept.

(b) Component energy absorption distribution, normalized by initial kinetic energy, 6S-1 concept.

Figure 7.16: Distribution of energy dissipated across components. ALLFD refers to energy dissipation due to friction. Different thicknesses for floor beams and struts change the load paths and cause a redistribution of energy dissipated.

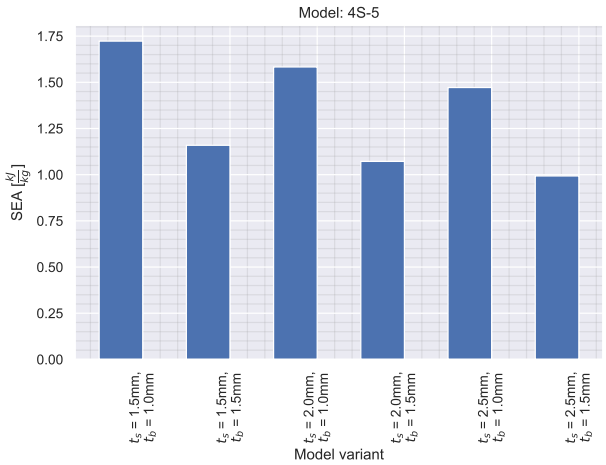

Figure 7.17: SEA for the 4S-5 concept. Variants with thinner floor beams and struts show to have higher specific energy absorption.

Secondly, considering Figure 7.18a, it is also evident that, for increasing floor struts thickness, the energy absorbed by the floor beam decreases. This is consistent with the considerations made in subsection 7.5.1. The fraction of energy dissipated by the floor struts only slightly changes, while, in turn, plastic deformation energy of the frames increases significantly. This is an index that thicker floor struts themselves will not absorb more energy, but will be able to favor plastic deformation of the frames. Another reason for this is that, once the floor struts buckle, they will start to fold, and the energy-absorbing capabilities of this deformation behavior are not significantly affected by an increase in thickness. This is particularly evident if one is to compare variants with 1 mm floor beam thickness, and 2 mm and 2.5 mm floor struts thicknesses, where energy absorption of the frames increases significantly, while that of the floor structure and of the floor struts actually decreases. In essence, the floor struts are able to transfer the load from the floor beams to the frames, and, thus, 1) end up deforming less (and thus absorb fewer energy themselves), and 2) prevent the floor structure to deform significantly.

Lastly, regarding the energy dissipated by plastic deformation of the skin, data shows that for configurations with thicker floor struts, the skin will also dissipated more energy. This phenomenon is correlated with the plastic deformation of the frames, to which the skin is tied. When the frames bend, the skin deforms with them, and, as mentioned, thicker floor struts favor bending of the frames.

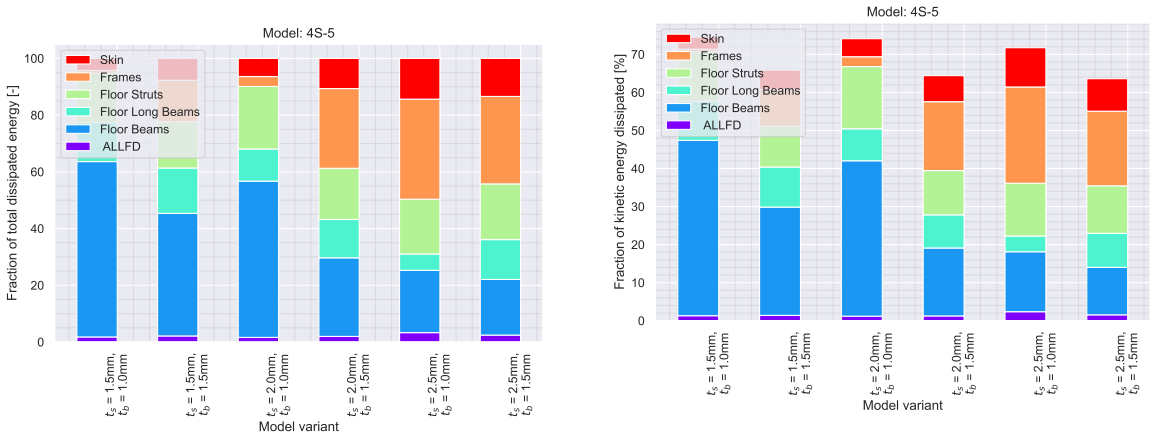

(a) Component energy absorption distribution, 4S-5 concept.

(b) Component energy absorption distribution, normalized by initial kinetic energy, 4S-5 concept.

Figure 7.18: Distribution of energy dissipated across components. ALLFD refers to energy dissipation due to friction. Configurations with thin floor struts dissipate more energy thru the deformation of the floor structure, while thicker struts will cause the frames to deform more.

7.5.3. HB Analysis

The best configuration for the HB concept is HB-1, with a DRI of 22.2 units. The SEA and normalized dissipated energy distributions for HB-1 are thus presented in Figure 7.19 and Figure 7.20, respectively.

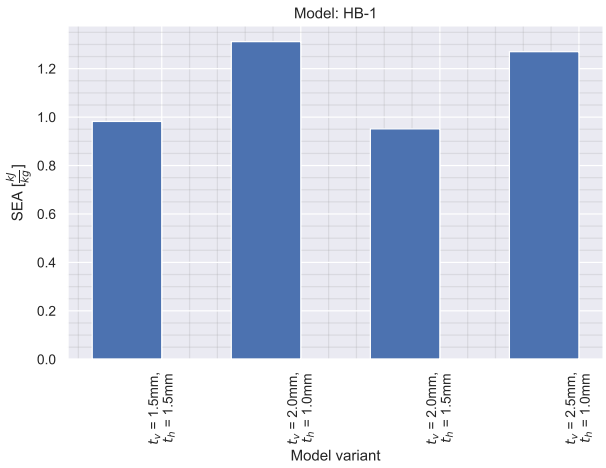

Figure 7.19: SEA for the HB-1 concept. Variants with thinner beams and struts show to have higher specific energy absorption.

First and foremost, it is significant to note that in HB-1 configuration, the vertical strut almost does not absorb any energy. Data shows that it is hovering about 0.1% across all configurations, which is the reason for which it is not visible in the stacked bar charts. This is also visible in Figure 7.9, as well as in Figure A.1 (Appendix A), where the contour plot of plastic strains of the deformed section shows no plastic deformation of the vertical strut. This is caused by the out-of-plane bending of the horizontal beam, after it has been pushed down by the vertical struts: once the horizontal beam has been bent downwards, then, two possible scenarios can occur. The first one was the design intent, namely that the vertical strut keeps pushing the horizontal beam down, which will thus induce tension in the beam, stiffening the assembly, increasing the load and favoring the crushing of the vertical strut. The second option, which is the one that occurred, of the horizontal beam out of plane displacement, and the rotation of the entire assembly about the floor beam. Compared to tension, bending is a mush lower energy state, and is thus the preferred deformation option. This is a deformation mode similar to that of concept HBH, as shown in Figure 7.11; compared to the HBH concept, however, the single

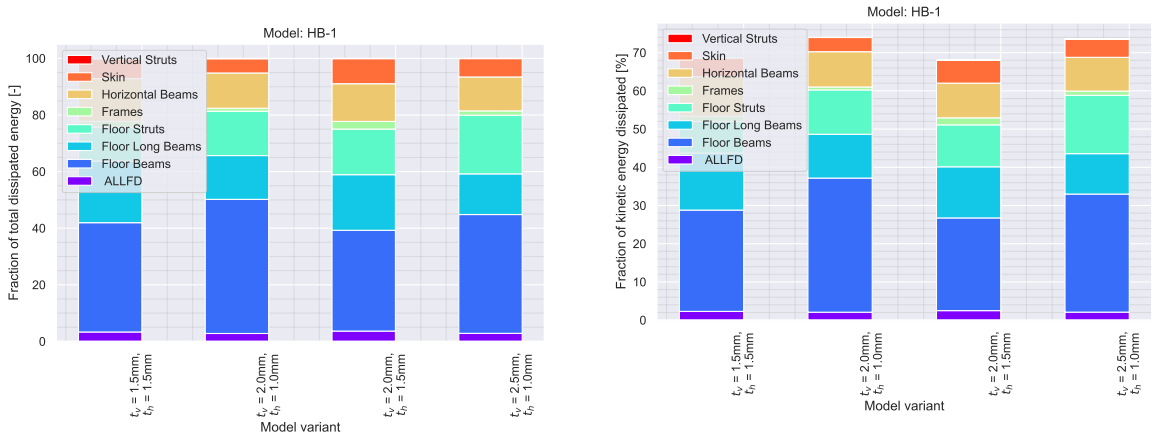

(a) Component energy absorption distribution, HB-1 concept.

(b) Component energy absorption distribution, normalized by initial kinetic energy, HB-1 concept.

Figure 7.20: Distribution of energy dissipated across components. Frames are contributing very little to energy absorption, due to lower load introduced by the floor struts, and most of the work is in turn being done by the floor structure. The vertical strut dissipates ≈0.1% of the energy, and is thus not visible in the bar chart. ALLFD refers to energy dissipation due to friction.

strut present in the HB-1 concept is significantly thicker ($1.5\text{mm} < t_v < 2.5\text{mm}$), and, thus, it does not deform plastically.

A second observation is that the frames absorb little energy, compared to 6S and 4S concepts. In fact, ≈60% of the dissipated energy, is absorbed by the floor structure itself, thus, the loads are hardly transferred to the frames. Actually, this means that the frames are not able to even dissipate their own kinetic energy, thus, have an overall negative effect on the crash properties of the section: after the impact, the frames will rebound and, only during this phase, then, their kinetic energy is dissipated by other structural elements. Additionally, about 15-20% of the dissipated energy is absorbed by the floor struts, and only about 12-15% by the horizontal beams.

The thickness of the vertical struts has virtually no effect on the energy absorption (which is expected, considering that they do not plastically deform), while, regarding horizontal beams, an increase in thickness will cause the absorbed energy to overall slightly decrease: likely, a stiffer horizontal beam will slow down the floor assembly by storing more elastic energy and, thus, when plastic deformation occurs, fewer kinetic energy will be dissipated plastically.

Lastly, regarding SEA, a slight decrease is shown for thicker vertical struts, which is expected, as the mass mass contribution of the vertical strut alone is small, compared to the longer horizontal beam. A larger decrease is however noticed for increased horizontal beam thickness. The decrease in SEA is due to a more significant increase of crushable mass, as, overall, as mentioned, variations in overall energy dissipated are small.

7.5.4. HBH Analysis

The version with the lowest DRI for concept HBH is HBH-2 (24.4 units). The SEA distribution for different variants of HBH-2 is shown in Figure 7.21, while normalized energy absorbed in presented in Figure 7.22.

Regarding SEA, it is clear how poorly effective the crash structure is, at absorbing energy. The vertical and horizontal floor beams add a significant amount of additional structure, which, however, due to the instability, does not pay off. Figure 7.22b shows that all variants approximately dissipate the same fraction of the pre-impact kinetic energy, while some variation in the contribution of the individual components. A general, obvious trend is observed, where lighter variants have higher SEA. Figure 7.22b shows that all the variants are able to dissipate roughly the same percentage of initial kinetic energy. Clearly, then, lighter ones will have higher SEA.

Interestingly, compared to concept HB-1, as shown in Figure 7.20, the frames are now absorbing a more

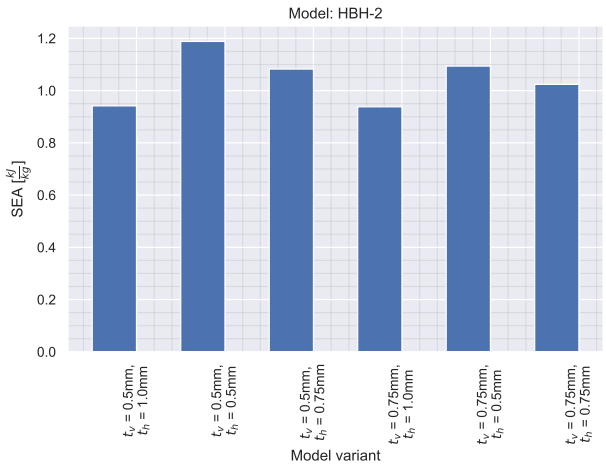

Figure 7.21: SEA for the HBH-1 concept. Variants with thinner beams and struts show to have higher specific energy absorption.

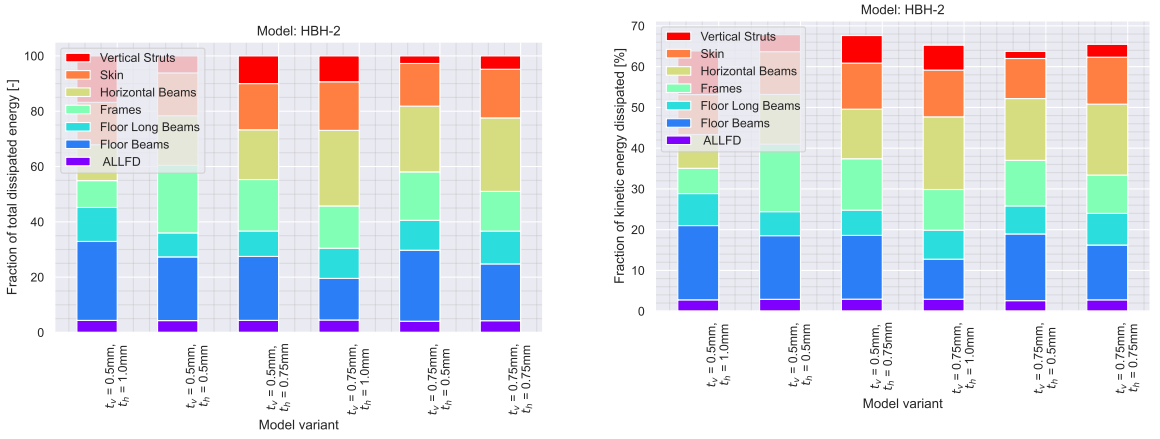

(a) Component energy absorption distribution, HBH-2 concept.

(b) Component energy absorption distribution, normalized by initial kinetic energy, HBH-2 concept.

Figure 7.22: Distribution of energy dissipated across components. All variants are approximately able to dissipate similar amounts of energy. Struts with thinner walls show an improvement in energy absorption, while the opposite is true for the horizontal beams.

significant portion of energy. In essence, this means that, before the structural instability is triggered, more load is transferred through the horizontal beams to the frames; this is further proven by the more significant portion of energy that is dissipated thru the horizontal beams, hovering about 20%, and less by the floor structure. As expected the vertical struts perform quite poorly, as they are in fact never crushed. The fraction of energy absorbed by the fuselage skin is in turn more similar to that of concepts 4S and 6S. As mentioned in subsection 7.5.2, the energy dissipated by the skin is closely related to that dissipated by the frames; this is thus consistent with that observation.

Overall, a trend can be hardly identified, due to the complexity of the observed failure mode. However, in general, the vertical struts seem to be performing best when thinner, while the opposite is true for the horizontal beams. This is logical as the structural instability is not caused by Euler buckling of the struts, but, rather, by out-of-plane displacement of the horizontal beams. Subsequently, having a thinner wall for the vertical struts will allow them to deform before and during the instability occurs, while thicker horizontal beams will delay the aforementioned instability.

7.6. Discussion on the Results

First and foremost, it is worth noting that the crushable mass represents a small percentage of the fuselage section mass. This fraction becomes even smaller considering that floor beams have also been included in the determination of the crushable mass, the design of which is however determined not solely by crashworthiness requirements, but also by structural sizing constraints. All in all, differences in mass fractions across crash concepts will always be small. Despite that, crash performance is shown to change significantly.

From the data presented above, none of the explored concepts was able to meet the requirements that have been laid in chapter 2. The best-performing one is 4S-5, with an equivalent DRI of 18.2 units, significantly higher than the required 16. The main bottleneck is the lack of plastic deformation of the frames, which, in conventional aircraft, dissipate the vast majority of the kinetic energy. In the simulations on the F-28 section, presented in chapter 5, it was shown that the F-28 section was able to dissipate about 80% of the initial kinetic energy, after the first impact. ≈70% of the dissipated kinetic energy is absorbed by the frames. In the proposed concepts, only one is able to get close to this figure, 4S-2, at 78%. 4S-5, in turn, stops at 72%, ≈35% of which is taken by the frames. The high rigidity of the structure also causes an increase in DRI.

Considering concepts 6S and 4S, it is concluded that, given the already high stiffness of the frames, it will not be beneficial for crashworthiness, to have a large number of floor struts. It is, instead, recommended to only consider designs employing four struts, in future studies. As shown in Part III, frames are a crucial element for crashworthiness, also for high-eccentricity sections. While their sizing will mostly be determined by operational loads, for future design iterations, it is of extreme importance to focus on the deformation of the frames to absorb energy. As proven by concepts HB and HBH, disregarding this aspect has not worked, at least within this research. Furthermore, it is worth emphasizing once again, at this point, that in the current research, the frames geometry has been simplified significantly. The consequence of this is that, although on average, the bending stiffness is kept approximately constant, it is highly overestimated at the locations where plastic deformation occurs, in the vicinity of the floor struts anchor points. As shown in Figure 6.3, this, in fact, corresponds to the region where the actual frame height is quite low. Thus, the approach taken significantly overestimates the bending stiffness at that critical location. It is thus highly likely that if a more accurate model has been developed, the crash properties of the analyzed section would have improved significantly. This will be in part confirmed by the sensitivity analysis study, where the thickness of the frames is varied in order to check for the significance of the simplifications made. However, while it is true that in those critical regions, the frame stiffness is overestimated, it should be noted that in other regions, such as the center of the keel, it is underestimated. An increase in stiffness of the central part of the keel would prevent flattening of the lower portion of the frames, likely causing deformations that are completely different from those seen in conventional aircraft configuration. Accurate modeling of the section is thus left as a future study.

The unconventional HB and HBH concepts are poorly performing, as they are not able to dissipate large amounts of energy, and are prone to large rebounds as a consequence of that. In particular, HBH is highly subjected to structural instability. It has been mentioned, earlier in this report, that, since concepts HB and HBH are significantly more complex than 4S (and 6S).

In terms of overall deformations, all concepts are subjected to large floor beam compliance; this is more limited in 4S and 6S, where the floor beam is better supported by the floor struts, while it is significantly more pronounced in HB and HBH. This was by design, as HB and HBH were conceived to absorb energy by means of floor beam deformation, while a larger focus on frames' plastic hinge creation was given for 6S and 4S. In addition, the large compressive load present in the floor struts of the latter concepts does have a stabilizing behavior on the floor beams, thus, further limiting their deformation.

Compliance of the floor beams, by itself, is not a negative outcome, as it allows for an increase in the impact time and, thus, reduces the acceleration experienced by the passengers. Excessive deformation of the floor beams, however, during a crash, might damage the interior floor panels, and, overall, render the evacuation process more cumbersome. This is an unwanted result, especially in light of recent proposals from US lawmakers, to create more stringent and real-life alike cabin egress

requirements[1,2].

To summarize, data shows a clear direction towards the design of a crashworthy FV typical section, which calls for a conventional floor beam-and-struts approach, with localization of the loads at a single anchor point, in order to achieve a plastic hinge on the frames. Some deformation of the floor beam will likely be beneficial as well, however, stringent requirements should be set on the allowed deformation, in order to favor the egress of the occupants from the cabin. A coupled static-dynamic optimization is highly recommended, in order to directly include crashworthiness requirements among the structural sizing requirements of the airframe, as well as to have a more accurate model of the FV fuselage section for the drop test analysis.

Lastly, a few considerations need to be made, regarding the limits of this current study:

- **Tail-impact first and rigid body rotation:** The current assessment of the crashworthiness of the FV aircraft relies on currently accepted means of compliance by regulators, namely, a simple drop test of the typical fuselage section. While this is a simple and traditionally effective method to assess aircraft crashworthiness, it also relies on the experience gained from decades of aviation history. Compared to conventional aircraft fuselages, the FV's is more rigid and stronger. As a reference, post-crash pictures of the Boeing 737 aircraft, show the fuselage to fracture in three distinct sections, after a crash-landing: one forwards of the central wingbox, one containing the central wingbox, and a tail section[3]. During a tail-impact first crash landing, it is possible for the FV's outer wings to be damaged and even separate from the main body. This would dissipate energy, and could be beneficial for crashworthiness. However, the stiffer and stronger fuselage section would also likely be affected by rigid body dynamics effect. When the tail strikes the ground, the resultant upwards force will induce a strong pitch-down moment on the aircraft, and subsequent rotation. The front-most part of the cabin will thus have a higher vertical impact velocity than the aft, resulting in higher accelerations experienced by the occupants. A proper evaluation of the FV rigid body dynamic motion has not been performed as part of this research, and will thus be left as a recommendation for future studies.
- **Fuel and sloshing:** the FV aircraft will store fuel aft the (trailing edge) wing-fuselage spar. While it is unlikely that fuel will be stored in the tank in a 'wet structure' configuration, fuel, fire and environmental are critical elements to be considered, when evaluating aicraft crashworthiness. In current analyses, fuel mass has been unaccounted for, mainly due to lack of fuel mass distribution data for the FV aircraft. Once again, this is left for future studies. However, besides the fuel mass itself, a critical factor that might emerge is damage caused by the sloshing of the fuel itself, after the impact. The accident investigation following the tragic accident of the Aérospatiale/BAC Concorde of 2001, determined that the root cause of the damage to the fuel tank of the aircraft was not the direct impact of tire debris, but the displacement of the (incompressible) fuel caused by the impact and the subsequent pressure surge [54]. Considering the vicinity of the passengers to the fuel tanks in the FV aircraft, it will be of prime importance to ensure reliable separation of the fuel from the cabin, even during higher-speed impacts, which are still survivable. As such, it is recommended, for future studies, to 1) include, to the aforementioned analyses, one that will take into account the interaction between fuel sloshing and structure, during a crash landing, for different amounts of stored fuel. In addition, it is recommended to include bulkheads in fuel tanks, at the location where the FV wing-fuselage is likely to fracture into separate sections, to ensure that, even in such an event, fuel will still be contained.

[1] https://www.chicagotribune.com/opinion/commentary/ct-opinion-faa-plane-evacuation-standards\-duckworth-20221230-leowchniknb2rd623xbgrhz7jm-story.html. Accessed on 27-Jan.-2023.

[2] https://www.reuters.com/world/us/us-senators-want-faa-rewrite-aircraft-evacuation-standards\-2022-12-08/. Accessed on 27-Jan.-2023.

[3] https://christinenegroni.com/boeing-workers-warn-of-737-ng-structural-problems-then-4\-planes-fracture/. Accessed on 28-Jan.-2023.

8

Sensitivity Analysis

The preliminary assessment on the crashworthiness of the FV aircraft presented in chapter 7 was based on the model of a fuselage section which relied on some simplifications and assumptions, that helped to reduce the number of modeling variables and modeling time, but, crucially, might have had an effect on the results. As such, a series of sensitivity analyses have been performed on the following set of parameters:

- Mesh size
- Floor beams thickness
- Floor beams flange width-to-web height ratio
- Floor struts thickness
- Floor struts flange width-to-web height ratio
- Frames thickness

The reasons for the choice of each of the aforementioned parameters will be discussed in the relevant section. Results on the mesh size sensitivity analysis will be presented in section 8.1; those on floor beams geometric parameters in section 8.2, while those on the floor struts geometric parameters in section 8.3. Lastly, data on the sensitivity analysis on the fuselage frames thickness will be shown in section 8.4.

Almost all variants are contained within a narrow band where DRI is between 18 and 19, and the fraction of absorbed energy is between 70% and 73%. The three exceptions to this are the two variants tested with different frame thicknesses, and one with a thinner floor beam, as visible from Figure 8.1.

8.1. Mesh Size

Compared to the F-28 section, the overall size of the structure is obviously increased; as such, the element size for all the structural elements, for the FV section, was kept the same at best, if not decreased, in order to have sufficient confidence in the accuracy of the analysis. A sensitivity analysis was thus performed to check the hypothesis's validity. The mesh size sensitivity analysis was performed by using the F-28 mesh size as a baseline, and then refining it further, twice, so that the global element size would be that of the baseline, multiplied by a factor of 0.9 and 0.8.

The results are tabulated in Table 8.1, and further presented in Figure 8.2 and Figure 8.3. Pictures of the deformed sections are, in turn, provided in Appendix B.

The baseline model consists of 178947 elements and 193896 nodes. In the 0.9x model, the number of elements increased to 217246, corresponding to a total of 233948 nodes. Lastly, in the 0.8x model, the number of elements further increased to 272197 elements and 290789 nodes. From the mesh

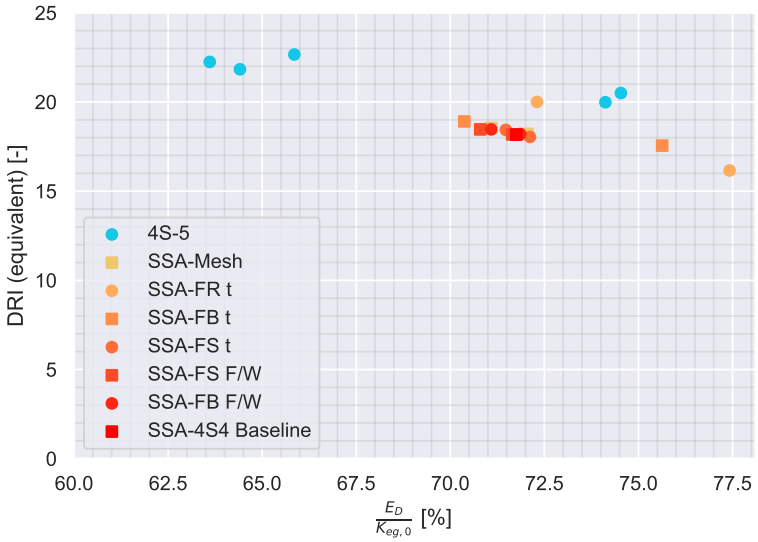

Figure 8.1: Comparison between 4S-5 concept variants and sensitivity analysis models. Overall, large differences in DRI and energy-absorption levels can be observed to be mainly occurring for variations in frames and floor beam thicknesses. Other quantities have a smaller effect.

Table 8.1: Comparison of DRI, kinetic energy dissipated, and SEA for different mesh refinement levels. All metrics show good agreement with the baseline mesh size, giving confidence on the accuracy of the solution.

Version	DRI [-]	$\frac{E_D}{K_{EG}}$ [%]	SEA [kJ/kg]
Baseline	18.2	72	1.47
0.9x mesh size	18.2	72	1.46
0.8x mesh size	18.5	71	1.45

refinement, the skin is excluded, as, other than plastic bending, it does not undergo more complex deformations.

Data shows little to no difference to be present between the three variants. An overall slight decrease in energy absorption (and, thus, SEA) is observed. Due to the small magnitude of the variation, it was not possible to determine the exact cause of the decrease; however, the data follows a consistent trend with that of the F-28 fuselage section, presented in section 4.4, where, as indicated by the kinetic energy time history plots (Figure 4.7), a slight decrease in overall absorbed energy was observed. Additionally, Figure 8.3 shows a slim decrease in the energy absorbed by the floor struts and a tiny increase in that absorbed by the frames. Once again, this is consistent with what was found for the F-28 fuselage section (Figure 4.8, Figure 4.9 and Figure 4.11).

The most significant difference is the increase in equivalent DRI measured, from 18.2 units to 18.5 units (which, however, in theory, corresponds to an increase in the probability of spinal injury from 12.5% to 15.7%). This is likely due to the increase in the crippling load of the floor struts associated with a more refined mesh. Once again, this is consistent with data presented in section 4.4, where DRI also increased with refined mesh.

Overall, the sensitivity analysis data provides confidence that the results determined with the ‘baseline’ mesh size are sufficiently accurate and trustworthy.

8.2. Floor Beams Geometric Parameters

As mentioned in the chapter introduction, two distinct floor beams geometric parameter sensitivity analyses have been performed: one on the thickness of the floor beams, and another on the ratio between

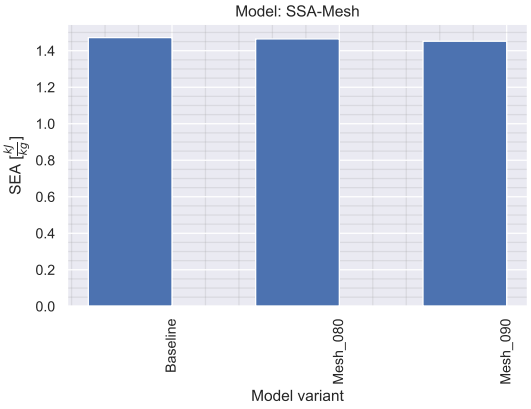

Figure 8.2: SEA for mesh sensitivity analysis variants. All models have almost identical SEA.

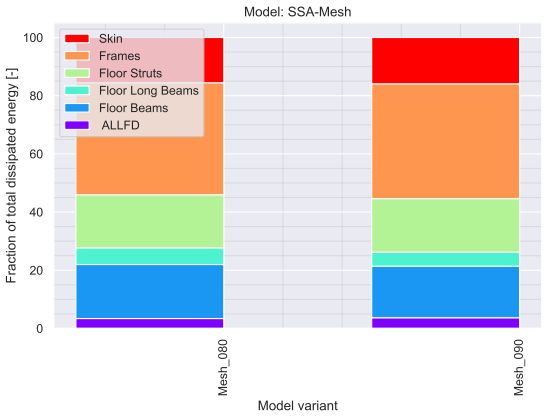

Figure 8.3: Energy absorption distribution by component, mesh sensitivity analysis. No significant variations are noted, for different mesh refinement levels. The '080' and '090' values denote a global element size equal to 0.80x and 0.90x that of the baseline, respectively.

the beam's web height and flange width. The results of the former are provided in subsection 8.2.1, while those of the latter are in subsection 8.2.2.

8.2.1. Floor Beam Thickness

Starting with the analysis on the floor thicknesses, it is clear that a thinner floor beam is highly beneficial for crashworthiness. This was already observed and pointed out earlier in this report, in subsection 7.5.2. A thinner floor beam will deform more and, thus, absorb more energy, as well as decrease overall the crushable mass, causing a large increase in SEA. As more energy is absorbed by the floor beam itself, the frames will be more lightly loaded, and, thus, contribute less. The energy fraction absorbed by the floor struts, instead, remains approximately constant, as their bucking and crippling loads are unvaried.

It is worth noticing, however, that, although not specified in the context of this research, a requirement on the maximum allowed bending of the passenger floor beam must be set, especially if optimization is to be performed, considering the high sensitivity of the crash characteristics to the thickness of the floor beam.

Table 8.2: Comparison of DRI, kinetic energy dissipated, and SEA for different floor beam thicknesses. All metrics show how thinner floor beams can significantly reduce DRI and energy absorption levels. This, however, comes with the penalty of significant floor beam deformation.

Version	DRI [-]	$\frac{E_D}{K_{EG}}$ [%]	SEA [kJ/kg]
t_b =0.75 mm	17.6	76	1.82
t_b =1.0 mm (baseline)	18.2	72	1.47
t_b =1.25 mm	18.9	70	1.25

8.2.2. Floor Beam Flange Width-to-Web Height Ratio

As mentioned in subsection 6.3.2, the floor beams cross-section consists of an I-beam, with a web height-to-flange width ratio equal to 3. It was of interest to check whether different ratios would have a positive, negative or neutral effect on the crash properties. The hypothesis is that variants with a lower ratio will be more stable (no LTB), as the flange width increases. In order to isolate other variables, it was decided to conduct this study by keeping the beam's flexural rigidity constant. As the width of the flanges with respect to the web height will increase, then, overall, the height of the beam's web needs to be decreased. Using the thin-walled approximation, (8.1) was derived, which allows determining the new beam height, as a function of the old beam height, and the respective flange width-to-web height

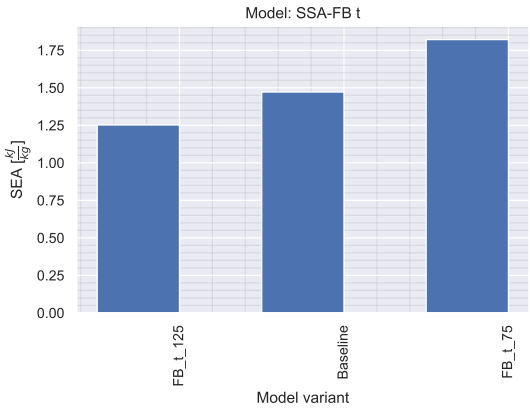

Figure 8.4: SEA for floor beam thickness sensitivity analysis. SEA increases for thinner floor beams due to 1) lighter beams and 2) an increase in energy absorption.

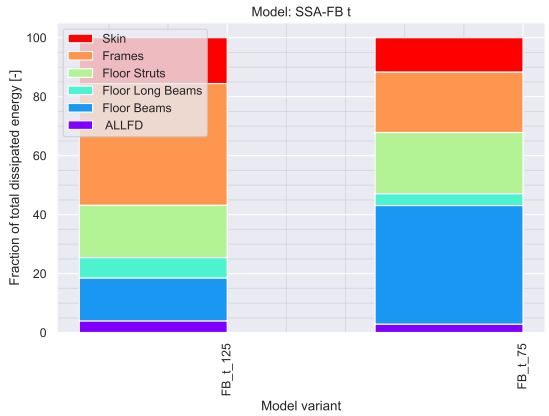

Figure 8.5: Energy absorption distribution by component, floor beam thickness sensitivity analysis. The energy absorbed by the floor beams increases significantly as they become thinner.

ratios, for an I-beam, keeping the flexural rigidity constant:

$$h_2 = h_1 \left(\frac{\frac{1}{12} + \frac{n_1}{2}}{\frac{1}{12} + \frac{n_2}{2}} \right)^{\frac{1}{3}} \tag{8.1}$$

where h_1 and h_2 are the old and new beam heights, while and n_1 and n_2 are the old and new flange width-to-web height ratios, respectively. For the baseline variant, $n_1 = \frac{1}{3}$. This resulted in a floor beam web height of $209\,\text{mm}$ for $n = \frac{1}{2}$ and $h = 244\text{mm}$, for $n = \frac{1}{4}$. As mentioned, earlier in this report, $h = 230\text{mm}$ for $n = \frac{1}{3}$.

The sensitivity analysis data is presented in Table 8.3, Figure 8.6 and Figure 8.7. For consistency with the plots, in Table 8.3, the variants are denoted using the inverse of n.

Table 8.3: Comparison of DRI, kinetic energy dissipated, and SEA for different ratios of floor beam web height-to-flange width. Within the analyzed range, no significant differences are noted.

Version	DRI [-]	$\frac{E_D}{K_{EG}}$ [%]	SEA [kJ/kg]
FB $\frac{F_w}{W_h} = 2$	18.5	71	1.38
FB $\frac{F_w}{W_h} = 3$ (baseline)	18.2	72	1.47
FB $\frac{F_w}{W_h} = 4$	18.2	72	1.48

Data clearly shows that, overall, the ratio of the flange-to-web dimensions has in fact little effect on the crash properties, of course, within the examined range. Likely, for more extreme configurations, this will differ. The energy absorption distribution by components, shown in Figure 8.7, are essentially unaffected, as well as the total absorbed energy, in Table 8.3. An increase in SEA for variants with higher $\frac{F_w}{W_h}$ is noted; this is attributed to the natural lightening of the floor beam when the height is increased and the flexural rigidity is kept constant, as it is more efficient to place material further away from the neutral axis. Lastly, an increase in DRI is noted for the variant with the lowest $\frac{F_w}{W_h}$. This is likely because, although the beam's second moment of area is constant, the height is decreased, which, overall, leads to lower stresses and, thus, reduced buckling.

Figure 8.6: SEA for floor beam height-to-width ratio sensitivity analysis. SEA only slightly increases for larger ratios since, when keeping flexural rigidity constant, the floor beam becomes lighter for higher ratios.

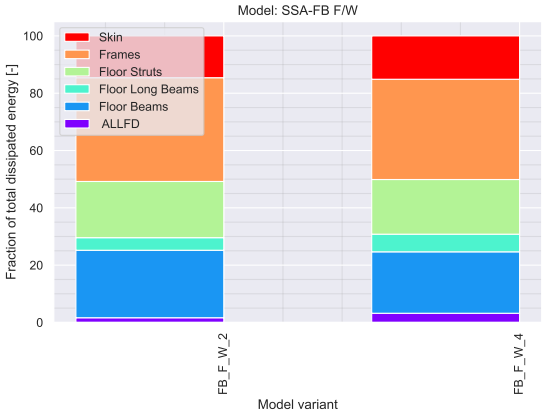

Figure 8.7: Energy absorption distribution by component, floor beam height-to-width ratio sensitivity analysis. Within the analyzed range, a changing ratio has little to no effect.

8.3. Floor Struts Geometric Parameters

Regarding the floor struts, a similar sensitivity analysis has been performed compared to the floor beams: one on the thickness, and another on the ratio between the struts' web height and flange width. The results of the former are provided in subsection 8.3.1, while those of the latter are in subsection 8.3.2.

8.3.1. Floor Struts Thickness

Starting with the floor struts thickness, data shows that the overall energy absorbed remains approximately unchanged. As evident from Figure 8.9, in variants with thicker floor struts, frames are able to absorb a bit more energy. On the other hand, the floor structure is subjected to fewer plastic deformation. Consequently, SEA is higher for thinner struts, as, simply, the crushable structure is lighter.

Table 8.4: Comparison of DRI, kinetic energy dissipated, and SEA for small variations in floor struts thickness. Thinner floor struts allow for greater floor beam deformation, thus, lowering the DRI while still allowing the structure to absorb the same amount of energy.

Version	DRI [-]	$\frac{E_D}{K_{EG}}$ [%]	SEA [kJ/kg]
t_s =2.25 mm	18.0	72	1.55
t_s =2.50 mm (baseline)	18.2	72	1.47
t_s =2.75 mm	18.4	71	1.41

8.3.2. Floor Struts Flange Width-to-Web Height Ratio

Regarding the floor struts' flange width-to-web height ratio, similar to what was done for the floor beams, it was decided to keep the flexural stiffness constant when changing the ratio. As the floor struts buckle during the crash, it was decided to keep constant the flexural rigidity about the minor axis (i.e. the axis about which I_{xx} is the lowest), since that is the one critical for buckling. In a C-section, this corresponds to that which is parallel to the web. Again, using the thin-walled approximation, (8.2) was derived, linking the web heights of C-sections with different flange width-to-web height ratios.

$$h_2 = h_1 \left(\frac{\frac{n_1^3}{6} + 2\frac{n_1^3}{(4n_1+2)^2} + \frac{n_1^4}{(2n_1+1)^2}}{\frac{n_2^3}{6} + 2\frac{n_2^3}{(4n_2+2)^2} + \frac{n_2^4}{(2n_2+1)^2}} \right)^{\frac{1}{3}} \tag{8.2}$$

The parameters h_i and n_i are the same as those presented for (8.1). This resulted in $h = 32$mm for

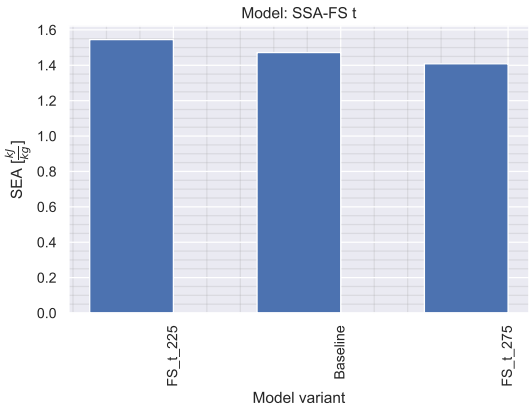

Figure 8.8: SEA for floor struts thickness sensitivity analysis. A slight decrease in SEA is attributed to heavier crushable mass, due to the increase in struts thickness.

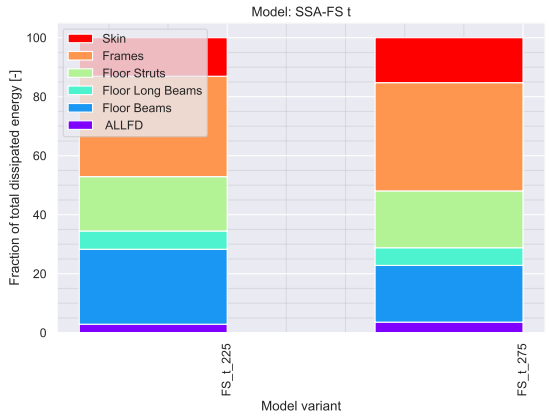

Figure 8.9: Energy absorption distribution by component, floor beam thickness sensitivity analysis. Small variations in floor struts thickness have little to no effect on the energy-absorption characteristics.

$n = 1$, and $h = 87$mm for $n = \frac{1}{3}$. For the baseline configuration, as mentioned in subsection 7.2.1, $h = 60$mm and $n = \frac{1}{2}$. The results are presented in Table 8.5, Figure 8.10, and Figure 8.11.

Table 8.5: Comparison of DRI, kinetic energy dissipated, and SEA for different floor struts flange width-to-web height ratios. Floor beams with width-to-height ratios closer to 1, within the analyzed range, tend to be more flexible, and, thus, have lower DRI.

Version	DRI [-]	$\frac{E_D}{K_{EG}}$ [%]	SEA [kJ/kg]
FS $\frac{F_w}{W_h} = 1$	17.9	73	1.59
FS $\frac{F_w}{W_h} = 2$ (baseline)	18.2	72	1.47
FS $\frac{F_w}{W_h} = 3$	18.1	72	1.37

The data is consistent with what was expected and found earlier in this report. Floor struts with a 1:1 ratio between the web and the dimensions of the flanges will tend to have more similar flexural rigidity about the two principal axes. As the ratio increases, since the stiffness about the minor axis was kept the same, then the second moment of area about the major axis will increase. Overall, consequently, the floor strut becomes stiffer. Indeed, as shown in Figure 7.7, floor struts do purely buckle only about their minor axis, but also twist. The twisting motion is of course affected by the stiffness about both principal axes, and not only the minor one ($J = I_{xx} + I_{yy}$ [49], with J being the polar second moment of area).

In short, floor struts in variants with values of n closer to 1 (but less than 1) will be, overall, more flexible. As seen earlier more flexible struts allow to have a lower DRI, as, instead, more energy is absorbed by the floor structure. This trend can indeed be observed by Figure 8.7. Lastly, regarding SEA, it is higher as floor struts in variants with n closer to 1 are lighter.

8.4. Frames Thickness

Lastly, a sensitivity analysis on the frames thickness was performed. Once again, data is tabulated in Table 8.6, and further presented in Figure 8.13 and Figure 8.14. Data clearly shows how, above all, the the frames thickness and, by extension, the frames' bending stiffness have a massive impact on the FV's crash properties. This is significant, since, one of the early modeling assumptions, was to keep the frames height and thickness constant. The results of this sensitivity analysis prove that this approach has been overly-conservative and that a much higher fidelity model will have significantly better crash characteristics.

Figure 8.10: SEA for floor struts height-to-width ratio sensitivity analysis. A decrease in SEA is associated with an increase in crushable mass, for larger web height-to-flange width ratios

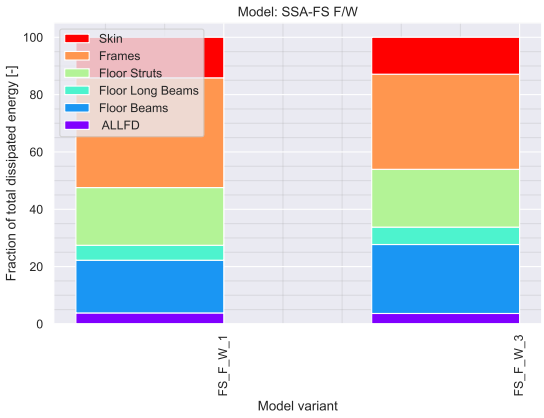

Figure 8.11: Energy absorption distribution by component, floor struts height-to-width ratio sensitivity analysis. No significant changes in the energy absorption distribution can be observed.

Assuming that the bending stiffness varies linearly with the shell thickness (which is reasonable when using the thin-walled approximation), then a 30% reduction in bending stiffness (from 6.7 mm to 4.7 mm, considering the two external versions) results in a DRI decrease of 4 units, which is significant: in theory, the risk of spinal injury would be reduced from approximately 30%, to just over 3%. As mentioned in chapter 2, a DRI of 16 is generally accepted for certification purposes.

Table 8.6: Comparison of DRI, kinetic energy dissipated, and SEA for variations in fuselage frames thickness. It is likely that in the current research, the frame bending stiffness has been overestimated in critical locations, and, thus, the results are overly-conservative. By reducing the frame bending stiffness, DRI can be significantly reduced. SEA does not increase in version with thinner frames since, for concept evaluating purposes, frames are not included in the calculation of the crushable mass.

Version	DRI [-]	$\frac{E_D}{K_{EG}}$ [%]	SEA [kJ/kg]
$t_{FR} = 4.7$mm	16.2	77	1.53
$t_{FR} = 5.7$mm (baseline)	18.2	72	1.47
$t_{FR} = 6.7$mm	20	72	1.52

The decrease in DRI is the result of a softer impact caused by a significant plastic deformation of the frames, which, in aicraft crashworthiness, is highly desired. Figure 8.12 shows the deformed section of the variant with 4.70 mm frames thickness.

From inspection of the crashed section, a significant rotation of the frames is evident, with a flattening crushing behavior. It is also evident a more significant collapse of the floor beams. In conventional aircraft configurations, the bending stiffness of the frames and that of the floor struts are of a comparable order of magnitude. As a consequence, the floor struts are able to influence the deformation pattern of the frames. As shown earlier in this report, it is the floor struts that dictate the location of the creation of the plastic hinges. Here, instead, the opposite is the case: the frames are significantly stiffer than the struts and, as a consequence, when the frames deform, the floor struts are dragged by them. This means that, when the frames deform, a significant bending load is introduced in the floor struts which, subsequently, buckle prematurely. An increase in floor struts thickness and overall dimensions might be able to further allow the creation of a plastic hinge and better support the floor.

Considering Figure 8.13, SEA only slightly increases for the thinner frames variant, since, as mentioned in section 7.4, the frames mass was not included in the calculation of the crushable mass. Additionally, Figure 8.14 clearly shows that frames thickness plays a crucial role on how components absorb energy.

Lastly, some plastic deformation of the spar occurs. As mentioned earlier, sizing of the currently chosen concept of the wing spar has not been sized yet, thus is it unknown whether the assumed spar orthogrid

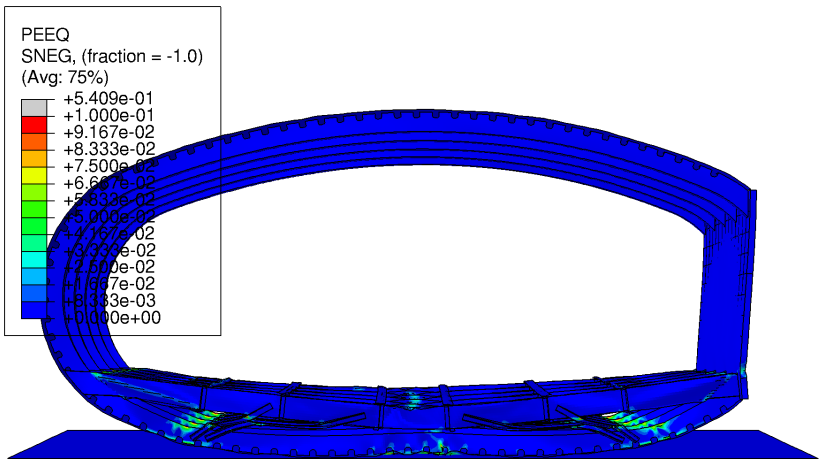

Figure 8.12: Fuselage section with thinner frames, post-crash. PEEQ is the keyword used by Abauqs to denote the equivalent plastic strain. The frames are able to deform significantly, showing a flattening crashing behavior.

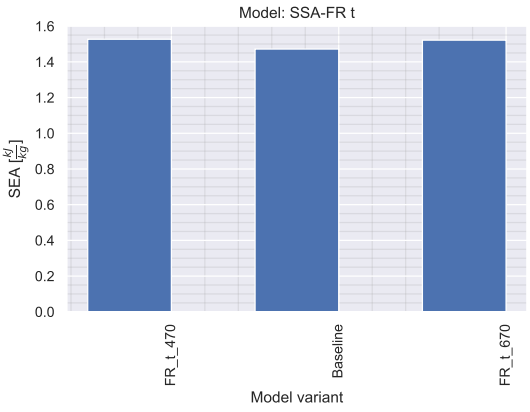

Figure 8.13: SEA for thickness sensitivity analysis. Although thinner frames absorb significantly more energy, no variation in SEA is observed as the frames are not included in the calculation of the crushable mass.

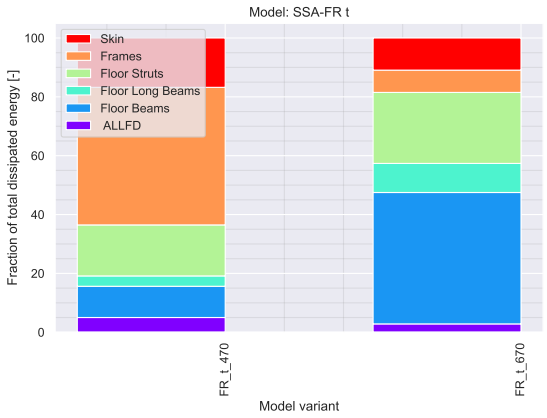

Figure 8.14: Energy absorption distribution by component, frames thickness sensitivity analysis. The frames' bending stiffness has a significant impact on the energy-absorption characteristics of the section.

parameters are conservative or not. The plastic energy dissipated by the wing spar is not shown in Figure 8.14, as for all previously tested variants, no plastic deformation of the spar plates occurred and, thus, plastic deformation energy for the spar was not requested in Abaqus' history output. Regardless, this results highlights an important aspect regarding the FV's crashworthiness: fire. In the FV aircraft, fuel tanks are located next to the passenger's cabin, on the other side of the wing spar. Figure 8.12 clearly shows that the high impact forces are able to bend the spar, and possibly crack it. By design, this should be avoided and the consequences mitigated. Although, in all likelihood, fuel will be stored in a bladder, fracture of the wing spar during a crash event might puncture the bladder itself, creating an hazardous, direct path between the fuel tanks and the passenger cabin.

8.5. Discussion on the Results

Results from the sensitivity analysis show that, in terms of mesh size, little to no variation is present between the baseline and the refined models, with the greatest difference being an increase in DRI of 0.3 units, attributed to the highest crippling resistance associated with a more refined mesh. Although, in order to define the model converged, more data points would be necessary, to show an asymptotic trend (the three data points presented here are the minimum required), the results give good confi-

dence that the model output is sufficiently close to the ‘converged’ one, and, thus, the results are to be considered accurate.

Regarding the floor struts and floor beams, the ratio between the web height and flange widths of the beams has a limited effect on the crash and energy-absorption capabilities of the fuselage section, as the second moment of area about the major axis was kept constant. Changing ratios without fixing the flexural rigidity of the beam, in turn, is certain to have, significant results on the crash properties. This is demonstrated by the fact that the simulation output is affected even by small variations in floor beam thickness (largely), and by small variations in floor struts thickness (to a lesser extent), and these variations in thickness have a direct effect on the beam’s flexural rigidity.

As already expected from the results presented in chapter 7, more flexible structures, and, in particular, flexible floor beams, have a significantly beneficial effect on the DRI. This is further confirmed in this sensitivity analysis study. While in the results presented in chapter 7 the variations have been as large as 0.5 mm, this value has been halved for the sensitivity analysis, and, still, significant variations in DRI and energy-absorption capabilities have been observed. It is worth emphasizing that, for cabin egress reasons, the deflection of the floor structure should be limited. In addition, the floor beam also does play an active role in keeping the FV fuselage shape during pressurization cycles, for which, a stiffer floor beam is likely to be required. Eventually, a final design shall be able to satisfy both requirements.

Furthermore, the sensitivity analysis on the frames’ thickness gives good confidence that, in the future, it will be possible to design a crashworthy fuselage section. In the current study, the frame bending stiffness has been largely overestimated in crucial areas that correspond to those where a plastic hinge would be created, and, thus, the frames acted as springs rather than absorbers. With reduced frame thickness, their energy-absorption capabilities increased significantly (and the opposite is equally true for increasing thickness). In future design iterations, crashworthiness requirements will likely influence the frame bending stiffness distribution, and that of other structural components of the section. It is possible, for instance, that a reduced bending stiffness of the frames can be traded off for stiffer floor beams, especially if, as mentioned earlier, a requirement on their maximum deflection is to be set.

Lastly, it is evident from visual inspection of the post-crash section, that large plastic strains are transmitted to the spar. While it is possible that, since no precise sizing data about the spar for this configuration was available, the wing spar strength has been underestimated, on the other hand, considering that the spar is an important separation barrier between the fuel tanks and the cabin, proper analyses need to be performed, in order to ensure that either the spar will not crack due to the local loads introduced by the connection with the frames, or that separation of the frames from the spar can occur before the spar itself will be damaged.

This page intentionally left blank.

V

Back Matter

This page intentionally left blank.

Summary, Conclusions and Recommendations

The scope of this report was to document all the activities, results, and analyses performed in the context of a M.Sc. thesis research project, in order to explore the feasibility to achieve a crashworthy design for the Flying-V aircraft typical fuselage section. At the beginning of this report, from this main research objective, a set of research sub-questions has been derived. Each of those will be thus addressed in the 'Conclusions' section of this chapter, where an overview of the obtained results will be given. Based on this, recommendations for future work will be provided.

8.6. Summary

The research towards the definition of a crash concept for the FV aircraft has started by acquiring and documenting current state-of-the-art research that has been performed on aircraft crashworthiness, all of which focuses on conventional aircraft configurations. This is the literature study. Design requirements have also been set as part of it. In particular, an equivalent dynamic response index not greater than 16 units has been set in order to define a typical section to be crashworthy.

Successively, a series of parametric studies have been performed, on the typical section of the Fokker F-28 airliner. The aim of the parametric studies was to understand how will mean accelerations and dynamic response index (DRI) experienced by the occupants be affected by increased fuselage eccentricity and variations in floor beam height. Data show that both parameters have a significant effect on the crash properties, and on mean accelerations in particular. A significant increase in DRI has been observed for significantly eccentric sections, compared to conventional, circular ones. There are two root causes to this: 1) overall, the passenger space in the cabin was kept approximately constant. This resulted in a decrease in crushable length, which largely affects the DRI, as the impact time duration becomes shorter; 2) due to the ovalization, fuselage frames lose part of their ability to absorb energy. As a result, more energy is dissipated by the deformation of the floor struts, when they hit the ground. This causes a sudden increase in peak load, as the crushing behavior is no longer progressive. An overall 7.5% decrease in energy absorbed has been observed between the zero-eccentricity and the most oval sections tested. While this value might seem to be relatively small, as it will also be observed in the Flying-V design chapter, even a 5-10% increase in absorbed energy can result in a significant improvement of the crash properties. Consistent results have been observed when varying the floor beam height. Data shows that even increments as small as 50 mm can allow for a significant decrease in DRI, as the impact duration increases. Small increments in floor beam height have, in turn, little to no effect on the overall energy absorbed.

In terms of suitable crash concepts for the FV aircraft, a total of four have been explored, with two being more similar to those already employed in conventional aircraft (oblique struts supporting the floor beam) and which aim to create a plastic hinge on the frames to absorb energy (6S and 4S), and other two including horizontal and vertical struts, with the purpose of dissipating energy thru the deformation of the floor beam (HB and HBH). All the concepts have been evaluated in terms of DRI and absorbed energy. Concept 6S has been discarded rather soon as it uses six floor struts to support the floor beam. However, the fuselage frames of the FV aircraft already provide high stiffness in the outboard regions of the floor beam. The additional struts at that location created an overly-stiff region, which directly transmitted high loads to the occupants, yielding high DRIs. The best-performing variant for the 6S concepts has an equivalent DRI of 23.5 units, which is significantly larger than the 16 required to deem the section crashworthy. The 6S best variant is able to dissipate 72% of the initial kinetic energy, and the crushable mass is 1.64% of the total section mass. The crushable mass is computed considering all the elements that have been treated as a design variable: floor beams and support structure.

Regarding concept 4S, the version with the lowest DRI is 4S-5, and the best-performing variant of which shows a DRI of 18.2 units, which is, however, still above the required maximum of 16. Similar to the 6S one, 4S-5 is able to dissipate 72% of the initial kinetic energy, and the crushable mass is 1.60% of the total section mass. The decrease in crushable mass is directly related to the removal of two of the floor struts. In addition, it is clear that, by removing the struts, more compliance is allowed, and, while the overall absorbed energy remains approximately constant, this directly results in a decrease in DRI.

For concept HB, the best performing one is HB-1, which features two oblique struts, and horizontal beam between the keel and the passenger floor beam, and a vertical strut which connects the former to the latter. The measured DRI is of 22.2 units, and a total of 69% of the initial kinetic energy is dissipated. In general, the main issue with concept HB was secondary bending introduced by the offset of the vertical struts' neutral axis, with that of the horizontal and floor beams, which, induced a rotation of the struts, rather than compression. This caused them to be less effective, in addition to excessive floor beam deflection.

Initially, concept HBH seemed to be a promising one, since it has many vertical crushable elements, and, thus, potential for high energy absorption by deformation of the floor beam. However, it was highly susceptible to structural instability, meaning that, instead of being crushed, the vertical struts rotated about the horizontal beams, almost rigidly. This has resulted in HBH the concept with, on average, the lowest rate of energy absorption, and with the highest DRI, as the lowest measured one was of 24.4 units. Overall, after a few design iterations, this concept was discarded.

Throughout the studies it has constantly been observed that, in order to have a good crushing behavior, a good balance between rigidity and flexibility is required. An overly rigid section was that of concept 6S, and, although decent energy absorption was achieved, a high DRI was measured, as a result of the high loads resultant from a rigid section. On the other hand, the structural instability present in concept HB, to a lesser extent, and HBH more significantly, caused large elastic deformations. While large deformations are generally desired for crashworthiness, if elastic, this will mean that energy is restituted from the structure to the occupants, which, overall, will increase the accelerations and, thus, the risk of spinal injury.

The sensitivity analysis has been performed on the overall best concept, 4S-5, and involved five different variables: mesh size; floor struts thickness; floor struts flange width-to-web height ratio; floor beams thickness; floor beams flange width-to-web height ratio; frames thickness. Data from the sensitivity analysis performed on the flange width-to-web height ratio, for both floor beams and struts, shows that, overall, such parameter has little influence on the overall crash properties of the section, provided that the flexural rigidity of the beams is kept constant. In turn, energy absorption properties and DRI are largely affected by floor beam thickness: a more compliant floor beam can greatly improve the crash properties, as it allows for large, plastic deformations. The same is true for the floor struts, from which, however, the crash properties are less sensitive. Thinner floor struts will buckle at a lower load, and, thus, allow for greater floor beam deformations. Overall, however, it is fundamental noting that excessive floor beam deformations, while they do reduce accelerations experienced by the occupants, they will also cause impeding during a post-crash evacuation, thus, reducing accident survivability. A requirement thus needs to be generated, in order to quantify the maximum allowed deflection of the floor beam.

Regarding mesh size sensitivity, the mesh has been refined up to 80% of its 'baseline' global size, and no significant variations have been observed. A slight increase in DRI, from 18.2 to 18.5 units has been observed, and this is likely due to the increase in crippling resistance of floor struts and frames, as a more refined mesh is able to better capture crippling of a structure. Overall, however, results gave good confidence on the accuracy of the analysis.

Lastly, regarding the sensitivity analysis on the frames thickness, data shows that frames bending stiffness is a crucial parameter for crashworthiness. In the fuselage section used in the analyses, as a result of simplifications made in order to reduce modeling time, the frames bending stiffness is highly overestimated in the regions where plastic hinges are set to occur, and this is one of the main causes for the little deformation of the frames observed. The sensitivity analysis shows that a 17% reduction in the frames bending stiffness yields a DRI of 16.6 units, which is just above the 16 units threshold. On the opposite, an increase in thickness of 17%, yielded a DRI of 20 units. In future work, accurate

modelling of the frames will be essential to obtain reliable results.

Conclusions

To conclude, looking back at the research questions, it is clear from the data that crash properties, in terms of average accelerations, DRI and energy absorption are deteriorated for high-eccentricity fuselages, as shown by the parametric studies. The frames will absorb less energy, and this is in part compensated by the floor struts (not fully). Accelerations experienced by the occupants will increase due to 1) higher peak loads caused by a high-speed impact of the struts with the ground, and 2) larger rebound due to less energy being dissipated from plastic deformation.

The most suitable crash concept identified within this research calls for a conventional approach, placing two floor struts underneath the floor beam. The struts will need to be optimally placed, such that the frames will plastically deform as much as possible, dissipating energy and limiting the post-crash rebound. Unstable designs for the floor supporting structure will result in little to no plastic deformation of the frames, large rebounds, and high DRIs. Flexible structures are to be generally preferred to rigid ones, in order to lower loads experienced by the occupants. However, a good degree of rigidity will be still required, in order to achieve good plastic deformations.

While within the current research it was not possible to design a crashworthy typical section, the acquired data gives good confidence, however, that with additional research this will be an achievable objective. The concept to be pursued in future work, to design a crashworthy typical section, is 4S, with an optimization to be performed with (at least) the positioning of the floor struts, and their dimensions to be design variables.

Recommendations for Future Work

From the literature study, it was evident how little to no research has been performed, to date, on crashworthiness of unconventional aircraft configurations. The current research focused on the typical section of the FV aircraft, by means of a drop test. However, while the FV does have constant cross-sections regions, that can be stretched in order to create a family of aircraft, the V-joint section of the fuselage, in turn, presents other features that are more common with blended-wing-body aircraft, and is significantly wider than the analyzed sections. In addition, the forward section of the FV aircraft will also likely experience larger vertical accelerations, due to rigid body motion effect, when, during a crash-landing, the FV would impact the ground tail-first. Thus, the first reccomendation for future work is to investigate the crash properties of the forward section of the FV aircraft, due to rigid body rotation of the FV during a crash landing, and of unconventional aircraft configurations in general.

In terms of design recommendations for the FV aircraft, it is strongly advised to pursue the design of a crashworthy typical section for the FV aircraft, using the 4S-5 structural concept. In addition, it will be beneficial to raise the floor beam as high as possible, while still preserving sufficient vertical space within the cabin. A coupled static-dynamic analysis is recommended to be performed, in order to achieve an optimal design that will be able to fulfill requirements in terms of both operational loads, and crashworthiness. The suggested workflow required to perform such an analysis, is presented in Figure 8.15.

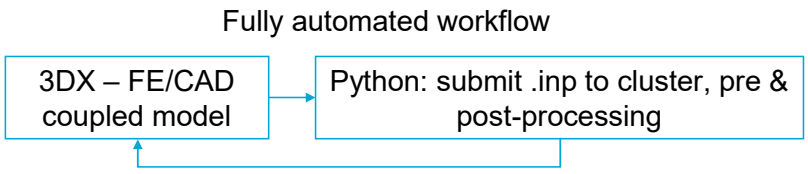

Figure 8.15: Recommended workflow for future design iterations and optimization.

In future analyses care should be taken to evaluate the effects of a crash on the structural integrity of the wing spar, in order to guarantee separation between the fuel and passenger compartments, also during impacts that can cause serious injuries, but are deemed to be survivable. As found in the

literature study, the implementation of crashworthy seats to reduce accelerations experienced by the passengers is not excluded a priori by regulators and, thus, exploring the feasibility of such option is also highly recommended.

Bibliography

[1] W. J. Oosterom. “Flying-V Family Design (MSc thesis)”. PhD thesis. Delft University of Technology, 2021.

[2] Federal Aviation Administration. *AC 20-107B - Composite Aircraft Structure - Change 1*. 2010.

[3] Climate Action Network et al. *Contribution of the Global Aviation Sector to Achieving Paris Agreement Climate Objectives*. 2018.

[4] D. S. Lee et al. “Aviation and global climate change in the 21st century”. In: *Atmospheric Environment* 43.22-23 (July 2009), pp. 3520–3537. ISSN: 13522310. DOI: 10.1016/j.atmosenv.2009.04.024.

[5] V. K. Poorte. “Design of a crash energy ab-sorber for a composite air-craft fuselage using a combined analytical-numerical approach (M.Sc. thesis)”. PhD thesis. Delft University of Technology, 2021.

[6] R. D. Hussein et al. “An analytical model of square CFRP tubes subjected to axial compression”. In: *Composites Science and Technology* 168 (Nov. 2018), pp. 170–178. ISSN: 02663538. DOI: 10.1016/j.compscitech.2018.09.019. URL: https://linkinghub.elsevier.com/retrieve/pii/S0266353818306900.

[7] M. Mohsenizadeh et al. “Additively-manufactured lightweight Metamaterials for energy absorption”. In: *Materials and Design* 139 (Feb. 2018), pp. 521–530. ISSN: 18734197. DOI: 10.1016/J.MATDES.2017.11.037. URL: https://doi.org/10.1016/j.matdes.2017.11.037.

[8] G. Yoon et al. *Challenges in fabrication towards realization of practical metamaterials*. Sept. 2016. DOI: 10.1016/j.mee.2016.05.005.

[9] I. Savage. “Comparing the fatality risks in United States transportation across modes and over time”. In: *Research in Transportation Economics* 43.1 (July 2013), pp. 9–22. ISSN: 07398859. DOI: 10.1016/J.RETREC.2012.12.011. URL: http://dx.doi.org/10.1016/j.retrec.2012.12.011.

[10] Federal Aviation Administration. *Part 25 - Airworthiness Standards: Transport Category Airplanes*. 2022.

[11] European Union Aviation Safety Agency. *Certification Specifications and Acceptable Means of Compliance for Large Aeroplanes (CS-25) - Amendment 27*. 2021.

[12] Federal Aviation Administration. *Special Conditions: Boeing Model 787-8 Airplane; Crashworthiness*. 2007.

[13] Federal Aviation Administration. *Special Conditions: Airbus A350–900 Airplane; Crashworthiness, Emergency Landing Conditions*. 2014.

[14] Transport Aircraft Crashworthiness and Ditching Working Group. *Transport Aircraft Crashworthiness and Ditching Working Group Report to FAA (Rev. B)*. Tech. rep. Oct. 2018.

[15] G. Lamanna et al. “Development of a Head Injury Criteria-Compliant Aircraft Seat by Design of Experiments”. In: (). DOI: 10.3390/aerospace6090095. URL: www.mdpi.com/journal/aerospace.

[16] J. W. Coltman et al. *Aircraft Crash Survival Design Guide: Volume II - Aircraft Design Crash Impact Conditions and Human Tolerance*. Tech. rep. Phoenix, Airzona: Simula Inc., Dec. 1989.

[17] G. Olivares et al. *List of Occupant Injury Criteria*. Tech. rep. Wichita, Kansas: National Institute for Aviation Research, Feb. 2018. URL: http://www.faa.gov/go/oamtechreports.

[18] A. M. Eiband. *Human Tolerance to Rapidly Applied Accelerations*. Tech. rep. Cleveland, Ohio: National Aeronautics and Space Administration, June 1959.

[19] G. Olivares et al. “Anthropomorphic Test Dummy Lumbar Load Variation”. In: *International Technical Conference on the Enhanced Safety of Vehicles* (2018). URL: https://www.researchgate.net/publication/327306747.

[20] J. W. Brinkley et al. *Dynamic Simulation Techniques for the Design of Escape Systems: Current Applications and Future Air Force Requirements*. Tech. rep. Dayton, Ohio: Aerospace Medical Research Laboratory - Wright-Patterson Air Force Base, Dec. 1971.

[21] P. R. Payne et al. *Dynamic Models of the Human Body*. Tech. rep. Englewood, Colorado: Aerospace Medical Research Laboratory - Wright-Patterson Air Force Base, Nov. 1969.

[22] R. Eppinger et al. *Development of Improved Injury Criteria for the Assessment of Advanced Automotive Restraint Systems-II*. Tech. rep. National Highway Traffic Safety Administration, Nov. 1999.

[23] P. Prasad et al. “The position of the United States delegation to the ISO Working Group 6 on the use of HIC in the automotive environment”. In: *SAE Technical Papers* (1985). ISSN: 26883627. DOI: 10.4271/851246.

[24] A. Taylor. “Comparison of the Hybrid II, FAA Hybrid III, and THOR-NT in Vertical Impacts”. In: Atlantic City, New Jersey: Eighth Triennial International Fire & Cabin Safety Research Conference, Oct. 2016.

[25] P. Xue et al. “Crashworthiness study of a civil aircraft fuselage section”. In: *Latin American Journal of Solids and Structures* 11.9 (2014), pp. 1615–1627. ISSN: 1679-7825. DOI: 10.1590/S1679-78252014000900007.

[26] D. I. Gransden et al. “Development of a finite element model for comparing metal and composite fuselage section drop testing”. In: *International Journal of Crashworthiness* 22.4 (July 2017), pp. 401–414. ISSN: 17542111. DOI: 10.1080/13588265.2016.1273987.

[27] H. M. Lankarani et al. “A modern aerospace modeling approach for evaluation of aircraft fuselage crashworthiness”. In: *International journal of crashworthiness* 8.4 (2003), pp. 401–413. ISSN: 1754-2111. DOI: 10.1533/ijcr.2003.0234.

[28] M. Mahé et al. “Composite fuselage crash FE modelling dedicated to enhance the design in correlation with full scale drop test”. In: *Mécanique & Industries* 2.1 (Jan. 2001), pp. 5–17. ISSN: 1296-2139. DOI: 10.1016/S1296-2139(00)01081-2.

[29] S. M. Hashemi et al. “A systematic approach to aircraft crashworthiness and impact surface material models:” in: *http://dx.doi.org/10.1243/0954410001532051* 214.5 (Dec. 2005), pp. 265–280. ISSN: 09544100. DOI: 10.1243/0954410001532051. URL: https://journals.sagepub.com/doi/10.1243/0954410001532051.

[30] A. Abromowitz et al. *Vertical Drop Test of a Narrow-Body Transport Fuselage Section With a Conformable Auxiliary Fuel Tank Onboard*. Tech. rep. Washington, D.C.: Federal Aviation Administration, Sept. 2000.

[31] A. Abramowitz et al. “Vertical Drop Test of a Narrow-Body Transport Fuselage Section with Overhead Stowage Bins”. In: *World Aviation Congress & Display*. Phoenix, Arizona: SAE International, Nov. 2002. DOI: https://doi.org/10.4271/2002-01-2995.

[32] Z. Xianfei et al. “Evaluate the crashworthiness response of an aircraft fuselage section with luggage contained in the cargo hold Evaluate the crashworthiness response of an aircraft fuselage section with luggage contained in the cargo hold”. In: *International Journal of Crashworthiness* 22.4 (Apr. 2017), pp. 347–364. ISSN: 1754-2111. DOI: 10.1080/13588265.2016.1258957. URL: https://www.tandfonline.com/action/journalInformation?journalCode=tcrs20.

[33] K. E. Jackson et al. *Crash Simulation of Vertical Drop Tests of Two Boeing 737 Fuselage Sections*. Tech. rep. Hampton, Virginia: NASA Langley Research Centre, Aug. 2002.

[34] M. Lützenburger. “Studies about the Utilisation of the Aircraft Cargo Compartment as Additional Passenger Cabin by use of Numerical Crash Simulation”. In: *The Fifth Triennial International Fire & Cabin Safety Research Conference* (Nov. 2007).

[35] G. Beuck et al. *Multi-deck passenger aircraft having impact energy absorbing structures (Airbus)*. Aug. 1996. URL: https://patents.google.com/patent/US5542626.

[36] M. Sankrithi et al. *Aircraft with multipurpose lower decks and associated methods of manufacture (Boeing)*. Nov. 1999. URL: https://patents.google.com/patent/EP1413513A3/un.

[37] K. H. Lyle et al. "Application of Probability Methods to Assess Airframe Crash Modeling Uncertainty". In: *Journal of Aircraft* 44.5 (Sept. 2007), pp. 1568–1573. ISSN: 15333868. DOI: 10.2514/1.27722. URL: https://arc.aiaa.org/doi/10.2514/1.27722.

[38] J. Blesa Gracia et al. "Increase in buckling loads of plates by introduction of cutouts". In: *Acta Mechanica* 230.8 (Aug. 2019), pp. 2873–2889. ISSN: 00015970. DOI: 10.1007/S00707-019-02435-6/TABLES/2. URL: https://link.springer.com/article/10.1007/s00707-019-02435-6.

[39] K. E. Jackson et al. *Finite Element Simulations of Two Vertical Drop Tests of F-28 Fuselage Sections*. Tech. rep. Hampton, Virginia, USA: NASA Langley Research Center, Feb. 2018. URL: http://www.sti.nasa.gov.

[40] M. Desiderio. *Data set: Fokker F-28 Fellowship typical fuselage surface model for crashworthiness*. Mar. 2023. DOI: 10.5281/ZENODO.7702919. URL: https://doi.org/10.5281/zenodo.7702918.

[41] Dassault Systèmes. *ABAQUS Documentation*. Mar. 2006.

[42] K. R. Obee. "Structural Design: A description of the design philosophy followed for the principal load carrying structures, the materials employed and details of the structural test programme". In: *Aircraft Engineering and Aerospace Technology* 39.9 (Sept. 1967), pp. 22–28. ISSN: 00022667. DOI: 10.1108/EB034293/FULL/PDF.

[43] G. Kay. *Failure Modeling of Titanium 6Al-4V and Aluminum 2024-T3 With the Johnson-Cook Material Model*. Tech. rep. Washington DC, USA: Federal Aviation Administration, Sept. 2003.

[44] K. H. Lyle et al. "Application of Probability Methods to Assess Airframe Crash Modeling Uncertainty". In: *https://doi.org/10.2514/1.27722* 44.5 (May 2012), pp. 1568–1573. ISSN: 15333868. DOI: 10.2514/1.27722. URL: https://arc.aiaa.org/doi/10.2514/1.27722.

[45] M. Waimer et al. "Contribution to an improved crash design for a composite transport aircraft fuselage-development of a kinematics model and an experimental component test setup". In: *CEAS Aeronautical Journal* 4 (2011), pp. 265–275. DOI: 10.1007/s13272-013-0070-3.

[46] M. Waimer. "Development of a Kinematics Model for the Assessment of Global Crash Scenarios of a Composite Transport Aircraft Fuselage Matthias Waimer Deutsches Zentrum für Luft- und Raumfahrt Institut für Bauweisen- und Konstruktionsforschun". PhD thesis. 2013. URL: https://elib.dlr.de/88358/.

[47] J. Benad. "The Flying V - A new Aircraft Configuration for Commercial Passenger Transport". In: *Deutscher Luft- und Raumfahrtkongress*. Nov. 2015. URL: https://www.dglr.de/publikationen/2015/370094.pdf.

[48] D. P. Raymer. *Aircraft design: a conceptual approach*. 6th ed. Blacksburg, Virginia: American Institute of Aeronautics and Astronautics, 2018, p. 1062. ISBN: 9781624104909.

[49] T. Megson. *Aircraft Structures for engineering students*. 6th ed. Butterworth-Heinemann, 2017.

[50] T. P. Dotman. "A Structural Sizing Methodology for the Wing-Fuselage of the Flying-V (M.Sc. Thesis)". PhD thesis. Delft: Delft University of Technology, Dec. 2021.

[51] Alan Poston. *Human Engineering Design Data Digest*. Tech. rep. Washington, DC: United States Department of Defence, Apr. 2000.

[52] E. Alfaro-Bou et al. "Crashworthy Design Considerations for General Aviation Seats". In: *SAE Transactions* 94 (1985), pp. 438–451.

[53] D. F. Shanahan. "Human Tolerance and Crash Survivability". In: *Pathological Aspects and Associated Biodynamics in Aircraft Accident Investigation*. Madrid, Spain: North Atlantic Treaty Organization, 2004.

[54] BEA. *Accident on 25 July 2000 at La Patte d'Oie in Gonesse (95) to the Concorde registered F-BTSC operated by Air France*. Tech. rep. Bureau Enquêtes-Accidents, 2000.

This page intentionally left blank.

VI

Appendix

This page intentionally left blank.

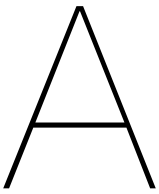

Plots of Deformed Sections

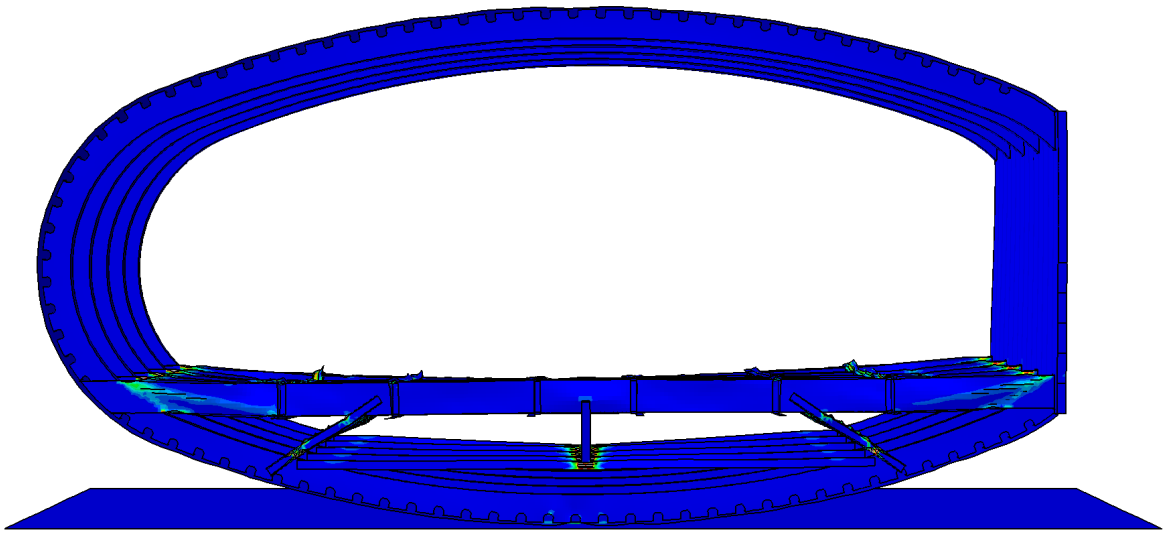

Figure A.1: Equivalent plastic strain, HB-1, t_v =1.5 mm, t_h =1.5 mm

B

Sensitivity Analysis Deformed Sections

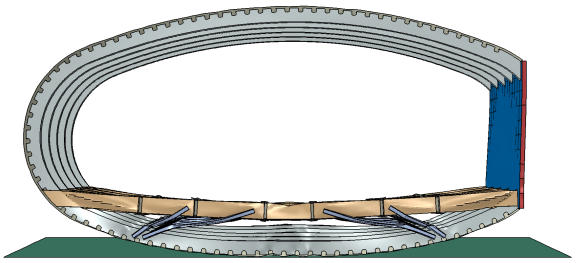

Figure B.1: Mesh sensitivity analysis, 0.80x.

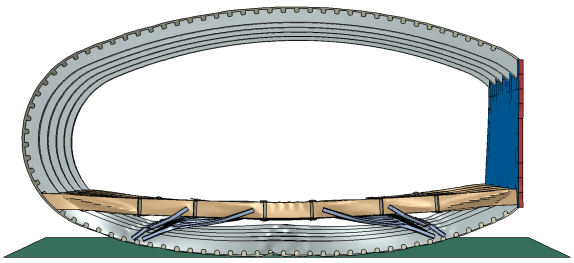

Figure B.2: Mesh sensitivity analysis, 0.90x.

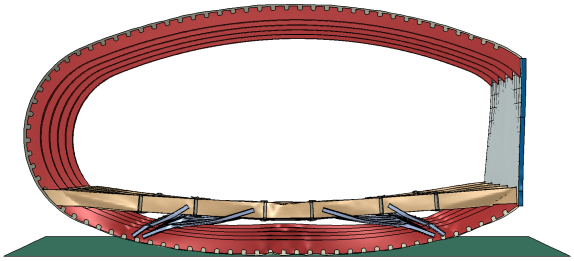

Figure B.3: Sensitivity analysis: FB thickness 1.25mm

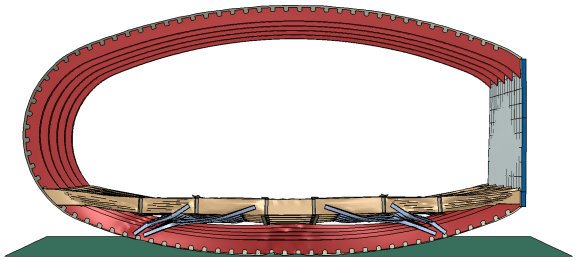

Figure B.4: Sensitivity analysis: FB thickness 0.75mm

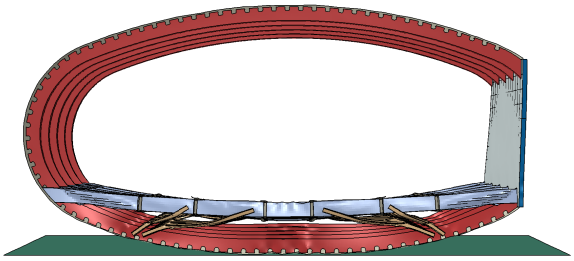

Figure B.5: Sensitivity analysis: Floor Beam Flange Width-to-Web Height Ratio of 2.

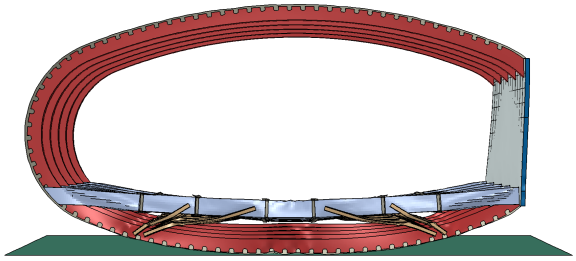

Figure B.6: Sensitivity analysis: Floor Beam Flange Width-to-Web Height Ratio of 4.

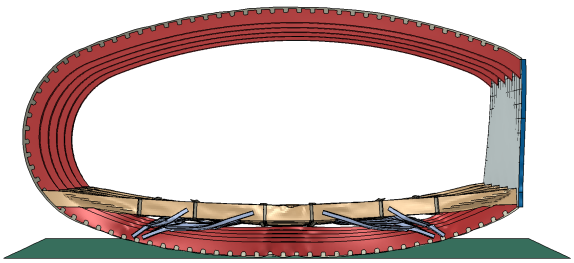

Figure B.7: Sensitivity analysis: FS thickness 2.25mm

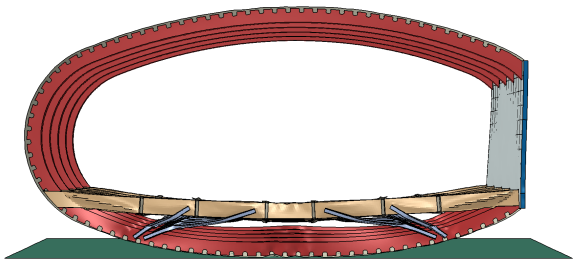

Figure B.8: Sensitivity analysis: FS thickness 2.75mm

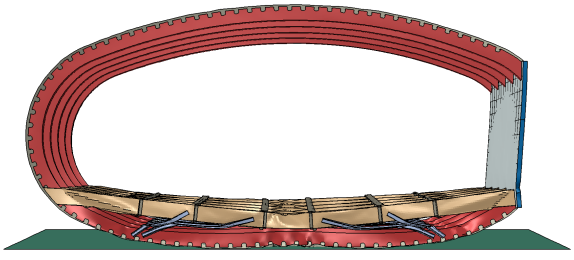

Figure B.9: Sensitivity analysis: frames thickness 4.7mm

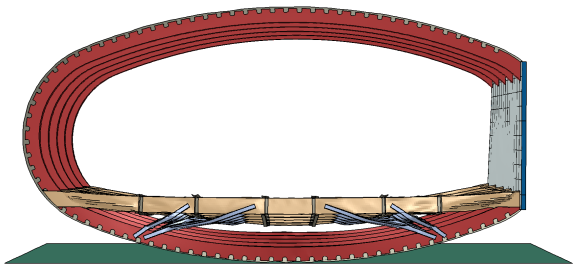

Figure B.10: Sensitivity analysis: frames thickness 6.7mm